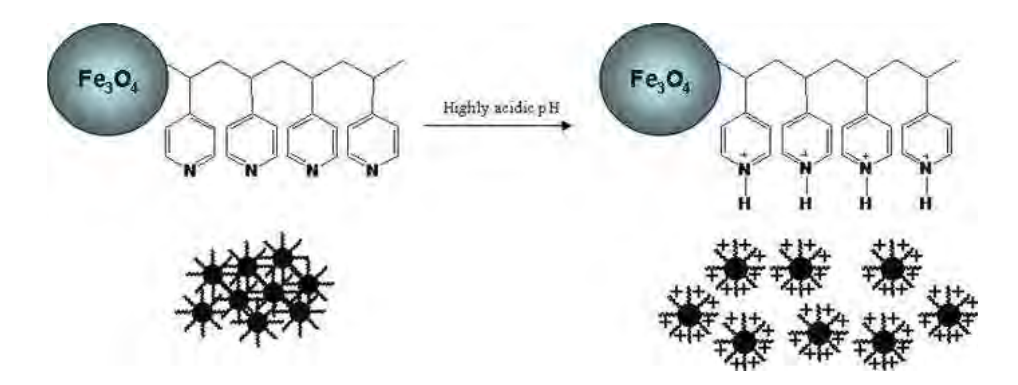
Fig. 4 The proposed stabilization mechanism of P4VP-coated MNP via electrostatic repulsion due to positively charged surface particle



charged surface particle (Fig. 4). The particles after 6 h of ATRP surface modification showed similar dispersibility of the particles in aqueous dispersions at the same pH range, implying that their dispersibility was not dependent on the chain length of P4VP on the particle surface.

How is that the pH values of the stable dispersions $(pH \le 2)$ correlate with pK_a of the pyridyl ring? Because the reported pK_a of pyridine is 5.62 (Mori et al. 2003), we expected it to be fully protonated at pH around 3-4. The fully protonated dispersion at pH 2 seems to be two orders of magnitude lower than what we expected. However, the polymeric nature of the pyridine may decrease the pK_a by one or more unit because of the potential electrostatic repulsion of the many adjacent protonated pyridyl rings. One might suspect that the MNP complex may dissolve in aqueous solution at $pH \le 2$ and eventually form Fe²⁺/Fe³⁺ ions and the free polymers. Therefore, the dispersions were centrifuged (14,000 rpm) to aggregate the particles, which were then collected by a permanent magnet. It was found that the MNP complexes still well responded to an external magnet, indicating that the MNP complex did not dissolve at low pH solution. This was in good agreement with PCS and TEM results discussed later that the polymer-MNP complexes still retained in the dispersions at pH \leq 2. However, for uses in biomedical applications, the particles should exhibit excellent dispersions between pH 4 and 8. Formation of pyridinium ion on the particle surface via the reaction between alkyl halide and pyridyl rings of P4VP-coated MNP is another promising approach to obtain stable MNP dispersions at higher pH, and this warrants further studies.

Because pyridyl ring of P4VP is highly sensitive to protonation especially in acidic pH, it is thus interesting to understand how pH of aqueous solutions influences the hydrodynamic diameter and surface charge of the P4VP-coated MNP. The particles used in this study were surface modified with P4VP via ATRP reaction for 24 h. The pHs of the aqueous dispersions containing the P4VP-MNP complexes (0.2 mg/ml) were varied from 0.5 to 2.5, and their hydrodynamic diameters were determined via PCS technique. As pH of the dispersions decreased (more acidic pH), their hydrodynamic diameters rapidly decreased at pH ranging between 2.5 and 1.5, and reached the plateau state with pH decreasing between 1.5 and 0.5 (Fig. 5a). It was hypothesized that as pH of the

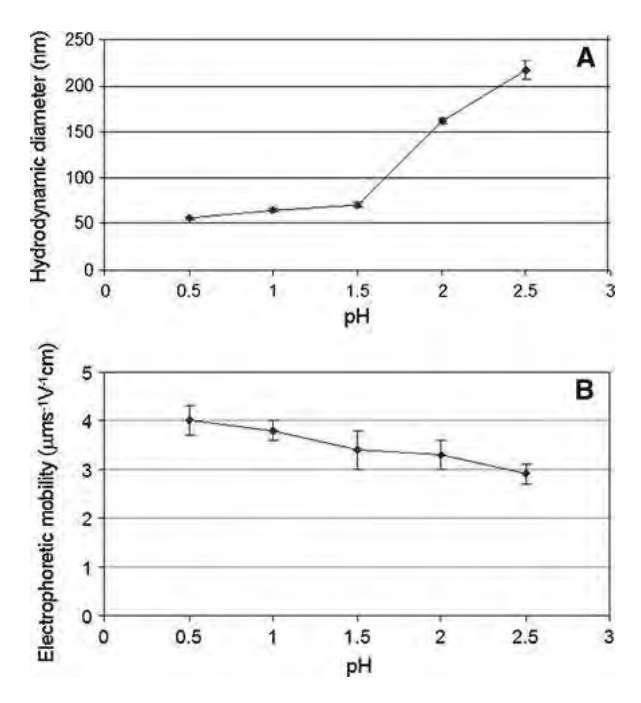


Fig. 5 a Hydrodynamic diameter and **b** electrophoretic mobility of P4VP-coated MNPs suspended in aqueous dispersions at various pHs. The particles were surface modified with P4VP via ATRP reaction for 24 h



dispersions decreased, the pyridyl rings on the surface of P4VP-coated MNP became more protonated. The formation of positive charges on their surfaces led to electrostatic repulsion toward neighboring particles, eventually preventing aggregation. These results supported the improved dispersibility of the particles at highly acidic pH.

The results from electrophoretic mobility measurements also supported this hypothesis. The samples were redispersed in the dispersions with pH ranging between 0.5 and 2.5 at ionic strength of 0.1 M for the electrophoretic mobility measurements. The obtained values were positive at all pH in the dispersions, implying that the surface of the P4VP-coated MNP have a net positive charge (Fig. 5b). The modified MNP showed an increase in electrophoretic mobility values with decreasing solution pH (more acidic pH). This was again attributed to the enhancement of protonation of pyridyl rings on the surface of the complex at highly acidic pH. It was also observed that the hydrodynamic diameter of P4VP-coated MNP steadily increased at the pH range of 0.5-1.5 and drastically changed at the pH range of 1.5-2.5, while its electrophoretic mobility showed a gradual change at the same pH range.

The dependence of ATRP reaction time on hydrodynamic diameter and electrophoretic mobility of P4VP-coated MNP was also investigated. According to the results in Fig. 6, when the ATRP reaction time was increased, the hydrodynamic diameters of the complex at pH 1.5 consistently decreased, while their surface charges became more positive. This result implied that increasing ATRP reaction time promoted the progressive growth of P4VP on the particle surface, leading to the increase in both steric and electrostatic repulsions of the protonated P4VP grafted onto the particle surface.

One might wonder if either steric or electrostatic repulsions of the grafted P4VP contributed a major effect on the particle stabilization. In order to demonstrate how well the P4VP stabilizing brushes can really perform, KNO₃ solution as background electrolyte was thus added in the dispersion to screen electrostatic repulsions. Others have reported on the effect of background electrolyte on the surface-enhanced Raman spectra (SERS) of pyridinium, and it was found that an obvious decrease of the intensity of pyridinium was observed as the concentration of KNO₃ background electrolyte was increased up to

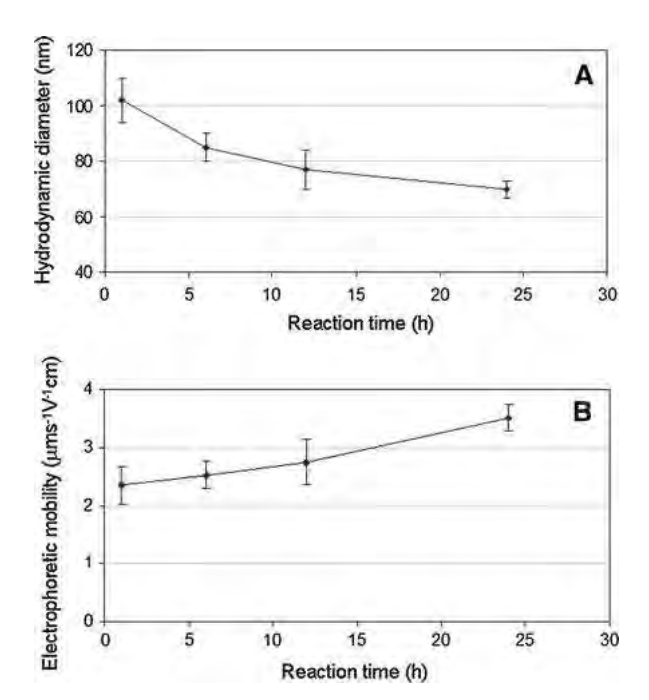


Fig. 6 a Hydrodynamic diameter and **b** electrophoretic mobility of P4VP-coated MNP at different ATRP reaction times. The P4VP-coated MNPs withdrawn at different time intervals were dispersed in pH 1.5 aqueous solutions

1.5 mol/L (Sun et al. 1985). According to this reported procedure, pH of the dispersion was monitored and carefully adjusted with HNO_3 to obtain pH = 2. Therefore, in the present study, an excess of 1.5 mol/L KNO₃ solution was added in P4VP-coated MNP dispersion to lessen the electrostatic repulsion of P4VP. It was found that the particles aggregated even though they were surface modified with P4VP via ATRP for 24 h. This result signified that electrostatic repulsion of the negatively charged surface played a major role on the particle stabilization. The chain length of the P4VP brush (the molecular weight of 5,300 g/mol) might be too short, and/or the grafting density of P4VP (0.66 chain/nm²) might be too low to stabilize the particles sterically. Increase of the molecular weight of P4VP grafted on MNP surface might enhance the steric stabilization mechanism. This can be achieved by optimization of the ATRP conditions such as reaction temperature, time, solvent and the catalytic complex (type and ratio ligand:catalyst).

The particles size and size distribution of the P4VP-coated MNP were investigated via TEM. The particles obtained from the 24 h ATRP reaction were resuspended in acidic aqueous dispersion at pH 1.5



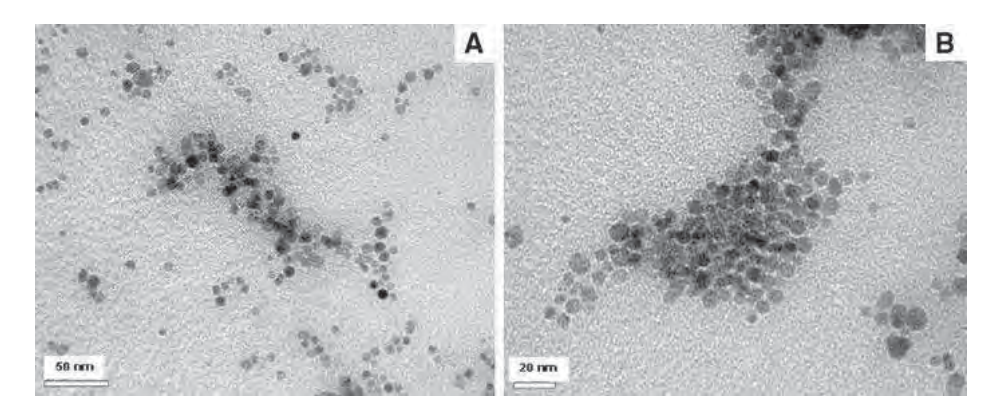


Fig. 7 TEM images of P4VP-coated MNP after 24 h of ATRP reaction, showing their good dispersibility and some nano-scale aggregation in pH 1.5-aqueous dispersions

before deposition on a TEM grid. From the TEM images (Fig. 7), the particle size was in the range of 6-11 nm with the average diameter of 8 nm. Although they were well dispersible in the media, some nanoscale aggregation of multiple particles was apparent. These particle clusters still existed in the TEM images even though the dispersions with more degree of dilution just enough to observe the presence of the particles were used for the TEM sample preparation. This indicated that these clusters were not drying artifact from the TEM sample preparation. The observation of these nanoclusters in TEM experiments was in good agreement with the PCS results that the hydrodynamic diameter of the particles (after 24 h of ATRP reaction) was in the range of 65-75 nm in aqueous solution at pH 1.5. This implies that the dispersions did not possess only the dispersed single particles, but also some stabilized clusters thoroughly dispersed in the system. It is striking to note that although these nano-clusters presented in the dispersions, these complexes were well dispersible in acidic aqueous dispersion without macroscopic aggregation visibly observed.

TGA experiments of P4VP-coated MNP at various ATRP reaction times were also performed to investigate the relative amounts of the organic components that can be grafted to the MNP surface. It should be noted that the P4VP-grafted MNP was repetitively extracted from other species in the reaction mixture with the use of ultracentrifugation and an external magnet. It was assumed that, at 600 °C under oxygen atmosphere, the weight residual was the weight of iron oxide core and the weight loss was thus attributed to the weight of the organic components including

BTPAm and P4VP that was coated onto the particles surface. Hence, percent weight residual of bare MNP and MNP coated with BTPAm were investigated to obtain the percentage of BTPAm in the complex. According to TGA results, percentage of BTPAm in the complexes was about 2 wt%. Using a similar strategy, percentages of P4VP in each complex can be determined. It was found that percentages of P4VP in the P4VP-coated MNP at 1, 6, 12 and 24 h of ATRP reaction times increased from 13, 24, 35 and 53, respectively (Fig. 8). This was a supportive result to FTIR and PCS experiments that the chain length of P4VP was increased with increasing the ATRP reaction time.

The *M*–*H* curves of bare MNP and P4VP-coated MNP were shown in Fig. 9. They showed superparamagnetic behavior at room temperature as indicated by the absence of remanence and coercivity when the external applied magnetic field was removed. From the results in Fig. 9, the decrease of saturation

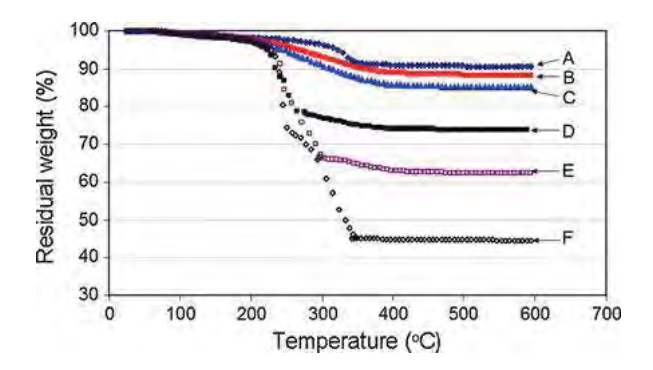


Fig. 8 TGA thermograms of (a) bare MNP. (b) BTPAm-coated MNP. P4VP-coated MNP at (c) 1 h, (d) 6 h, (e) 12 h, (f) 24 h of ATRP reactions



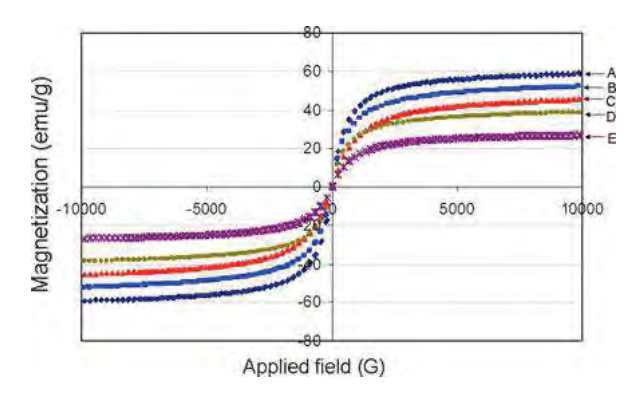


Fig. 9 *M*–*H* curves of (*a*) bare MNP, P4VP-coated MNP at (*b*) 1 h, (*c*) 6 h, (*d*) 12 h, (*e*) 24 h of ATRP reactions

 Table 1
 Percentage of magnetite in the complexes and their magnetic properties

Sample	emu/g sample ^a	% Fe ₃ O ₄ ^b	emu/g Fe ₃ O ₄
Bare MNP	58	100	63
P4VP-coated MNP at			
1 h of ATRP	52	85	61
6 h of ATRP	45	73	62
12 h of ATRP	38	62	61
24 h of ATRP	27	44	61

^a Estimated from the saturation magnetization (M_s) at 10,000 G from VSM technique

magnetization (M_s) from 58 emu/g of bare MNP to 27–52 emu/g of P4VP-coated MNP was attributed to the presence of the organic coating, including BTPAm and P4VP, on their surface. The M_s values also dropped with increasing ATRP reaction time because of the growth of P4VP, resulting in the decrease of the percentage of magnetite core in the complexes. Interestingly, when taking percentage of magnetite in the complex (estimated from TGA technique) into account, the M_s values (in an emu/g magnetite unit) were almost constant, implying that magnetic properties of the magnetite core were not sacrificed after the surface modification (Table 1).

Conclusions

This study presented a "grafting from" strategy for surface modification of magnetite nanoparticles with a pH sensitive polymer, poly(4-vinylpyridine) (P4VP), via ATRP reaction. The living ATRP allowed a very good control on the growth of P4VP on the particle surface by tuning the ATRP reaction time. Many techniques, including FTIR, PCS, TGA, and VSM, were employed to confirm the growth of P4VP with increasing ATRP reaction time. The P4VP-coated MNP was well dispersible in acidic aqueous solutions with some nanoclusters observed. Decreasing the pH of the aqueous dispersions was proposed to promote protonation of the P4VP on their surface and enhance the magnetite nanoparticles' stabilization because of positively charged repulsion mechanism. These nanocomplexes with magnetically guidable properties might be used as an anion capture in aqueous solutions.

Acknowledgments The authors thank the Thailand Research Fund (TRF), the Commission on Higher Education (CHE) (RTA5280002), and The National Research Council of Thailand (NRCT) for providing financial supports. MR acknowledges T. Inphotha for the assistance in the syntheses, Dr.R.Traiphol and O. Ketchart for the discussions in electrophoretic mobility results, and Dr. Y. Udnan and Dr. P. Masawat for the discussions in the study on the addition of background electrolyte.

References

Casula MF, Floris P, Innocenti C, Lascialfari A, Marinone M, Corti M, Sperling RA, Parak WJ, Sangregorio C (2010) Magnetic resonance imaging contrast agents based on iron oxide superparamagnetic ferrofluids. Chem Mater 22: 1739–1748

Chang CC, Lo CT (2011) Effect of particles on the structure of solvent-annealed block copolymer/nanoparticle composite thin film. J Phys Chem B 115:2485–2493

Chen Z, Yang Q, Peng K, Guo Y (2011) Surface-initiated nitroxide-mediated radical polymerization of 4-vinylpyridine on magnetite nanoparticles. J Appl Polym Sci 119:3582–3590

Cheng G, Zhao J, Tu Y, He P, Fang Y (2005) A sensitive DNA electrochemical biosensor based on magnetite with a glassy carbon electrode modified by muti-walled carbon nanotubes in polypyrrole. Anal Chem Acta 533:11–16

Coessens V, Pintauer T, Matyjaszewski K (2001) Functional polymers by atom transfer radical polymerization. Prog Polym Sci 26:337–377

Cook GL, Church FM (1957) Correlations of the infrared spectra of some pyridines. J Phys Chem 61:458–462

Gil ES, Hudson SM (2004) Stimuli-responsive polymers and their bioconjugates. Prog Polym Sci 29:1173–1222

Gohy J, Lohmeijer BGG, Varshney SK, Decamps B, Leroy E, Boileau S, Schubert US (2002) Stimuli-responsive aqueous micelles from an ABC metallo-supramolecular triblock copolymer. Macromolecules 35:9748–9755



^b Estimated from % char residual at 600 °C from TGA technique

- Golas PL, Louie S, Lowry GV, Matyjaszewski K, Tilton RD (2010) Comparative study of polymeric stabilizers for magnetite nanoparticles using ATRP. Langmuir 26:16890–16900
- Gupta AK, Gupta M (2005) Synthesis and surface engineering of iron oxide nanoparticles for biomedical applications. Biomaterials 26:3995–4021
- Hawker CJ, Bosman AW, Harth E (2001) New polymer synthesis by nitroxide mediated living radical polymerizations. Chem Rev 101:3661–3688
- Hayashi K, Ono K, Suzuki H, Sawada M, Moriya M, Sakamoto W, Yogo T (2010) One-pot biofunctionalization of magnetic nanoparticles via thiol-ene click reaction for magnetic hyperthermia and magnetic resonance. Chem Mater 22: 3768–3772
- Hermann High LR, Holder SJ, Penfold HV (2007) Synthesis of star polymers of styrene and alkyl (meth)acrylates from a porphyrin initiator core via ATRP. Macromolecules 40: 7157–7165
- Hertler WR, Boettcher FP, Sogah DY (1990) Group transfer polymerization on a polymeric support. Macromolecules 23:1264–1268
- Kobayashi M, Matsuno R, Otsuka H, Takahara A (2006) Precise surface structure control of inorganic solid and metal oxide nanoparticles through surface-initiated radical polymerization. Sci Technol Adv Mater 7:617–628
- Laurent S, Forge D, Port M, Roch A, Robic C, Elst LV, Muller RN (2008) Magnetic iron oxide nanoparticles: synthesis, stabilization, vectorization, physicochemical characterizations, and biological applications. Chem Rev 108: 2064–2110
- Lellouche J, Senthil G, Joseph A, Buzhansky L, Bruce I, Bauminger ER, Schlesinger J (2005) Magnetically responsive carboxylated magnetite-polydipyrrole/polydicarbazole nanocomposites of core-shell morphology. Preparation, characterization, and use in DNA hybridization. J Am Chem Soc 127:11998–12006
- Liu X, Xing J, Guan Y, Shan G, Liu H (2004) Synthesis of amino-silane modified superparamagnetic silica supports and their use for protein immobilization. Colloids Surf A: Physicochem Eng 238:127–131
- Liu G, Yan X, Lu Z, Curda SA, Lal J (2005) One-pot synthesis of block copolymer coated cobalt nanocrystals. Chem Mater 17:4985–4991
- Liu JY, Cheng L, Song YH, Liu BF, Dong SJ (2011) Simple preparation method of multilayer polymer films containing Pd nanoparticles. Langmuir 17:6747–6750
- Marinescu G, Patron L, Culita DC, Neagoe C, Lepadatu CI, Balint I, Bessais L, Cizmas CB (2006) Synthesis of magnetite nanoparticles in the presence of amino acids. J Nanopart Res 8:1045–1051
- Matsuno R, Yamamoto K, Otsuka H, Takahara A (2004) Polystyrene- and poly(3-vinylpyridine)-grafted magnetite nanoparticles prepared through surface-initiated nitroxidemediated radical polymerization. Macromolecules 37:2203– 2209
- Matyjaszewski K, Xia J (2001) Atom transfer radical polymerization. Chem Rev 101:2921–2990
- Milano G, Musumeci D, Gaglione M, Messere A (2010) An alternative strategy to synthesize PNA and DNA magnetic

- conjugates forming nanoparticle assembly based on PNA/DNA duplexes. Mol Biosys 6:553–561
- Mori H, Müller AHE, Klee JE (2003) Intelligent colloidal hybrids via reversible pH-induced complexation of polyelectrolyte and silica nanoparticles. J Am Chem Soc 125:3712–3713
- Mornet S, Vekris A, Bonnet J, Duguet E, Grasset F, Choy JH, Portier J (2000) DNA–magnetite nanocomposite materials. Mater Lett 42:183–188
- Pan BF, Gao F, Gu HC (2005) Dendrimer modified magnetite nanoparticles for protein immobilization. J Colloid Interface Sci 284:1–6
- Pei W, Kumadaa H, Natusmea T, Saitoa H, Ishio S (2007) Study on magnetite nanoparticles synthesized by chemical method. J Magn Magn Mater 310:2375–2377
- Perrin DD (1965) Dissociation constants of organic bases in aqueous solution. IUPAC Chem Data Ser, Buttersworth
- Pinkrah VT, Snowden MJ, Mitchell JC, Seidel J, Chowdhry BZ, Fern GR (2003) Physicochemical properties of poly(*N*-isopropylacrylamide-co-4-vinylpyridine) cationic polyelectrolyte colloidal microgels. Langmuir 19:585–590
- Rutnakornpituk M, Puangsin N, Theamdee P, Rutnakornpituk B, Wichai U (2011) Poly(acrylic acid)-grafted magnetic nanoparticle for conjugation with folic acid. Polymer 52:987–995
- Sonvico F, Mornet S, Vasseur S, Dubernet C, Jaillard D, Degrouard J, Hoebeke J, Duguet E, Colombo P, Couvreur P (2005) Folate-conjugated iron oxide nanoparticles for solid tumor targeting as potential specific magnetic hyperthermia mediators: synthesis, physicochemical characterization, and in vitro experiments. Bioconjugate Chem 16: 1181–1188
- Sun SC, Bernard I, Birke RL, Lombardi JR (1985) The effect of pH, Chloride ion and background electrolyte concentration on the SERS of acidified pyridine solutions. J Electroanal Chem 196:359–374
- Sun Y, Ding X, Zheng Z, Cheng X, Hu X, Peng Y (2007) Surface initiated ATRP in the synthesis of iron oxide/polystyrene core/shell nanoparticles. Eur Polym J 43:762–772
- Tamami B, Farjadian F (2011) Synthesis and applications of polyvinylpyridine-grafted silica containing palladium nanoparticles as a new heterogeneous catalyst for heck and suzuki coupling reactions. J Iran Chem Soc 8:S77–S88
- Thiessen W, Dubavik A, Lesnyak V, Gaponik N, Eychmüller A, Wolff T (2010) Amphiphilic and magnetic behavior of Fe₃O₄ nanocrystals. Phys Chem Chem Phys 12:2063–2066
- Tian J, Zheng F, Zhao HY (2011) Nanoparticles with Fe₃O₄-nanoparticle cores and gold-nanoparticle coronae prepared by self-assembly approach. J Phys Chem C 115:3304–3312
- Woo K, Hong J, Choi S, Lee HW, Ahn JP, Kim CS, Lee SW (2004) Easy synthesis and magnetic properties of iron oxide nanoparticles. Chem Mater 16:2814–2818
- Xu FJ, Neoh KG, Kang ET (2009) Bioactive surfaces and biomaterials via atom transfer radical Polymerization. Prog Polym Sci 34:719–761
- Yang X, Shi J, Johnson S, Swanson B (1998) Growth of ultrathin covalently attached polymer films:# uniform thin films for chemical microsensors. Langmuir 14:1505–1507
- Zhang J, Misra RDK (2007) Magnetic drug-targeting carrier encapsulated with thermosensitive smart polymer:



- Core–shell nanoparticle carrier and drug release response. Acta Biomater $3\colon\!838\!-\!850$
- Zhang Y, Kohler N, Zhang M (2002) Surface modification of superparamagnetic magnetite nanoparticles and their intracellular uptake. Biomaterials 23:1553–1561
- Zhou Y, Wang S, Ding B, Yang Z (2008) Modification of magnetite nanoparticles via surface-initiated atom
- transfer radical polymerization (ATRP). Chem Eng J 138:578–585
- Zhou LL, Yuan JY, Yuan WZ, Sui XF, Wu SZ, Li ZL, Shen DZ (2011) Synthesis, characterization, and controllable drug release of pH-sensitive hybrid magnetic nanoparticles. J Magn Magn Mater 321:2799–2804





Contents lists available at SciVerse ScienceDirect

Talanta





FRET detection of DNA sequence via electrostatic interaction of polycationic phenyleneethynylene dendrimer with DNA/PNA hybrid

Paitoon Rashatasakhon^a, Kunnigar Vongnam^b, Warathip Siripornnoppakhun^a, Tirayut Vilaivan^a, Mongkol Sukwattanasinitt^{a,*}

- ^a Center for Petroleum, Petrochemicals and Advanced Materials, Department of Chemistry, Faculty of Science, Chulalongkorn University, Phayathai Road, Pathumwan, Bangkok 10330, Thailand
- b Program of Petrochemistry and Polymer Science, Faculty of Science, Chulalongkorn University, Phayathai Road, Pathumwan, Bangkok 10330, Thailand

ARTICLE INFO

Article history:
Received 23 October 2011
Received in revised form
13 November 2011
Accepted 14 November 2011
Available online 19 November 2011

Keywords: DNA Dendrimer Fluorescence sensor FRET Peptide nucleic acid

ABSTRACT

Interaction between a polycationic compound and DNA is a useful phenomenon for development of a new DNA sensing system. In this work, dendritic polycationic phenyleneethynylene fluorophores are investigated as a Förster resonance energy transfer (FRET) donor for the detection of DNA hybridization in conjunction with a fluorescein-labeled pyrrolidinyl peptide nucleic acid (Fl-acpcPNA) probe. The first generation dendrimer is an efficient energy donor for the fluorescein acceptor but also shows nonspecific FRET signal with Fl-acpcPNA. The addition of *N*-methyl 2-pyrrolidone can virtually completely remove the non-specific interaction between Fl-acpcPNA and the dendrimer. Under the optimal condition, the complementary DNA gives a distinctively high FRET ratio (1.42) comparing with those of the non-complementary (0.26) and singly mismatched (0.51) DNAs. The FRET ratio responses linearly with the DNA concentration with the detection limit lower than 1 nM. The FRET ratio is even higher for the complementary target DNAs with extra hanging nucleotide sequences, which is a more frequently encountered scenario in real applications.

© 2011 Elsevier B.V. All rights reserved.

1. Introduction

Detection of DNA sequences is indispensable in medical diagnostics and biochemical analyses. During the past decades, we have witnessed several major developments of various techniques for the detection of DNA sequences based on DNA hybridization process including fluorimetry [1-3], colorimetry [4,5], electrochemistry [6-8], and surface plasmon resonance [9,10]. Homogeneous fluorescence analysis in solution is considered as one of the most convenient and sensitive methods. Direct use of fluorescent dyes which are capable of intercalating or binding into the grooves of double-stranded DNA (dsDNA) with concomitant fluorescence enhancement, such as ethidium bromide, SYBR Green® and PicoGreen®, as reporters for DNA hybridization is probably the most simple and common practice. Enhanced fluorescent signals by mismatched hybridized or even unhybridized singlestranded DNAs (ssDNA) are also often encountered due to their significant binding to these dyes [11,12]. To increase specificity of the analytical method, Förster resonance energy transfer (FRET) between energy donor and acceptor fluorophores has been successfully exploited [13,14]. One of the most intriguing developments

involves the use of a polycationic π -conjugated polymer as a FRET donor and a flurophore-labeled ssDNA as a FRET acceptor [15,16]. Fluorescein-labeled peptide nucleic acid (Fl-PNA), a neutral peptide analog of DNA, has also been applied in a FRET-based detection of specific DNA sequences via PNA/DNA Watson–Crick hybridization [17–19]. The successful use of PNA probe has been attributed to two main reasons. First, PNA/DNA hybrid electrostatically interacts with the polycationic FRET donor more strongly, and second, the neutral unhybridized PNA and the PNA/DNA duplex is more readily and specifically formed than the analogous DNA/DNA duplex [20–23]. As a result, the use of PNA in place of DNA significantly increased the specificity such that even a single mismatched base in the DNA target can be readily distinguished with a considerably lower FRET signal [19].

Comparing with small molecule, conjugate polymers containing multiple fluorogenic moieties offer advantages in signal amplification and large molecular optical cross section [24–26]. The use of polycationic conjugated polymers as FRET donors for the detection of PNA/DNA hybridization however have been limited to a class of linear poly(phenylene-co-fluorene). The linear conjugated polymers usually possess broad distribution of molecular weights which may be not readily reproducible from lab to lab or even batch to batch. Unpredictable secondary structures of linear polymeric chains in aqueous media also add subtle issues in the interpretation of its intermolecular interaction. We are interested in exploring

^{*} Corresponding author. Tel.: +66 2 2187620; fax: +66 2 2187598. E-mail address: smongkol@chula.ac.th (M. Sukwattanasinitt).

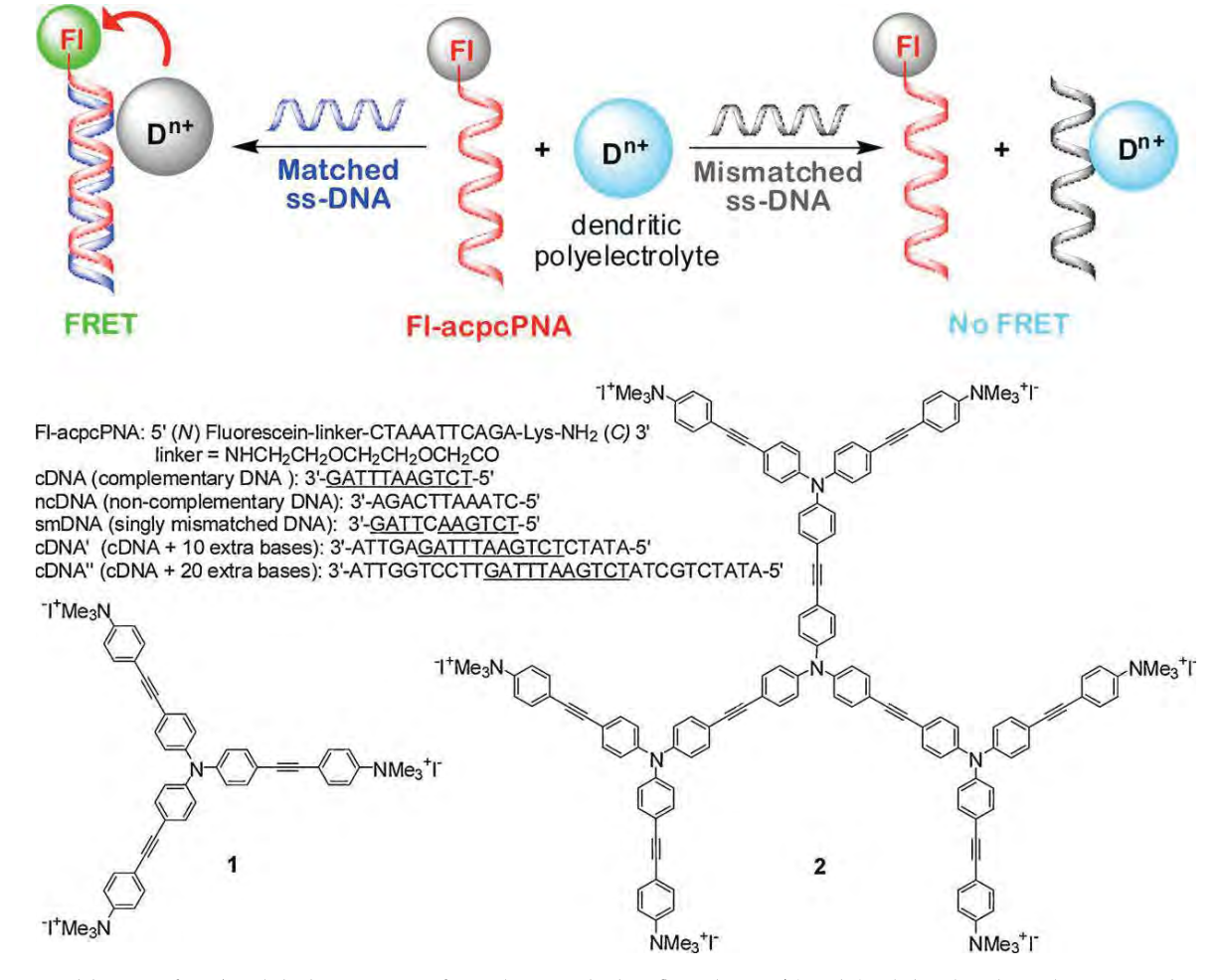


Fig. 1. Proposed detection of DNA/PNA hybridization via FRET from polycationic dendritic fluorophores Dⁿ⁺ (1 and 2) including their chemical structures and sequences of FI-acpcPNA and DNAs used.

a class of polycationic fluorophores with definite molecular sizes and charges to be used as fluorescent transducers. Dendrimers are good candidates as their sizes and shapes can be controlled via convergent synthetic approach [27–30]. Recently, applications of dendritic phenylene-ethynylene polyelectrolytes as fluorescent signal transducer in sensing systems have been reported [31–36]. In this present work, we investigated the use of polycationic phenylene-ethynylene dendrimers 1 and 2 (Fig. 1) as a FRET donor in the detection of DNA sequence via the PNA/DNA hybridization principle. The specific PNA used in this work is a conformational constrained fluorescein-labeled pyrrolidinyl PNA (Fl-acpcPNA) derived from proline/2-aminocyclopentanecarboxylic acid backbone which exhibited superior specificity in DNA hybridization than the classical PNA [37,38].

2. Experimental

2.1. Chemicals and materials

Dendritic cationic fluorophores, **1** and **2**, were prepared as described in our previously reported procedures [34]. The acpcPNA probe was labeled at the *N*-terminus by 5(6)-carboxyfluorescein *N*-hydroxysuccinimidyl ester via an aminoethoxyethoxyacetyl spacer (–NHCH₂CH₂OCH₂CH₂OCH₂CO–) and was purified by HPLC after removal from the solid support [37,38]. HPLC-purified DNA

oligo-nucleotides were purchased from Biodesign-Co., Ltd. (Thailand). Reagent grade formamide and N-methyl-2-pyrrolidinone were purchased from Merck and used without further purification.

2.2. Instruments

The UV–vis absorption spectra were recorded on a Varian Cary 50 UV–vis spectrophotometer. Fluorescence measurements were carried out with solution samples in a 3 mL quartz cuvette at room temperature using a Varian Cary Eclipse spectrofluorometer at 90° detection angle. The FRET ratios were calculated as the fluorescent intensity of the acceptor (fluorescein) over the intensity of the donor (2).

2.3. PNA/DNA sample preparation

Solutions of Fl-acpcPNA ($0.6\,\mu\text{M}$) and DNA ($0.6\,\mu\text{M}$) in 10 mM phosphate saline buffer pH 6.9 were mixed and allowed for hybridization at room temperature for overnight to provide a $0.3\,\mu\text{M}$ Fl-acpcPNA/DNA duplex stock solution. For the fluorescence measurement, this stock solution was mixed with the fluorophore solution and the total volume was adjusted by 10 mM phosphate saline buffer pH 6.9, to give the final concentration of 1.0 μ M for the fluorophore 0.1 μ M for the DNA and PNA.

3. FRET experiments

To 1 mL of Fl-acpcPNA or Fl-acpcPNA/DNA stock solution (0.3 μ M) was added 30 μ L of 1 or 2 solution (100 μ M), and the designated amount of 1-methyl-pyrrolidinone (NMP) or formamide at room temperature (25 °C). The final volume of the mixture was adjusted to 3 mL by 10 mM phosphate saline buffer pH 6.9 to afford the final concentration of 1 μ M for the fluorophores and 0.1 μ M for PNA and DNA. After the solution was thoroughly mixed for 1 min, the emission spectrum (410–700 nm) was recorded at room temperature with an excitation wavelength of 400 nm. The FRET signal and ratio were observed as the intensity of the fluorescein band peaked at 530 nm from the spectrum with the donor peak at 440 nm normalized.

4. Results and discussion

The basis of this work, as illustrated in Fig. 1, relies on the assumption that there is no significant interaction between the cationic dendritic fluorophores $\mathbf{D^{n^+}}$ (1 or 2) and the electrostatically neutral Fl-acpcPNA. The addition of ssDNA with a complementary base sequence (cDNA) should give rise to a formation of a negatively charged DNA/PNA duplex, which in turn preferentially bind with the cationic dendrimer as a result of Coulombic interaction. A close proximity between $\mathbf{D^{n^+}}$ and the fluorescein moiety on the acpcPNA should result in a FRET signal observed as enhanced fluorescein emission and reduced $\mathbf{D^{n^+}}$ emission. On the other hands, if the DNA sequence has a non-complementary base sequence (ncDNA), there should be only the DNA/ $\mathbf{D^{n^+}}$ complexation, which gives no FRET signal.

The emission spectra of 1 and 2 along with the absorption and emission spectra of Fl-acpcPNA are shown in Fig. 2. Although the emission band of 1 has an ideal full overlapping integral with the absorption spectrum of Fl-acpcPNA, its broad emission band also cover a large portion of Fl-acpcPNA emission band. This precludes an efficient function of 1 as a FRET donor because the FRET signal detected from fluorescein emission would be greatly interfered by the donor emission. On the other hand, the emission band of the first generation dendrimer 2 advantageously appears at a significantly shorter wavelength probably due to its slower geometrical relaxation as a result of the bulkier dendritic arms. With a shorter emission wavelength, the overlapping area between the emission band of 2 and Fl-acpcPNA is considerably reduced and thus dendrimer 2 is a better choice as a FRET donor for Fl-acpcPNA. In

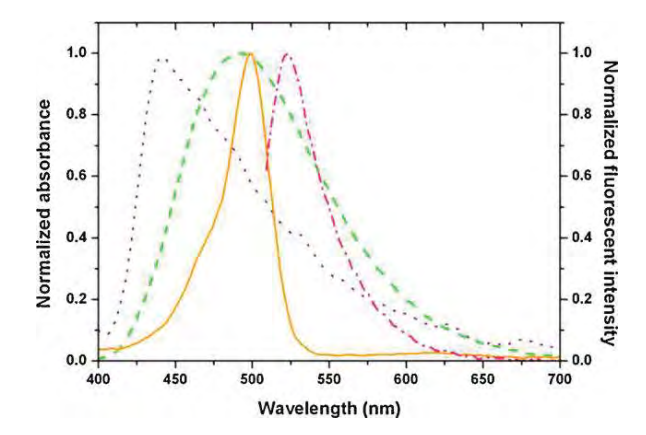


Fig. 2. Absorption spectrum of Fl-acpcPNA (-) and emission spectra of $\mathbf{1}$ (---), $\mathbf{2}$ (-) and Fl-acpcPNA (---).

addition, the higher number of positive charge (6+) on **2** should also provide a stronger electrostatic interaction with the PNA/DNA duplex that in turn enhance the efficiency of the FRET process.

Our initial FRET measurements showed that the use of 1 as the energy donor failed to give any distinguishable FRET signal even in the presence of the complementary DNA (Fig. 3a). On the other hand, the experiment with dendrimer 2 showed promising results. The strong emission signal of fluorescein was observed at 530 nm, especially for the system with cDNA (Fig. 3b). For the system with ncDNA, a much weaker FRET signal was observed. Interestingly, we observed a relatively strong FRET signal from the solution of only 2 and Fl-acpcPNA in the absence of any DNA. This result is somewhat deviate from our postulation proposed in Fig. 1 and it indicates a significant interaction between the donor and Fl-acpcPNA itself. This undesirable non-specific FRET signal may result from a relatively strong hydrophobic interaction between the dendritic core of ${\bf 2}$ and the PNA backbone. Drastic reduction of the FRET signal in the presence of ncDNA implies that the Coulombic interaction of ncDNA with **2** is likely to be much stronger than the hydrophobic interaction between 2 and Fl-acpcPNA.

Recently, formamide has been successfully used as an additive to reduce non-specific hydrophobic interaction between DNA and PNA [39] while *N*-methylpyrrolidinone (NMP) has been used to reduce such interaction between DNA and cationic polyelectrolyte fluorophore [40]. These additives are known for their ability to

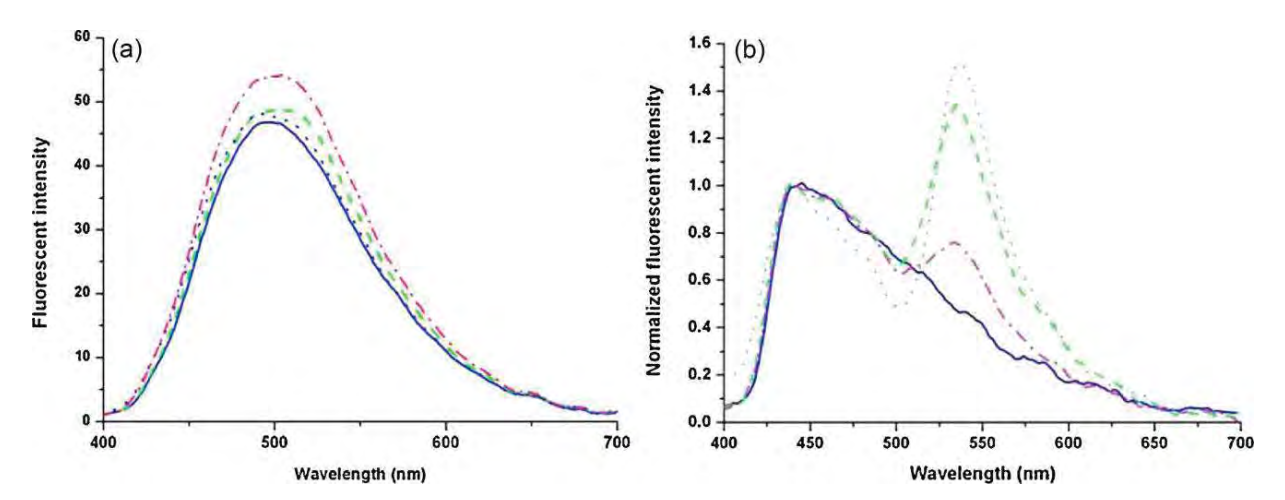


Fig. 3. (a) Emission spectra of 1 (-), 1:Fl-acpcPNA (---), 1:Fl-acpcPNA:cDNA (···) and 1:Fl-acpcPNA:ncDNA (···) in phosphate saline buffer pH 6.9; [1] = 1.0 μM; [Fl-acpcPNA] = [DNA] = 0.1 μM. (b) Emission spectra of 2 (-), 2:Fl-acpcPNA (---), 2:Fl-acpcPNA:cDNA (···) and 2:Fl-acpcPNA:ncDNA (···) in phosphate saline buffer pH 6.9; [2] = 1.0 μM; [Fl-acpcPNA] = [DNA] = 0.1 μM.

Table 1 Effects of additives on FRET ratios.

Additive	2 + Fl-acpcPNA	2 + Fl-acpcPNA + cDNA	2 + Fl-acpcPNA + ncDNA
None	1.23 ± 0.14	1.40 ± 0.13	0.72 ± 0.11
Formamide (20%, v/v)	1.34 ± 0.16	1.66 ± 0.15	1.03 ± 0.09
NMP (20%, v/v)	0.58 ± 0.05	0.90 ± 0.07	0.47 ± 0.01
NMP (10%, v/v)	0.39 ± 0.15	1.42 ± 0.13	0.26 ± 0.18

solvate the PNA and DNA chain primarily via hydrogen bonding, which consequently reduce the hydrophobic interaction. In our tests, Table 1 shows that formamide cannot reduce the FRET ratio observed in the system containing only **2** and Fl-acpcPNA while NMP drastically decreases the FRET ratio of this system. At 10% (v/v) of NMP, the non-specific FRET ratio decreases without deteriorating the FRET signal generated from the desired Fl-acpcPNA/cDNA hybridization. Importantly, the FRET ratio of the PNA/ncDNA pair is also significantly reduced by NMP. Accordingly, the cDNA gives remarkably higher FRET signal than those of the ncDNA and the non-specific background in the presence of 10% (v/v) NMP (Fig. 4).

The effect of donor/acceptor ratio in the FRET process was studied at constant concentration of Fl-acpcPNA at $0.1~\mu M$ in the presence of 10% (v/v) NMP. The concentration of **2** was varied as 0.5, 1.0, and $1.5~\mu M$. We compared the FRET ratios obtained from each condition in the presence of cDNA, ncDNA, and single mismatched DNA (smDNA), as well as in the absence of DNA. The plot in Fig. 5 indicates that the 1:10~M ratio of Fl-acpcPNA/**2** provide the best detection of cDNA while the non-specific signal, observed in the absence of DNA, is suppressed at a much lower level. This optimum ratio is probably governed by the countered balance between two concentration effects i.e. the increases of donor/acceptor complexation and the fluorescence background of **2**. It is also important to note that the cDNA (fully complementary DNA) can be clearly distinguished from the smDNA (singly mismatched DNA) at this optimal ratio.

We next investigated the effect of target DNA chain length on FRET efficiency by using 21-mer (cDNA') and 31-mer DNA (cDNA"). Both cDNA' and cDNA" contain the complementary base sequence in the middle with extra base units extended from its both ends. The results are encouraging that the FRET ratio with cDNA' and cDNA" are successively higher than that in the case with cDNA (Fig. 6) and that the target DNAs with extra hanging nucleotide sequences is more likely the case encountered in real applications involving PCR-amplified or genomic DNA targets. The enhanced FRET signals by

longer DNA chains highlight the importance of electrostatic interaction between the segment of DNA/PNA duplex and the cationic dendrimer in the FRET process.

The FRET ratio of the sensing system increased with the cDNA and a plot between corrected FRET ratio ($F_{(530)}$ – $F_{0(530)}$) against concentration of cDNA yielded a linear line as shown in Fig. 7. The linear response suggests that the sensing system should be applicable for quantification of a designated DNA sequence. Fig. 7 also showed that the detection limit of this system is below 1 nM.

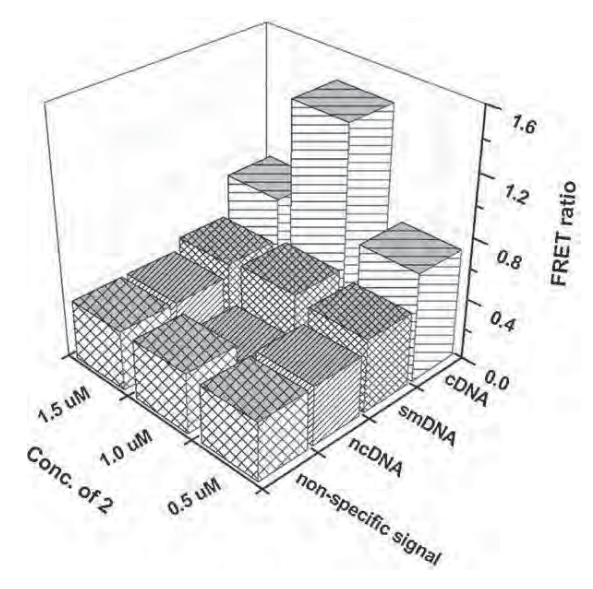


Fig. 5. FRET ratios obtained upon the addition of DNA $(0.1 \,\mu\text{M})$ to solutions containing varied concentrations of **2** and fixed Fl-acpcPNA concentration $(0.1 \,\mu\text{M})$.

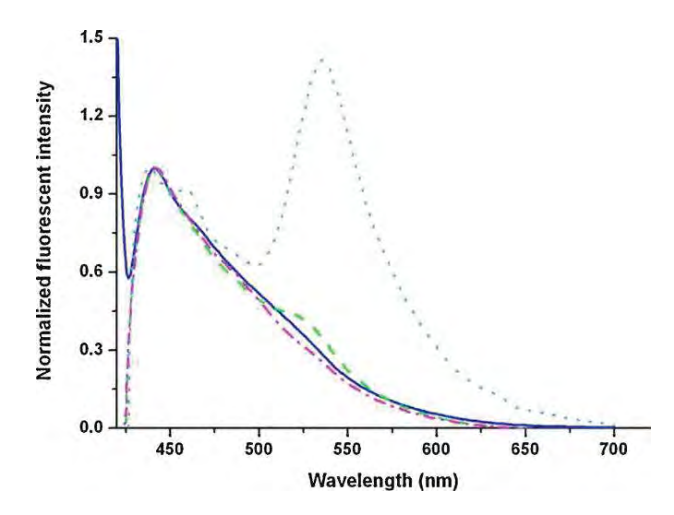


Fig. 4. Emission spectra of **2** (–), **2**:Fl-acpcPNA (---), **2**:Fl-acpcPNA:cDNA (\cdots) and **2**:Fl-acpcPNA:ncDNA (\cdots) in panel (a) phosphate saline buffer pH 6.9 with 10% (v/v) NMP [2] = 1.0 μ M; [Fl-acpcPNA] = [DNA] = 0.1 μ M.

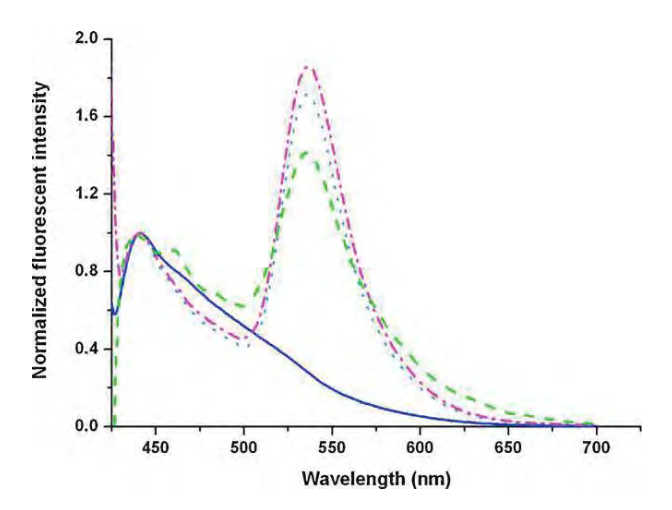


Fig. 6. Emission spectra of **2** (–), **2**:Fl-acpcPNA:cDNA(---), **2**:Fl-acpcPNA:cDNA' (\cdots) and **2**:Fl-acpcPNA:cDNA" (\cdots) in phosphate saline buffer pH 6.9 in the presence of 10% (v/v) NMP. [2] = $1.0~\mu$ M; [Fl-acpcPNA] = $0.1~\mu$ M; [DNA] = $0.1~\mu$ M.

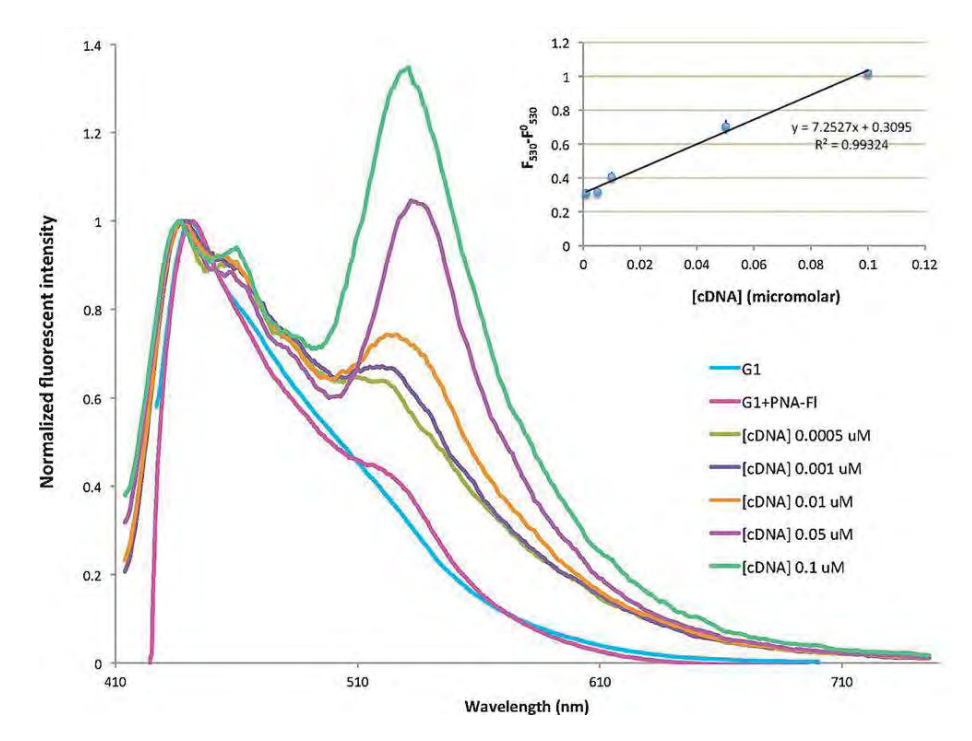


Fig. 7. Emission spectra and Linear plot between corrected FRET ratio ($F_{(530)}$ - $F_{0(530)}$) and concentration of cDNA in phosphate saline buffer pH 6.9 with 10% (v/v) NMP $[2] = 1.0 \,\mu\text{M}$; $[Fl-acpcPNA] = 0.1 \,\mu\text{M}$.

5. Conclusion

In conclusion, we have demonstrated a detection of DNA hybridization by Förster resonance energy transfer (FRET) employing a cationic phenyleneethynylene dendritic fluorophore as a FRET donor and a fluorescein-labeled pyrrolidinyl peptide nucleic acid (Fl-acpcPNA) as the energy acceptor. The first generation fluorescent dendrimer with six positively charged ammonium peripheries provide adequate electrostatic interaction and spectral overlap resulted in readily distinguishable signals for the cases with complementary and non-complementary DNA. The background signal, which may be caused by the hydrophobic interaction between the inner part of the fluorophore and the peptide backbone of the acpcPNA could be eliminated by the addition of N-methyl-2-pyrrolidinone (NMP). Under optimum sensing condition, the sensing system readily detected fully complementary sequence DNA at submicromolar concentration level and distinguished it from the DNA with a single mismatch base. The cationic phenyleneethynylene dendrimer showed even higher FRET signal for detecting the target DNAs with extra hanging nucleotide sequences that should be useful for detecting PCR-amplified or genomic DNA targets in real applications.

Acknowledgement

This work is part of the Project for Establishment of Comprehensive Center for Innovative Food, Health Products and Agriculture supported by the Thai government stimulus package 2 (TKK2555, SP2) and receives financial support from the Thailand Research Fund (RTA5280002), the National Nanotechnology Center, NSTDA (NN-B-22-FN9-10-52-06), the 90th Anniversary of Chulalongkorn University Fund, the National Research University of CHE and the Ratchadaphiseksomphot Endowment Fund (AM1006A). KV thanks the Faculty of Science, Chulalongkorn University (A1B1-5) for her research fellowship. We also would like to thank Ms. Chalothorn Boonlua for Fl-acpcPNA samples.

References

- [1] J. Zhu, Y. Lu, C. Deng, G. Huang, S. Chen, S. Xu, Y. Lv, K. Mitchelson, J. Cheng, Anal. Chem. 82 (2010) 5304-5312
- I. Saaem, K-S. Ma, A.N. Marchi, T.H. LaBean, J. Tian, ACS Appl. Mater. Interfaces 2 (2010) 491–497.
- [3] K. Boeneman, J.R. Deschamps, S. Buckhout-White, D.E. Prasuhn, J.B. Blanco-Canosa, P.E. Dawson, M.H. Stewart, K. Susumu, E.R. Goldman, M. Ancona, I.L. Medintz, ACS Nano 4 (2010) 7253–7266.
- [4] A. Baeissa, N. Dave, B.D. Smith, J. Liu, ACS Appl. Mater. Interfaces 2 (2010) 3594-3600.
- R. Kanjanawarut, X. Su, Anal. Chem. 81 (2009) 6122-6129.
- E.G. Hvastkovs, D.A. Buttry, Analyst 135 (2010) 1817-1829.
- J.-Y. Park, S.-M. Park, Sensors 9 (2009) 9513–9532.
- X. Zhang, K. Jiao, S. Liu, Y. Hu, Anal. Chem. 81 (2009) 6006-6012. [9] S. Ekgasit, G. Stengel, W. Knoll, Anal. Chem. 76 (2004) 4747-4755.
- [10] B.P. Nelson, T.E. Grimsrud, M.R. Liles, R.M. Goodman, R.M. Corn, Anal. Chem. 73
- [11] J.B. LePecq, C. Paoletti, J. Mol. Biol. 27 (1967) 87-106.
- [12] J.T. Petty, J.A. Bordelon, M.E. Robertson, J. Phys. Chem. B 104 (2000)
- [13] R. Flehr, A. Kienzler, W. Bannwarth, M.U. Kumke, Bioconjugate Chem. 21 (2010) 2347-2354.
- Y.-N. Teo, E.T. Kool, Bioconjugate Chem. 20 (2009) 2371–2380.
- [15] G. Liang, A.S. Susha, A.A. Lutich, F.D. Stefani, J. Feldmann, A.L. Rogach, ACS Nano 3 (2009) 4127-4131.
- R.R. Nayak, O.K. Nag, M. Kang, Y. Jin, H. Suh, K. Lee, H.Y. Woo, Macromol. Rapid Commun. 30 (2009) 633-638.
- [17] B.S. Gaylord, A.J. Heeger, G.C. Bazan, Proc. Natl. Acad. Sci. U.S.A. 99 (2002) 10954-10957
- [18] B.S. Gaylord, A.J. Heeger, G.C. Bazan, J. Am. Chem. Soc. 125 (2003) [19] B.S. Gaylord, M.R. Massie, S.C. Feinstein, G.C. Bazan, Proc. Natl. Acad. Sci. U.S.A.
- 102 (2005) 34–39. [20] E. Uhlman, A. Peyman, G. Breipohl, D.W. Will, Angew. Chem. Int. Ed. 37 (1998)
- 2796-2823.
- [21] P.E. Nielsen, Acc. Chem. Res. 32 (1999) 624-630.
- [22] B. Falkiewicz, Acta Biochim. Pol. 46 (1999) 509-529. [23] K.N. Ganesh, P.E. Nielsen, Curr. Org. Chem. 4 (2000) 931–943.
- [24] D.T. McQuade, A.E. Pullen, T.M. Swager, 2537-2574.
- [25] S.W. Thomas, G.D. Joly, T.M. Swager, Chem. Rev. 107 (2007) 1339-1386.
- [26] C. Chi, A. Mikhailovsky, G.C. Bazan, J. Am. Chem. Soc. 129 (2007) 11134-11145.
- C.J. Hawker, J.M.J. Fréchet, J. Am. Chem. Soc. 112 (1990) 7638–7647. [28] F. Zeng, S.C. Zimmerman, Chem. Rev. 97 (1997) 1681-1712.
- [29] S.M. Grayson, J.M.J. Fréchet, Chem. Rev. 101 (2001) 3819–3867.
- [30] P. Furuta, J.M.J. Fréchet, J. Am. Chem. Soc. 125 (2003) 13173–13181.

- [31] B. Sandanaraj, R. Demont, S. Aathimanikandan, E.N. Savariar, S. Thayumanavan, J. Am. Chem. Soc. 128 (2006) 10686–10687.
 [32] S. Jiwpanich, B.S. Sandanaraj, S. Thayumanavan, Chem. Commun. 80 (2009) 6–808.
 [33] N. Niamnont, W. Siripornnoppakhun, P. Rashatasakhon, M. Sukwattanasinitt, Org. Lett. 11 (2009) 2768–2771.
 [34] N. Niamnont, R. Mungkarndee, I. Techakriengkrai, P. Rashatasakhon, M. Sukwattanasinitt Biosens Ricelectron 26 (2010) 863–867.

- wattanasinitt, Biosens. Bioelectron. 26 (2010) 863–867. [35] B.W. Davis, N. Niamnont, C.D. Hare, M. Sukwattanasinitt, Q. Cheng, ACS Appl. Mater. Interfaces 2 (2010) 1798–1803.
- [36] B.W. Davis, N. Niamnont, R. Dillon, B. Christopher, M. Sukwattanasinitt, Q. Cheng, Langmuir 27 (2011) 6401–6408.
 [37] T. Vilaivan, C. Srisuwannaket, Org. Lett. 8 (2006) 1897–1900.
 [38] C. Ananthanawat, T. Vilaivan, V.P. Hoven, X. Su, Biosens. Bioelectron. 25 (2010) 1602.

- 1064–1069. [39] B. Boontha, J. Nakkuntod, N. Hirankarn, P. Chaumpluk, T. Vilaivan, Anal. Chem. 80 (2008) 8178–8186.
- [40] F. Xia, X. Zou, R. Yang, Y. Xiao, D. Kang, A. Valle-Belisle, X. Gong, A.J. Heeger, K.W. Plaxco, J. Am. Chem. Soc. 132 (2010) 1252–1254.



Contents lists available at SciVerse ScienceDirect

Biosensors and Bioelectronics

journal homepage: www.elsevier.com/locate/bios



Phenylene-ethynylene trication as an efficient fluorescent signal transducer in an aptasensor for potassium ion

Wannapa Yuanboonlim, Warathip Siripornnoppakhun, Nakorn Niamnont, Paitoon Rashatasakhon, Tirayut Vilaivan, Mongkol Sukwattanasinitt*

Center for Petroleum, Petrochemicals and Advanced Materials, Department of Chemistry, Faculty of Science, Chulalongkorn University, Bangkok 10330, Thailand

ARTICLE INFO

Article history: Received 21 October 2011 Received in revised form 25 November 2011 Accepted 29 November 2011 Available online 30 December 2011

Keywords:
Aptamer
Biosensor
Fluorescence
Nucleic acid
Potassium detection
G-quadruplex

ABSTRACT

A tricationic phenylene–ethynylene (N^{3+}) fluorophore is investigated as a fluorescent transducer in homogeneous aptasensing system for potassium ion (K^+) assay in aqueous media. The enhancement of the fluorescent signal of N^{3+} by three K^+ aptamers consisting of 12, 15, and 21 nucleotides are observed and used for the determination of N^{3+} -aptamer binding affinities. The binding affinities increase with the length of the aptameric oligonucleotides and are proven to be important to the sensitivity and selectivity of the aptasensors. The enhanced fluorescent signal of each N^{3+} -aptamer solution is selectively quenched by K^+ due to the ability of K^+ in stabilizing the G-quadruplex structure of the aptamer. Among three aptamers, the 15-base aptamer provides optimal sensitivity and selectivity over other ions such as L^{1+} , N^{4+} , N^{2+} , N^{2+} , L^{2+} and L^{2+} . The sensing system shows the detection limit of 1 μ M of L^{2+} in clean buffered solution and 30 μ M of L^{2+} in the solution containing 4800-fold excess of L^{2+} , with wide linear dynamic ranges of micro- to millimolar concentration. This label-free fluorescence aptasensor is conveniently and effectively applicable for analysis of L^{2+} in urine samples.

© 2011 Elsevier B.V. All rights reserved.

1. Introduction

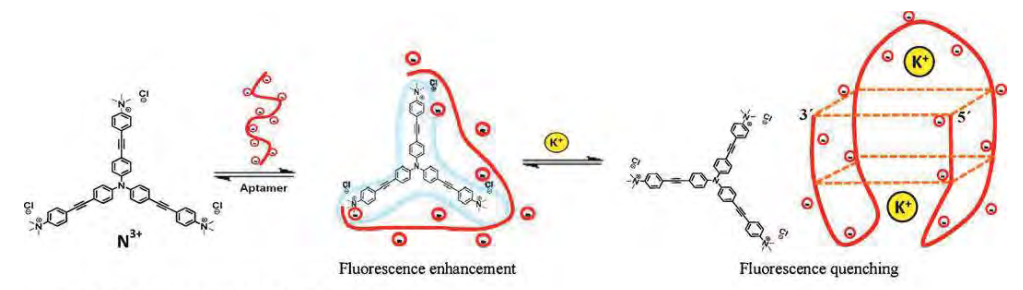
Potassium ion (K⁺) are involved in many biological functions, such as maintenance of extracellular osmolarity, regulation of other ions in organisms, production of electrical signals in nerve systems related to Na⁺-K⁺ pump process (Yu et al., 2001; Walz, 2000), regulation of blood pressure and pH, enzyme activation of Na⁺/K⁺-ATPase, and the formation of collagen or elastin (Kofuji and Newman, 2004; Suter, 1998; Pedersen et al., 2006). An abnormal potassium ion concentration in biological fluids can lead to several diseases such as kidney, Addison's and adrenal gland diseases (Modesto et al., 2006; Michaud and Strickberger, 2001). The normal concentration range of potassium ion in human blood plasma is 3.5–5 mM (Huang and Chang, 2008). The daily reference intakes (DRI) of 4000 mg potassium has been proposed (Karger, 2004) and a lower risk of stroke was found to be associated with a little higher intakes (D'Elia et al., 2011). Development of a sensing system for rapid and reliable quantification of potassium ion is thus of importance for medical diagnosis and nutritional analysis.

In common medical practice, potassium ion concentration is determined by a medical instrument operated based on ion selective electrode technique (Szmacinski and Lakowicz, 1999). An

optical method is a particularly interesting alternative to the electrochemical method as its detection is fast, sensitive and requires relatively inexpensive instrument. Among all optical methods, fluorometry is one of the most attractive methods due to its operational simplicity and high sensitivity. Simple fluorescent K⁺-sensing systems are often encountered with poor selectivity against Na⁺ ion, preventing them from practical usages (Yamauchi et al., 1999).

Recently, aptamer-based sensing systems, so-called aptasensors, have gained much attention due to their high sensitivity and selectivity. A typical aptamer is a single-stranded DNA or RNA chain, isolated from a large pool of random-sequence oligonucleotides, that is capable of binding a designated chemical or biological entity with high affinity and specificity (Zhang et al., 2008; Arthanari et al., 1998; Ho and Leclerc, 2004). Potassium aptamers are one of the best known classes of aptamers applied in sensing systems. They are G-rich oligonucleotides which can form the four-stranded helical conformation in solution with stacked arrays of G-quartets connected by Hoogsteen-type base pairing called G-quadruplex (Phan et al., 2006; Marathias and Bolton, 2000; Rujan et al., 2005; Radi and O'Sullivan, 2006). The stability of this conformation is greatly enhanced by K⁺, hence highly selective detection of K⁺ based on the formation of the G-quadruplex structure and fluorescent labeled probes have been reported (Ueyama et al., 2002; He et al., 2005; Chao et al., 2010). If the 5'- and 3'-ends of the aptameric oligonucleotide are labeled with a donor and an acceptor fluorophore, respectively, the formation of G-quadruplex structures

^{*} Corresponding author. Tel.: +66 2 2187620; fax: +66 2 2187598. E-mail address: smongkol@chula.ac.th (M. Sukwattanasinitt).



Apt12: d(5'- GGG GTT TTG GGG -3')

Apt15: d(5'- GGT TGG TGT GGT TGG-3')

Apt21: d(5'- GGG TTA GGG TTA GGG-3')

nApt15: d(5'- CAT TCA TGT CAT TCA-3')

Scheme 1. The proposed supramolecular interaction for K⁺ detection using potassium aptamer (Apt) and tricationic fluorophore (N³⁺).

can bring the two fluorophores close to each other, thus resulting in fluorescence resonance energy transfer (FRET) (Nagatoishi et al., 2006; Juskowiak, 2006; Nagatoishi et al., 2007). This type of probe, frequently called molecular beacon, shows high selectivity and sensitivity for K+ detection. However, it requires double labeling of the oligonucleotides which increase the cost of detection. Label-free aptasensors for potassium ion utilizing fluorescent dyes such as Oligreen (Huang and Chang, 2008), crystal violet (Kong et al., 2009), tetrakis-(diisopropylguanidino) zinc phthalocyanine (Qin et al., 2010), and Rhodamine B (Yu and Jiang, 2011) have also recently reported as a more economical alternative. The sensitivity and selectivity of these label-free sensing systems are likely to be interdependent on the supramolecular interactions among the signal transducing dye, the aptamer probe and the K⁺ analyte. It is thus of interest to investigate effects of the interaction between the aptamer and the dye molecule on the sensitivity and selectivity of the sensing system. In this study, we used three known potassium aptamers (Apt12, Apt15 and Apt21 in Scheme 1) as the probe and one of our recently reported tricationic fluorophores (Niamnont et al., 2009) (N3+) as the signal transducer. N³⁺ is selected based on its multi-cationic nature to ensure appreciable water solubility and strong electrostatic interaction with the polyanionic oligonucleotide aptamers. The principle of the detection system, as illustrated in Scheme 1, relies on the assumption that there is a strong Coulombic interaction between the aptamer and N³⁺ that resulted in a strongly enhanced fluorescent signal. The addition of K⁺ is expected to induce the aptamer to form a G-quadruplex which has a weaker interaction with $N^{3+}\mbox{ leading}$ to the reduction of the fluorescent intensity in relation to the K⁺ concentration.

2. Experimental

2.1. Chemicals and materials

The fluorophore N³+ with an iodide counter ion was prepared according to our previously reported procedures (Niamnont et al., 2009) and it was eluted through an anionic exchange resin column (Amberlite IRA-410 Cl⁻ form) by DI water to exchange iodide with chloride counter ion. Metal salts i.e. LiCl, NaCl, KCl, MgCl₂, CaCl₂, SrCl₂ and Tris−HCl buffers used in the fluorescence measurement were analytical grade purchased from chemical vendors such as Sigma–Aldrich (USA), Fluka (Switzerland) or Merck (Germany). Oligonucleotides were ordered from BioDesign. Co. Ltd. (Bangkok, Thailand). All chemicals were used as received without further purification. Water was purified using a Millipore filtration system.

2.2. General methods

UV–vis absorption spectra were recorded on a Varian Cary 50 UV–Vis spectrophotometer. Fluorescence measurements were carried out with solution samples in a 2 mL quartz cuvette at room temperature using a Varian Cary Eclipse spectrofluorometer at 90° detection angle. The quantum efficiency was measured relative to quinine sulfate standard in 0.1 M $\rm H_2SO_4$ (Φ_F = 0.54).

2.3. Fluorescence sensing study

The stock solutions of N^{3+} , aptamers and metal salts were prepared in Tris–HCl buffer pH 7.4 (10 mM). For spectrum measurements, the stock solutions of relevant compounds were mixed thoroughly and the total volumes were adjusted to 1.5 mL with the same buffer solution. The samples were allowed to equilibrate for at least 5 min at room temperature prior to the measurements. Each sample was prepared in triplicate solutions and each solution was measured for three times to provide the reported average values along with their standard deviation.

2.4. Fluorescence detection of K+

The fluorescence spectrum of the mixture of ${\bf N^{3^+}}$ (0.2 μ M), the aptamer (0.02 μ M) and one of the metal chlorides tested (LiCl, NaCl, KCl, NH4Cl, MgCl₂, CaCl₂, and SrCl₂; 10 mM) in Tris–HCl buffer pH 7.4 (10 mM) was acquired in the range of 400–700 nm with the excitation wavelength of 372 nm. The quenching efficiency, $1-(F/F_0)$, was plotted against the types of aptamers and metal ions, where F and F_0 are the fluorescence intensity in the presence and absence of the metal ion, respectively. For potassium concentration dependence study, the mixtures of ${\bf N^{3^+}}$ (0.2 μ M), Apt15 (0.02 μ M) and potassium ion at various concentrations (0.004, 0.02, 0.2, 1, 2, 3, 4, 5, 10, 50, 100, 140 and 196 mM) were used. For interference test, the mixtures of ${\bf N^{3^+}}$ (0.2 μ M), Apt15 (0.02 μ M), potassium ion (0.2 mM) and other metal chloride such as LiCl, NaCl, NH4Cl, MgCl₂ CaCl₂, and SrCl₂ at ten times of potassium ion concentration (2 mM) were measured.

2.5. Application for K^+ assays in real samples

A calibration curve was prepared from the Tris–HCl buffered solutions of potassium ion (0.04–20 mM) in the presence of other simulated extracellular ions including NaCl (145 mM), CaCl₂ (2.5 mM), and MgCl₂ (1.5 mM) in the presence of N^{3+} fluorophore (1 μ M) and Apt15 (0.1 μ M). Urine samples were collected from four

healthy volunteers, centrifuged at 3500 Rev/min for 5 min, kept at 4 °C overnight and filtered through 0.45 μm Teflon membranes. For recovery test, KCl (10 mM) was also added into the urine samples prior to the analyses. The urine samples were then diluted 100-fold with Tris–HCl buffer (10 mM, pH 7.4) containing Apt15 (0.1 μM) and N³+ fluorophore (1 μM) and analyzed by fluorometer. For method validation, the same urine samples were analyzed by Inductively Coupled Plasma-Optical Emission Spectroscopy (ICP-OES Spectrometer, iCAP 6000 SERIES ICP Consumables Kit).

3. Results and discussion

3.1. Synthesis and photophysical properties of the tricationic fluorophore

The tricationic fluorophore N³+ in the form of iodide salt was synthesized according to the previously reported procedures (Scheme S1) (Niamnont et al., 2009). This iodide salt however gradually lost its water solubility upon storage in its solid state. The ¹H NMR spectra of the samples stored for a week revealed significant degree of demethylation from the ammonium groups (Fig. S1). The mixture of demethylated salts became poorly soluble in water and it is not suitable for further study. Ion exchange of the strongly nucleophilic iodide ion with a less nucleophilic chloride ion was thus performed by eluting the aqueous solution of the iodide salt through an Amberlite IRA-410 (Cl⁻ form) anionic ion exchange resin column. The fluorophore containing chloride counter ion, N³+ 3Cl⁻, was found to be more stable that it retains good water solubility upon storage. This chloride salt is thus utilized for further study as an analytical fluorescent transducing agent.

The solution of N^{3+} in Tris–HCl buffer solution pH 7.4 displayed absorption maximum at 372 nm (Fig. S2) with molar absorptivity of 3.42×10^4 . When being excited at 372 nm, the fluorophore showed emission maximum at 486 nm and quantum efficiency of 13.6%. The addition of Apt15, a K⁺ aptamer consisting of 15 nucleotide bases, enhanced the fluorescent intensity over five folds and blue shifted it to 454 nm (Fig. S3a). With one equivalent of Apt 15, the system gave the quantum yield as high as 33.4%. These changes in the fluorescent signal reflect the expected interaction between the aptamer and N³⁺. The interaction reduces the geometrical relaxation and selfassociative quenching process resulting in the wavelength shift and intensity enhancement, respectively (Swager, 1998; Azagarsamy et al., 2010). The K⁺ detection experiment gave results in good agreement with the principle proposed in Scheme 1. The fluorescence spectra shown in Fig. S3a demonstrate that the enhanced fluorescent signal of N³⁺/Apt15 system decreases by over 50% upon the addition of 1 mM K⁺. The positively charged K⁺ is expected to bind with the aptamer reducing its binding with N^{3+} and reinstalling the self-associative quenching effect. To confirm that this behavior was a result of the specific binding between K⁺ and the aptamer, a non-aptameric oligonucleotide (nApt15) having a random sequence which cannot form a G-quadruplex structure was also tested. In this case, the addition of K⁺ did not cause any changes in the fluorescence intensity of the **N**³⁺/nApt15 mixture (Fig. S3b).

3.2. Fluorescence responses of the fluorophore to ODNs

To gain insight into interactions between the fluorophore and aptamer, we investigated the mixtures of $\mathbf{N^{3+}}$ and four oligonucleotides (ODN) i.e. Apt12, Apt15 Apt21 and nApt15 (Scheme 1). The first three ODNs are $\mathbf{K^{+}}$ aptamers while the last one is a nonaptameric ODN. At the same molar concentration, the ODNs with different lengths gave different enhancement and shift of the fluorescent signal of $\mathbf{N^{3+}}$ suggesting different binding affinity with the fluorophore (Fig. S4). With the assumption of 1:1 complexation

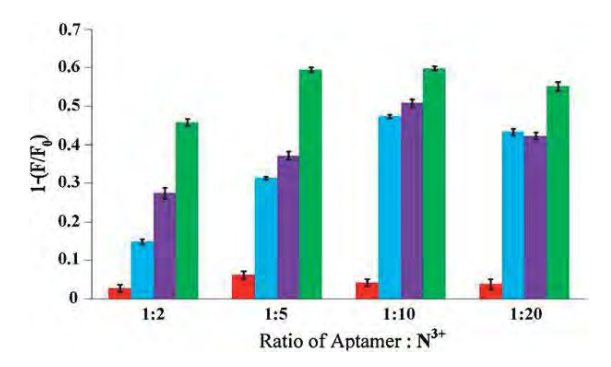


Fig. 1. Quenching efficiencies of K^+ in aptameric sensing systems using different ODNs: Apt12 (), Apt15 (), Apt21 () and nApt15 () at various ODN/fluorophore mole ratios.

between N^{3+} and the aptamer, the intercept/slope of a linear plot fit to the Benesi-Hildelbrand equation (Mukhopadhyay et al., 2005; Chakraborty and Guchhait, 2008; Upadhyay et al., 2007) gave the affinity constant (K_a) for each N^{3+} /ODN complex. The K_a values for Apt12, Apt15, Apt21 and nApt15 were determined as 3.2×10^7 , 9.1×10^7 , 3.0×10^8 and $9.4 \times 10^7 \, \text{M}^{-1}$, respectively (Fig. S5). The binding constants increase with the length of the ODNs in accordance to the increasing electrostatic interaction. The observation of similar values of the binding constants for the aptamer (Apt15) and non-aptamer (nApt15) also confirmed that the electrostatic force is the main binding contribution. Job's plot analysis of the fluorescence responses (Zachary, 1986) revealed that the Apt12 formed 2:1 complex with N3+, while all the other ODNs formed 1:1 complexes (Fig. S6). The K_a obtained from the plot for Apt12 is thus likely to be the product of two binding steps $(K_{a1} \times K_{a2})$ and each Apt 12 chain should have even much lower binding affinity than that obtained from the Benesi-Hildelbrand plot. We attribute the difference in binding ratios to the molecular length of ODN. From AM1 geometrical optimization, the distance between two ammonium groups of N³⁺ was determined to be 21.7 Å. Based on the length of a single nucleotide unit of 3.3 Å, the extended chain lengths of Apt12, Apt15 and Apt 21 are estimated to be 39.6, 49.5 and 69.3 Å, respectively. These values suggested that there is a good possibility of two Apt12 chains to interact with all three cationic sites of N^{3+} to form a 2:1 complex while only one chain of the longer aptamers (Apt15 and Apt21) is required to interact with all three cationic sites of N^{3+} (Fig. S7).

3.3. Condition for detection of K+

According to the sensing mechanism presented in Scheme 1, the fluorescence quenching involves the competitive binding between K^+ and $\hat{{\bf N}^{3+}}$ to the aptamer and greater sensitivity of K⁺ may be obtained at the aptamer/fluorophore ratio lower than its stoichiometric ratio. We therefore investigated the effect of aptamer/fluorophore ratio on the sensitivity by varying the concentration of the aptamer from 0.1 to 0.01 µM at a fixed fluorophore concentration of 0.2 µM. The optimum aptamer/fluorophore ratio is determined as the ratio giving the highest quenching efficiency $(1 - F/F_0)$ upon the addition of K⁺ at a physiological concentration (10 mM). Fig. 1 shows the highest quenching efficiency at the aptamer/fluorophore ratio of 1:10 for all aptameric ODN lengths. While reducing the aptamer/fluorophore ratio decreases the initial fluorescence signal (F_0) , this adverse effect can be offset by lower amount of K+ required for effective competitive complexation. It is important to note that the reported binding constant of K⁺ with Apt15 is $2 \times 10^6 \, \text{M}^{-1}$ (Wilcox et al., 2008), which is about 50 times lower than the K_a values of N^{3+} with Apt15. Fig. 1 also shows that Apt12 has the highest quenching sensitivity at all

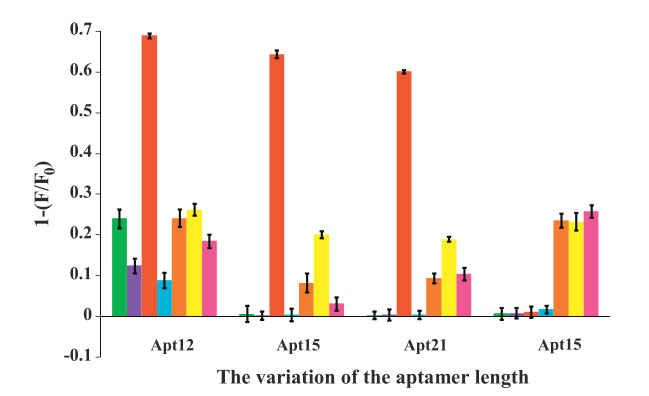


Fig. 2. Quenching efficiencies of physiological cations: Li $^+$ (\blacksquare), Na $^+$ (\blacksquare), NH₄ $^+$ (\blacksquare), Mg $^{2+}$ (\blacksquare), Ca $^{2+}$ (\blacksquare) and Sr $^{2+}$ (\blacksquare) in the sensing systems constructing from various ODNs.

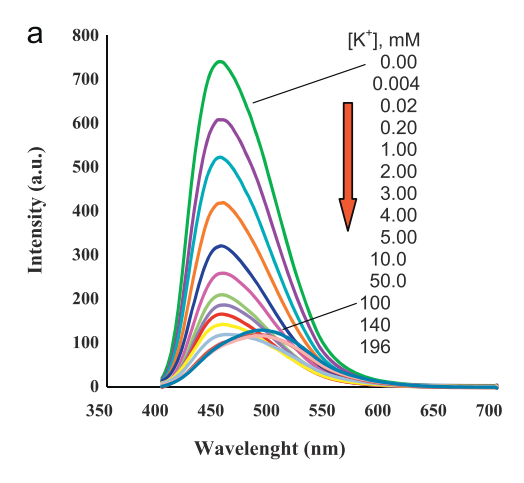
ratios as expected for its lower binding affinity to the fluorophore, for each individual chain. It is also important to point out that the lower aptamer/fluorophore ratio is translated into the lower amount of expensive aptameric ODN required for the detection. In this particular aptasensing system, the optimum condition for K⁺ sensing required only 20 nM of the aptamer and 200 nM of the fluorophore which is one of the lowest values have been reported (Huang and Chang, 2008; Kong et al., 2009; Qin et al., 2010). The plot also shows that K⁺ gives very low quenching efficiency for the non-aptameric ODN, nApt15, confirming that the detection is based on the specific aptamer–K⁺ interaction. Since the sensitivity of a sensor is generally traded off with selectivity, our next investigation is to compare the selectivity toward K⁺ against other cations.

We investigated the selectivity of each aptamer/ N^{3+} pair at the optimum 1:10 mole ratio by comparing the quenching efficiency of K^+ with other cations such as Li^+ , Na^+ , NH_4^+ , Mg^{2+} , Ca^{2+} and Sr^{2+} . Fig. 2 clearly reveals that the aptameric sensing systems have high sensing selectivity toward K^+ while the non-aptameric system gave no K^+ selectivity. Among three aptamers, Apt12 provided the lowest selectivity against other monovalent cations such as Li^+ , Na^+ and NH_4^+ that should again be attributed to its low binding affinity to the fluorophore. For the divalent cationic species such as Mg^{2+} , Ca^{2+} and Sr^{2+} , we observed lower selectivity against these ions. Comparing with the monovalent cations, the divalent cations

possess greater electrostatic attraction with the ODN chains that led to greater quenching effect to the sensing system. Interestingly, the selectivity against divalent cations is rarely reported for K^{+} aptasensors, it is thus important to point out that this tricationic fluorophore N^{3+} provided greater selectivity than the monocationic dye for K^{+} aptasensing system (Kong et al., 2009). We thus attributed the factors for high selectivity not only to the specific binding between K^{+} and the aptameric G-quadruplex structure but also to the binding affinity between the fluorophore and aptamer. Among the three aptamers, Apt15 presents the best choice for K^{+} sensor as it give high selectivity with only slightly lower sensitivity comparing to Apt12.

3.4. Quantitative analysis of K+

For quantitative analysis of K+, the fluorescent signal of Apt $15/N^{3+}$ (1:10) solution in the presence of KCl was measured. The fluorescent signal decreased with the increasing K⁺ concentration (Fig. 3a). At low K⁺ concentrations (\leq 50 mM or \leq 2.5 × 10⁵ equiv.), the fluorescent signal was quenched without any peak shift. When the concentration of K⁺ increased to 100 mM (\geq 5 × 10⁵ equiv.), the fluorescent signal was shifted to the original position of the free fluorophore. These results agree well with the stepwise formation of 1:1 and 2:1 complexes between K⁺ and Apt15 (Yoshikawa, 2001; Declan and Wallace, 1998; Baigl and Yoshikawa, 2005). The 1:1 complex of K⁺/Apt15 probably remains largely bound to N³⁺ while the 2:1 complex is likely to be dissociated from the fluorophore. This stepwise formation of 1:1 and 2:1 complexes is also evidenced from two linear dynamic ranges observed in the plot between quenching efficiency and log[K⁺] before reaching the saturation (Fig. 3b). At low K+ concentration, most complex formed is likely to be the 1:1 complex whereas the 2:1 complex becomes predominant at higher K⁺ concentration. The 2:1 complex has lower negative charge and thus its binding with N3+ is weaker resulting in greater quenching sensitivity and the greater slope of the second dynamic range. With K+ concentration higher than 100 mM (5×10^5) equiv.), the quenching effect is clearly saturated and the fluorescent signal returned to the original position of N^{3+} . The plot in Fig. 3b demonstrates useful concentration range for quantitative analysis of K⁺. The first linear dynamic range gave the limit of detection (LOD determined at the signal = $3 \times \text{noise}$) of K^+ as low as 9×10^{-7} M which is among the best for the label free systems reported to date (Huang and Chang, 2008; Kong et al., 2009; Qin et al., 2010).



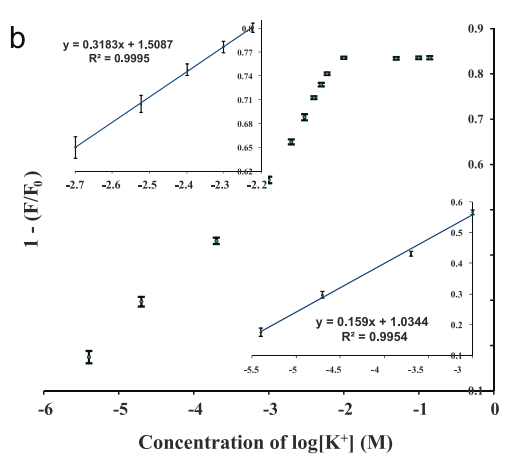


Fig. 3. (a) Fluorescence spectra (λ_{ex} = 372 nm) of the Apt15/N³+ (20/200 nM) in Tris–HCl buffer pH 7.4 (10 mM) in the presence of K⁺ at various concentrations. (b) Plot of the quenching efficiency (λ_{em} = 456 nm) as a function of log[K⁺]. The insets show two dynamic ranges of K⁺ concentration (4 μ M to 1 mM and 2–6 mM).

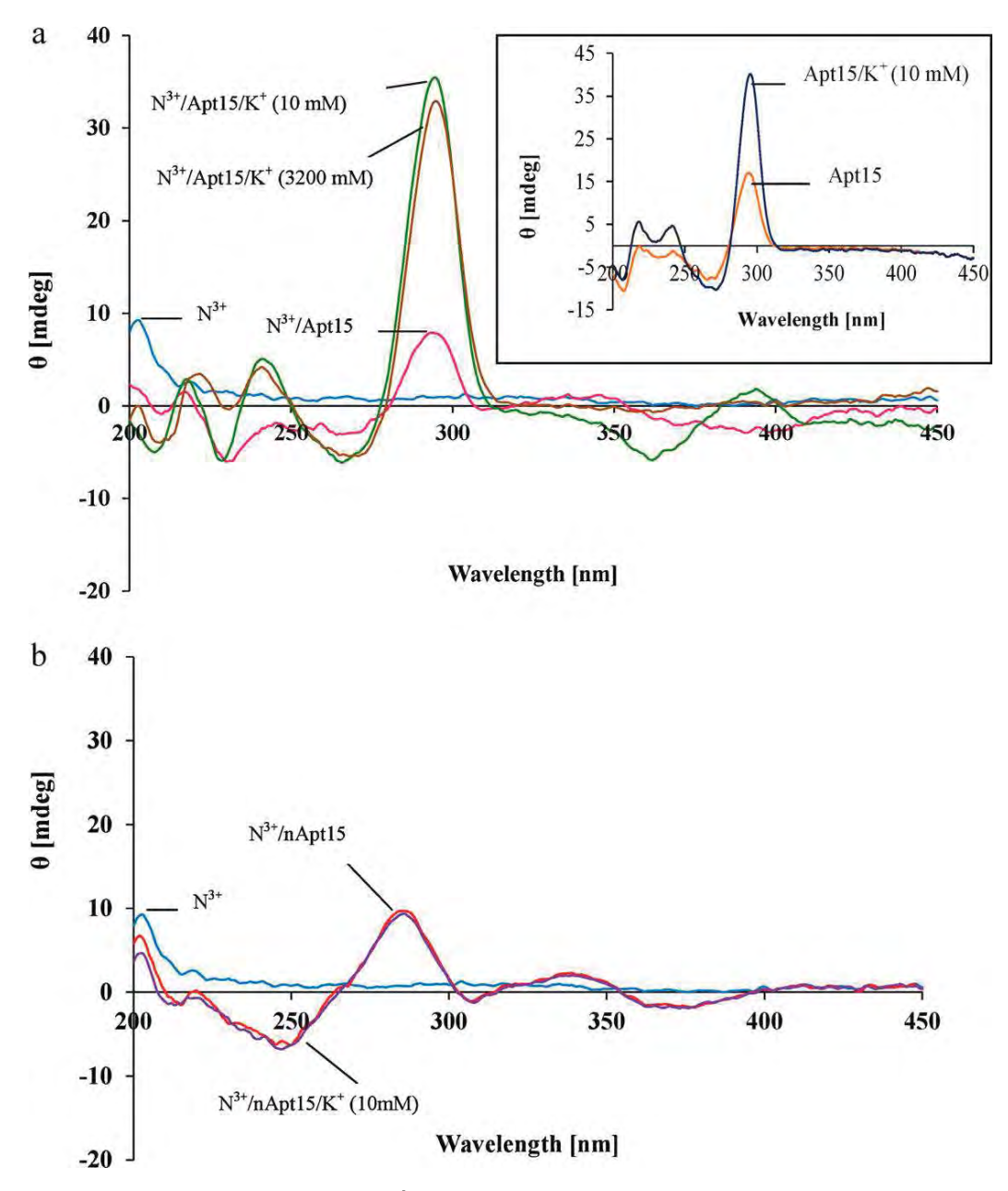


Fig. 4. Circular dichroism (CD) spectra of (a) aptameric system ([N^{3*}] = 10 μM, [Apt15] = 10 μM, [K*] = 10 and 3200 mM) and (b) non-aptameric system N^{3*} solution ([N^{3*}] = 10 μM, [Apt15] = 10 μM, [Apt15] = 10 μM, [K*] = 10 mM) in Tris-HCl buffer pH 7.4 (10 mM). Inset is the system without N^{3*} .

3.5. Supramolecular interaction study by circular dichroism (CD)

Circular dichroism (CD) spectroscopy was used to ascertain the changes in the interactions among N^{3+} , Apt15 and K^+ at different K^+ concentration levels. The negative CD signal near the absorption of N^{3+} around 385 nm signifies the interaction between Apt15 and N^{3+} (Fig. 4a). In the presence of 10 mM K^+ (1.0 \times 10 3 equiv.), the positive CD signal at 290 nm, corresponding to the signal of antiparallel G-quadruplex conformation of the aptamer (Kypr et al., 2009), is markedly increased. However, the signal near the absorption of N^{3+} did not return to the original nil value indicating some interaction between the aptamer and N^{3+} remained. The sign switching structure of the signal in this region also implies that the aptamer unevenly interacts with three branches of N^{3+} . Further addition of K^+ to 3.20 M (3.2 \times 10 5 equiv.) returns this CD signal back to zero

confirming the full dissociation of the potassium–G-quadruplex complex from $\mathbf{N^{3^+}}$. With similar interpretation, Fig. 4b confirms that the non-aptameric ODN, nApt15, interact with $\mathbf{N^{3^+}}$ but not with $\mathbf{K^+}$ as there is no CD signal change upon the addition of $\mathbf{K^+}$.

3.6. K^+ assay in urine samples

In the final stage of this work, the application of Apt15- N^{3+} aptasensing system for determination of K^+ concentration in real human urine samples was evaluated. Using synthetic urine solutions containing 145 mM NaCl, 2.5 mM CaCl₂, 1.5 mM MgCl₂ and various concentrations of K^+ (0–20 mM) (Nagatoishi et al., 2005), a linear calibration line was obtained in the range of 0.04–2.0 mM (Fig. S8). Although the linearity range of the K^+ assay shifted to somewhat higher concentration range because of the impact of the

Table 1 Analytical results for K⁺ content in urine samples from four healthy volunteers measured using the N³⁺-Apt15 fluorescence sensor^a and ICP-OES.

Sample	N^{3+} -Apt sensor Mean \pm SD/mM ($n = 5$)	ICP-MS Mean ± SD/mM (n = 5)	<i>F</i> -Test between two methods ^b	Add K ⁺ (mM)	Found K ⁺ (mM)	Recovery (%)
Urine 1	4.20 ± 0.006	4.15 ± 0.033	S	10	9.875	98.8
Urine 2	11.17 ± 0.004	11.22 ± 0.152	3.15	10	9.952	99.5
Urine 3	14.58 ± 0.003	14.59 ± 0.063	2.30	10	9.753	97.5
Urine 4	23.21 ± 0.012	23.75 ± 0.091	3.67	10	9.741	97.4

a $[N^{3+}]/[Apt15] = 1/0.1 \mu M$.

sample matrixes, as little as $30\,\mu\text{M}$ K⁺ could be detected, even in the presence of 145 mM Na⁺ (4800-fold of K⁺ concentration). On the basis of an F-test at a 95% confidence level, the K+ concentrations in four volunteers' urine samples determined by Apt15– N^{3+} sensor agree very well with the values obtained from inductively coupled plasma-optical emission spectrometry (ICP-OES) (Table 1). The recovery level of 97.4–99.5% of K⁺, intentionally spiked at 10 mM concentration into the urine sample solutions, also confirmed the effectiveness of this method for determination of K+ content in urine. It is important to point out here that this fluorescence aptasensing assay provides the advantages of simple sample preparation, rapid detection and low cost instrumentation that are amenable to high throughput analysis.

4. Conclusion

The tricationic phenylene–ethynylene (N^{3+}) is capable of transducing fluorescent signal in aptasensing system. The fluorescent signal of N3+ is enhanced upon electrostatic binding with the potassium aptamer. The addition of potassium ion selectively diminished this enhancement by inducing the formation G-quadruplex conformation of the aptamer chain which in turn weakens its electrostatic interaction with N3+. Sensitivity and selectivity of the sensing system was optimized by the variation of the aptamer length in order to tune the electrostatic interactions between the fluorophore and aptamer. The 15-base aptamer gave higher selectivity than the 12-base aptamer and higher sensitivity than the 21base aptamer. The N^{3+} -Apt15 aptasensor exhibits wide linear dynamic ranges from micro- to millimolar concentration of K+ with the detection limit just below 1.0 µM. The sensing system is conveniently applicable for rapid K+ assays in real urine samples.

Acknowledgements

The authors would like to acknowledge the financial support from the Research, Development and Engineering (RD&E) Fund through National Nanotechnology Center (NANOTEC), National Science and Technology Development Agency (Project NN-B-22-FN9-10-52-06). We would also like to thank The Thailand Research Fund (TRF: code RTA5280002) for research grants. This work is part of the Project for Establishment of Comprehensive Center for Innovative Food, Health Products and Agriculture supported by the Thai government stimulus package 2 (TKK2555, SP2) and National Research University of CHE and the Ratchadaphiseksomphot Endowment Fund (AM1006A). We would like to thank Assist. Prof. Dr. Narong Praphairaksit and his student for the experiments on the inductively coupled plasma-optical emission spectrometry (ICP-OES).

Appendix A. Supplementary data

Supplementary data associated with this article can be found, in the online version, at doi:10.1016/j.bios.2011.11.049.

References

Arthanari, H., Basu, S., Kawano, T.L., Bolton, P.H., 1998. Nucleic Acids Res. 26,

Azagarsamy, M.A., Yesilyurt, V., Thayumanavan, S., 2010. J. Am. Chem. Soc. 132, 4550-4551.

Baigl, D., Yoshikawa, K., 2005. Biophys. J. 88, 3486–3493.

Chakraborty, A., Guchhait, N., 2008. J. Incl. Phenom. Macrocycl. Chem. 62, 91–97.

Chao, S., Hongxi, G., Cuiping, M., 2010. Anal. Biochem. 400, 99–102.

Declan, A.D., Wallace, B.A., 1998. Biophys. J. 75, 635-640.

D'Elia, L., Barba, G., Cappuccio, F., Strazzullo, P., 2011. J. Am. Coll. Cardiol. 57, 1210-1219.

He, F., Tang, Y., Wang, S., Li, Y., Zhu, D., 2005. J. Am. Chem. Soc. 127, 12343–12346.

Ho, H.A., Leclerc, M., 2004. J. Am. Chem. Soc. 126, 1384–1387. Huang, C.C., Chang, H.T., 2008. Chem. Commun. 146, 1–1463.

Juskowiak, B., 2006. Anal. Chim. Acta 568, 171-180.

Karger, S., 2004. Ann. Nutr. Metab. 48, 1-16.

Kofuji, P., Newman, E.A., 2004. Neuroscience 129, 1045–1056.

Kong, D.M., Guo, J.H., Yang, W., Ma, Y.E., Shen, H.K., 2009. Biosens. Bioelectron. 25, 88-93.

Kypr, J., Kejnovska, L., Renciuk, D., Vorlickova, M., 2009. Nucleic Acids Res. 37, 1713–1725.

Marathias, V.M., Bolton, P.H., 2000. Nucleic Acids Res. 28, 1969-1977.

Michaud, G.F., Strickberger, S.A., 2001. J. Am. Coll. Cardiol. 38, 1224–1225. Modesto, K.M., Møller, J.E., Freeman, W.K., Shub, C., Bailey, K.R., Pellikka, P.A., 2006.

Am. J. Cardiol. 97, 1247-1249.

Mukhopadhyay, M., Banerjee, D., Koll, A., Mandal, A., Filarowski, A., Fitzmaurice, D., Das, R., Mukherjee, S., 2005. J. Photochem. Photobiol. A: Chem. 175, 94–99. Nagatoishi, S., Nojima, T., Juskowiak, B., Takenaka, S., 2005. Angew. Chem. Int. Ed.

Engl. 44, 5067-5070.

Nagatoishi, S., Nojima, T., Galezowska, E., Juskowiak, B., Takenaka, S., 2006. Chem. BioChem. 7, 1730–1737.

Nagatoishi, S., Nojima, T., Galezowska, E., Gluszynska, A., Juskowiak, B., Takenaka, S., 2007. Anal. Chim. Acta 581, 125-131.

Niamnont, N., Siripornnoppakhun, W., Rashatasakhon, P., Sukwattanasinitt, M., 2009. Org. Lett. 11, 2768-2771.

Pedersen, S.F., O'Donnell, M.E., Anderson, S.E., Cala, P.M., 2006. Am. J. Physiol. - Reg. I 291, R1-R25.

Phan, A.T., Kuryavyi, V.D., Patel, J., 2006. Curr. Opin. Struct. Biol. 16, 288–298. Qin, H., Ren, J., Wang, J., Luedtke, N.W., Wang, E., 2010. Anal. Chem. 82, 8356–8360.

Radi, A.E., O'Sullivan, C.K., 2006. Chem. Commun. 343, 2-3434.

Rujan, L.N., Meleney, J.C., Bolton, P.H., 2005. Nucleic Acids Res. 33, 2022–2031. Suter, P.M., 1998. Nutr. Rev. 56, 151–153.

Swager, T.M., 1998. Acc. Chem. Res. 31, 201–207.

Szmacinski, H., Lakowicz, J.R., 1999. Sens. Actuators B: Chem. 60, 8-18.

Ueyama, H., Takagi, M., Takenaka, S., 2002. J. Am. Chem. Soc. 124, 14286–14287. Upadhyay, S.P., Pissurlenkar, R.R.S., Coutinho, E.C., Karnik, A.V., 2007. J. Org. Chem. 72, 5709-5714.

Walz, W., 2000. Neurochem. Int. 36, 291-300.

Wilcox, J.M., Rempel, D.L., Gross, M.L., 2008. Anal. Chem. 80, 2365–2371.

Yamauchi, A., Hayashita, T., Nishizawa, S., Watanabe, M., Teramae, N., 1999. J. Am. Chem. Soc. 121, 2319-2320.

Yoshikawa, K., 2001. Adv. Drug Deliv. Rev. 52, 235–244. Yu., X., Jiang, Z., 2011. Anal. Lett. 44, 898–907.

Yu, S.P., Canzoniero, M.T., Choi, D.W., 2001. Curr. Opin. Cell Biol. 13, 405–411.

Zachary, D., 1986. J. Chem. Educ. 63, 162–170. Zhang, J., Wang, L., Pan, D., Song, S., Boey, F.Y.C., Zhang, H., Fan, C., 2008. Small 4, 1196–1200.

b The F-test value is 6.39 at a 95% confidence level.





BRIEF COMMUNICATION

A nested sequence-specific primer-polymerase chain reaction for the detection of *HLA-B*15:02*

S. Virakul¹, P. Kupatawintu², J. Nakkuntod¹, O. Kangwanshiratada³, T. Vilaivan⁴ & N. Hirankarn³

- 1 Medical Microbiology, Interdisciplinary Program, Graduate School, Chulalongkorn University, Bangkok, Thailand
- 2 National Blood Center, Thai Red Cross Society, Bangkok, Thailand
- 3 Department of Microbiology, Faculty of Medicine, Chulalongkorn University, Bangkok, Thailand
- 4 Department of Chemistry, Faculty of Science, Chulalongkorn University, Bangkok, Thailand

Key words

carbamazepine hypersensitivity; *HLA-B*15:02*; nested sequence-specific primer-polymerase chain reaction

Correspondence

N. Hirankarn, MD, PhD Lupus Research Unit Department of Microbiology Faculty of Medicine Chulalongkorn University Rama 4 Road Bangkok 10330 Thailand

Tel: +66 2 256 4132 ext. 624 Fax: +66 2 252 5952

e-mail: fmednpt@md.chula.ac.th

Received 21 July 2011; revised 29 November 2011; accepted 4 January 2012

doi: 10.1111/j.1399-0039.2012.01836.x

Abstract

In this study, we reported a new technique in detecting *HLA-B*15:02* by using a nested sequence-specific primer-polymerase chain reaction (SSP-PCR) that can be used on genomic DNA and whole blood for carbamazepine hypersensitivity prediction. We tested a total of 200 blind samples with known human leukocyte antigen (HLA)-B allelic types (44 positive for *HLA-B*15:02* and 156 negative for *HLA-B*15:02*) with this new nested SSP-PCR technique and compared its efficacy to that of commercial sequence-specific oligonucleotide probe-polymerase chain reaction (SSOP-PCR). Using starting materials from DNA and whole blood, we were able to detect *HLA-B*15:02* in 44 of our samples correctly. The test is very sensitive and is highly reproducible.

Certain human leukocyte antigen (HLA) alleles can be used as a marker for detecting Steven Johnson syndrome and toxic epidermal necrolysis. Although life-threatening drug hypersensitivities are rare, however, when it does occur, it can cause death in around 30% of its sufferers. In 2004, Chung et al. was the first to report using *HLA-B*15:02* as a genetic marker for predicting the patient's hypersensitivity to carbamazepine (1). Along the same lines, it has been reported that ethnicity plays an important role in patients becoming hypersensitive to certain drugs (2). *HLA-B*15:02* is strongly associated with carbamazepine hypersensitivity in Asians (3, 4) and not in Caucasians (5). As a result of this, the US Food and Drug Administration now recommends physicians to screen all Asian patients for the presence of *HLA-B*15:02* before initiating carbamazepine regimens (6).

Currently, HLA typing is frequently used in the field of transplantations, which require the detection of many alleles at the same time. However, for other medical fields, this is unnecessary, time consuming and costly. As a result of this, a simpler, cheaper and faster method to detect a

specific allele is urgently needed. It has been shown that to detect *HLA-B*15*, the most polymorphic group, a multiple set of different primers are needed (7, 8). For example, a sequence-specific primer-polymerase chain reaction (SSP-PCR) technique would require at least six sets of primers in order to distinguish *HLA-B*15:02* from *B*15:13* and *B*15:21* (7).

Although SSP-PCR is the most cost effective method used to detect *HLA-B*15*, however, its DNA extraction procedure is highly dependent on DNA extraction kits which are quite expensive. Other techniques used to extract DNA such as the standard salting out method is very cheap but very time consuming and can take approximately 6 h to complete. A number of attempts have been used to type HLA and amplify the target DNA directly from whole blood to reduce the total assay time as much as possible (9). Mutant Taq DNA polymerase and high pH buffer were used to overcome the inhibitor in the whole blood samples such as anti-coagulating agent, hemoglobin, immunoglobulin G and lactoferrin (10, 11). Here, we report an alternative method

HLA-B*15:02 nested SSP-PCR S. Virakul et al.

using a nested SSP-PCR in detecting *HLA-B*15:02* from purified genomic DNA and whole blood samples.

To find sequence-specific primers, all HLA-B sequences were obtained from the IMGT/HLA database (12). Nested PCR was used to increase the specificity of each round of amplification and to eliminate heterozygous combination from a number of separate reactions. Briefly, in the first PCR, some subtypes of *HLA-B*13*, *B*15*, *B*35*, *B*40*, *B*44* and *B*57* were amplified followed by a second PCR, which specifically amplified only *HLA-B*15:02*. All primer locations are shown in Figure 1 and all primer sequences are listed in Table 1. To predict which alleles will be amplified from the different

combinations of primers used in the nested SSP-PCR, 10 bases from 3' end of each primer sequence was entered into the PROBE and PRIMER Search Tool, IMGT/HLA database version 3.6 October 2011 (12). All possibilities of allele amplification from the prediction are shown in Table 2.

To test the specificity of primers, purified genomic DNAs were extracted from 13 samples with known HLA alleles identified by a commercial SSP-PCR Kit (Micro SSP™ HLA DNA Typing Trays, One Lambda, Inc., Canoga Park, CA) (Figure 2A). The results from the first PCR amplified the following alleles as expected: *HLA-B*13:01*, *15:02*, *15:13*, *15:21* and *15:25*. Other alleles commonly found (more than

	Primer F1		Primer F2
cDNA B*07:02:01° B*13:01:01 B*13:07N B*15:02:01 B*15:13 B*15:21 B*15:25:01 B*15:88 B*15:121 B*15:144	-A	CCGCGGGCGC CGTGGATAGA GCAGGAGGGG CCGGAGTATT C	G- G
		Primer R2 Primer F3	Primer R1
CDNA B*07:02:01* B*13:01:01 B*13:07N B*15:02:01 B*15:13 B*15:21 B*15:25:01 B*15:28 B*15:121 B*15:144	280 290 300 310 TACAAGGCCC AGGCACAGAC TGACCGAGAG AGCCTGCGGA -CA-A -CA	ACCTGCGCGG CTACTACAAC CAGAGCGAGG CCG GGTCTCA C-GC-T-C- T-GC-T-C- T-GC-T-C-	
cDNA B*07:02:01° B*13:01:01 B*13:07N B*15:02:01 B*15:13 B*15:21 B*15:25:01 B*15:88 B*15:121 B*15:144		420 430 440 450 TGACCAGTAC GCCTACGACG GCAAGGATTA CATCGCCCTG A -ATAC	

Figure 1 Primers were designed from regions within *HLA-B*15:02* exons 2 and 3. All these sequences were taken from IMGT/HLA database (12). For the first PCR, the sequences for *HLA-B*15:02* primers F1 are located in exon 2 and for R1, it is located in exon 3. For the second PCR, both F2 and R2 are all located in exon 2. The F3, a nested control primer is located in exon 2. All sequences for the primers are shown in Table 1. HLA, human leukocyte antigen.

^a *HLA-B*07:02:01* was used as the consensus sequence. A dash (–) indicated that the sequences were similar to each other, whereas the dot (.) represented sequence insertions or deletions.

S. Virakul et al. HLA-B*15:02 nested SSP-PCR

Table 1 Primers for HLA-B*15:02 nested SSP-PCRa

SSP-PCR primers for *HLA-B*15:02*F1:5'-GCGAGTCCGAGGATGGC-3'
R1:5'-AGCCATACATCCTCTGGATGA-3'
F2:5'-GGAGTATTGGGACCGGAAC-3'
R2:5'-TTGTAGTAGCCGCGCAGGT-3'
Primers for internal control (IFN-y)
IF: 5'-CCTCACATGATATGACTTTGACAT-3'
IR: 5'-AACATCAGAAGCATTGACCTTG-3'
Primers for nested control (HLA)
F3:5'-CTACTACAACCAGAGCGAGGC-3'
R1:5'-AGCCATACATCCTCTGGATGA-3'

HLA, human leukocyte antigen; SSP-PCR, sequence-specific primer-polymerase chain reaction.

^aIn the first PCR, *HLA-B*15:02* primers (F1 and R1) were added to the reaction with an internal control primer (IF and IR). In the second PCR, F2 and R2 is used, in addition with F3 and R1 as nested control primer.

1%) in the Thai population (*HLA-B*07:05*, *15:01*, *27:04*, *35:01*, *40:01*, *46:01*, *57:01* and *58:01*) were not amplified.

Using primers F2 and R2 in the second PCR, only *HLA-B*15:02* was amplified. PCR product sizes were detected by gel electrophoresis, which was performed on a 2% agarose at 100 V for 35 min with GeneRulerTM 50 bp (Fermentas, Glen Burnie, MD).

As shown in Table 2, some frequently found alleles were expected to be amplified in the first PCR such as *HLA-B*13:01*, *B*15:13*, *B*15:21* and *B*15:25* (430 bp). In the second PCR reactions, all other common alleles except *B*15:02* were expected to be eliminated. A sample would be identified as *HLA-B*15:02* if there was a positive band from F2&R2 (74 bp). To interpret the result, PCR products from first and second PCR were analyzed by gel electrophoresis. To avoid a false negative result, all samples must be positive from the internal control primer (150 bp) in the first PCR. In the second PCR, only positive samples from F1 and R1 will be amplified from the nested control primer (303 and/or 367 bp). The nested control primer (F3 and R1) will give a 303 bp band in the second PCR reaction. For *HLA-B*13:01*, products from F1 and R1 are fainter than other predicted

Table 2 Prediction of all possible amplified alleles and its frequencies (14) from different pairs of primers based on 10 mer from 3' end of each primer^a

Group	Alleles	Primers F1 and R1	Primers F2 and R2	Frequency in Thai population ^b	References	Frequency in Chinese population ^c	References
B*13	B*13:01	√		2.1-4.1	(15, 16)	3.6	(17)
	B*13:06	v		n/a	(,,	0.0	(18)
	B*13:07N	v V		n/a		0.0	(18)
	B*13:12	Ž		n/a		0.0	(18)
	B*13:13	Ž		n/a		0.0	(18)
	B*13:17	v		n/a		n/a ^d	(19)
	B*13:20	v		n/a		n/a ^d	(19)
	B*13:21	V		n/a		n/a ^d	(19)
	B*13:22	V		n/a		n/a ^d	(19)
	B*13:23	Ž		n/a		n/a ^d	(19)
	B*13:25	V		n/a		n/a ^d	(19)
	B*13:26	V		n/a		n/a ^d	(19)
	B*13:28	<i></i>		n/a		n/a ^d	(19)
	B*13:29	, _		n/a		n/a ^d	(19)
	B*13:36	<i></i>		n/a		n/a ^d	(19)
	B*13:39 ^e	V	√	n/a		n/a ^f	
	B*13:43			n/a		n/a ^f	
	B*13:50	√ ·		n/a		n/a ^f	
	B*13:51	, _		n/a		n/a ^f	
	B*13:52	√		n/a		n/a ^f	
B*15	B*15:02	√	\checkmark	8.2-8.5	(15, 16, 20)	12.87	(21)
	B*15:13	√ ·		0.1-1.8	(15, 20)	0.37	(21)
	B*15:20 ^e	√	\checkmark	n/a		0.74	(21)
	B*15:21	√		0.7 - 1.0	(16, 20)	0.74	(21)
	B*15:25 ⁹	√	\checkmark	2.0-2.5	(15, 16)	1.84	(21)
	B*15:36	\checkmark		n/a		0.0	(18)
	B*15:44	\checkmark		n/a		0.0	(18)
	B*15:77 ^e	\checkmark	\checkmark	n/a		0.0	(18)
	B*15:85 ^e	\checkmark	\checkmark	n/a		0.0	(18)
	B*15:88 ^h	\checkmark	\checkmark	n/a		0.0	(18)
	B*15:89	\checkmark		n/a		0.0	(18)
	B*15:121 ^h	\checkmark	\checkmark	n/a		n/a ^d	(19)
	B*15:139	\checkmark		n/a		n/a ^d	(19)

HLA-B*15:02 nested SSP-PCR S. Virakul et al.

Table 2 Continued

Group	Alleles	Primers F1 and R1	Primers F2 and R2	Frequency in Thai population ^b	References	Frequency in Chinese population ^c	References
	B*15:144 ^h	<i>√</i>	<i>√</i>	n/a		n/a ^d	(19)
	B*15:154 ⁹	Ţ	, V	n/a		n/a ^d	(19)
	B*15:194 ^h	J	, V	n/a		n/a ^f	
	B*15:204 ^e	<i></i>	Ż	n/a		n/a ^f	
	B*15:213 ^h	, _	ý	n/a		n/a ^f	
	B*15:214 ^h	, 	ý	n/a		n/a ^f	
	B*15:223 ^h	Ţ	Ž	n/a		n/a ^f	
B*35	B*35:46	J	·	n/a		0.0	(18)
B*40	B*40:137e	, _	√	n/a		n/a ^f	
B*44	B*44:08	, _	•	n/a		0.10	(17)
	B*44:57	1		n/a		n/a ^d	(19)
	B*44:60	v		n/a		n/a ^d	(19)
B*57	B*57:05	~		n/a		0.0	(18)

HLA, human leukocyte antigen; SSP-PCR, sequence-specific primer-polymerase chain reaction.

alleles, as there is one mismatch on F1. There are also fewer 303 bp products in the second PCR. The additional 367 bp fainted band can also be seen in B*15:21 and B*15:25 in the second PCR as a product from F2 and R1. It should be noted that HLA-B*15:02 and 15:13 can be amplified by F2 and R1 much better than F3 and R1. This can be explained by a perfect match of F2 primer to these two alleles and a melting temperature of each primer. F2 (60.6°C) has the same melting temperature as R1, while F3 has 64.5°C. Interestingly, HLA-B*15:25 failed to be amplified by F2 and R2, which was firstly predicted by 10 bases analysis. This is because the condition is stringent enough for nested control primer (F3 and R1) to overcome a reaction from the second PCR primer (F2 and R2). The nested control primer can bind 100% to HLA-B*15:25, whereas HLA-B*15:25 has two mismatches near 5' end of F2. The behavior of these primers implies that rare alleles such as HLA-B*13:39, 15:20, 15:77, 15:85, 15:154, 15:204 and 40:137 will not be amplified by this system, which will have only *HLA-B*15:88*, 15:121, 15:144, 15:194, 15:213, 15:214 and 15:223 as default

We validated our nested PCR with 104 purified genomic DNA collected from blood or bone marrow donors from

the Thai Red Cross Society, Bangkok, Thailand, which was approved by the Ethics Committee for Human Research Protection from the Faculty of Medicine, Chulalongkorn University, and consent forms were obtained from all subjects. These samples have been HLA typed by the commercial sequence-specific oligonucleotide probe-polymerase chain reaction (SSOP-PCR) (LABType® SSO B Locus, One Lambda, Inc., Canoga Park, CA). These 104 samples were then sent to us, blind. We detected 20/20 HLA-B*1502. Other HLA-B alleles (n = 84) were not detected by our system (Table 3). According to our primer design, rare alleles such as HLA-B*15:88, 15:121, 15:144, 15:194, 15:213, 15:214 and 15:223 were also expected to be amplified from this nested SSP-PCR technique by using 10 bases from 3' end of each primer to predict. However, these alleles are very rare worldwide, and we could not detect them, which suggests the specificity of this assay to be >99.9%, with 100% sensitivity.

Nested SSP-PCR was also performed directly from whole blood using KAPA Blood PCR Kit (Kapa Biosystems, Woburn, MA). For the first PCR reaction, a total final volume of 10 μ l consisted of the following components: final concentration of 1× KAPA Blood PCR Mix B, 1.0 μ M primer, 0.25 μ M internal control primer and 1.0 μ l of whole blood as

^aTo predict which alleles will be amplified from the different combinations of primers used in the nested SSP-PCR, 10 bases from 3' end of each primer were entered into the IMGT/HLA PROBE and PRIMER Search Tool, database version 3.6 October 2011. Frequencies of all alleles were from the Allele Frequency Net Database (14).

bFrequency of these alleles in the Thai population both from Bangkok and from the Northeast region which has the highest population in Thailand.

Frequency of these alleles in the Chinese population. Majority of the Asian population is composed of Chinese ethnicity. Because most of the data is available for the Chinese North Han population, this data is used here to determine the frequency of these alleles in the Chinese population.

^dThis data is only from Morocco Settat Chaouya population. The frequency of these alleles is 0.0%.

eThe behavior of these primers with *HLA-B*15:25* can imply that rare alleles such as *HLA-B*13:39*, 15:20, 15:77, 15:85, 15:154, 15:204 and 40:137 will not be amplified by this system.

^fThere are no frequency information about these alleles.

⁹*HLA-B*15:25* failed to be amplified by F2 and R2, which was first predicted by 10-base analysis. This is because the condition is stringent enough for nested control primer (F3 and R1) to overcome a reaction from the second PCR primer (F2 and R2). This is because nested control primer can bind 100% to *HI A-B*15:25* whereas *HI A-B*15:25* has two mismatches near 5′ end of F2.

hHLA-B*15:88, 15:121, 15:144, 15:194, 15:213, 15:214 and 15:223 are expected to be positive for both reactions. It should be noted that these alleles are extremely rare worldwide. This assay can be used to identify HLA-B*15:02 with very low false positive results.

S. Virakul et al. HLA-B*15:02 nested SSP-PCR

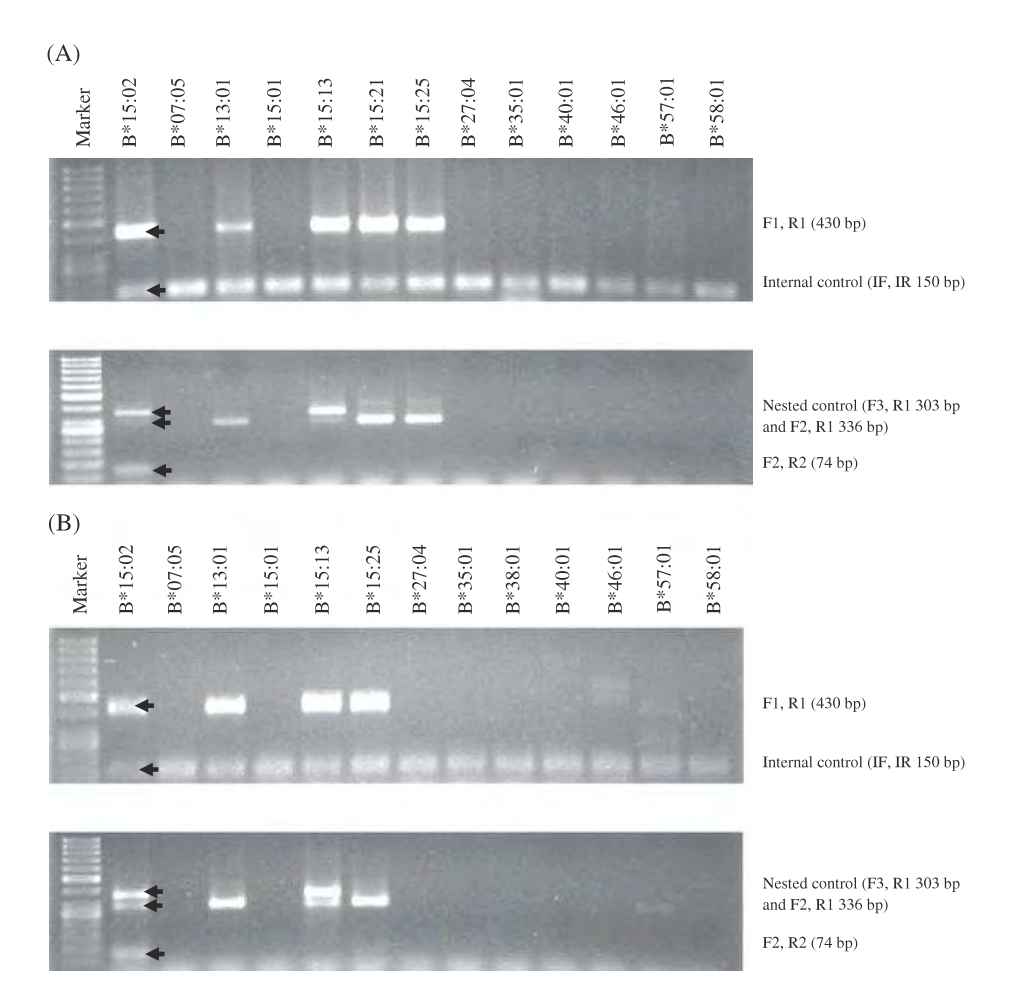


Figure 2 Migration patterns of *HLA-B*15:02* compared to other alleles. These products were detected by nested sequence-specific primer-polymerase chain reaction from both DNA (A) and whole blood samples (B). The composition of PCR from DNA the first PCR with a final volume of 10 μl contained the following components: final concentrations of 1× *Taq* buffer, 2.5 mM MgCl2, (Fermentas, Glen Burnie, MD) and total genomic DNA of 50 ng per reaction. For the second PCR, a total final volume of 10 μl reaction had the same components as the first PCR with 0.6 mM of nested control primer and had an additional 2.5 μl of 100 times diluted PCR product from the first step, region amplified by primers F1 and R1, as template. PCR cycles for both DNA and whole blood are the same. The first PCR was performed with an initial denaturation at 95°C for 5 min followed by a touchdown program of: (1) 5 cycles at 95°C for 30 s, 70°C for 30 s and 72°C for 30 s, (2) 5 cycles at 95°C for 30 s, 68°C for 30 s and 72°C for 30 s, (4) 10 cycles at 95°C for 30 s, 65°C for 30 s and 72°C for 30 s, and (5) 20 cycles at 95°C for 30 s, 65°C for 30 s and 72°C for 30 s. The final extension step was performed at 72°C for 5 min and later was held at 4°C. For the second PCR, denaturation was performed in one cycle at 95°C for 5 min and followed by 10 cycles at 95°C for 30 s, 70°C for 30 s and 72°C for 30 s. The final extension step was performed at 72°C for 30 s, 70°C for 30 s and 72°C for 5 min and held at 4°C. Two positive bands from the first (430 bp from F1 and R1) and second PCR (74 bp F2 and R2) will be reported as *HLA-B*15:02*. Alleles that are positive in the first step, but not *HLA-B*15:02*, will only be positive from nested control band (303 bp from F3 and R1) in the second step. Negative results will only have the internal control band (150 bp) from the first PCR. HLA, human leukocyte antigen. Arrow head (♣) indicates the expected product.

template. As for the second PCR, the same components from the first PCR were used with 0.6 mM of nested control primers and with an additional 2.5 µl of 100 times diluted PCR product from the first PCR, product amplified from using primers F1 and R1, as template. We tested our in-house nested SSP-PCR on another 96 independent blood samples from blood or bone marrow donors from the Thai Red Cross Society. These samples have been HLA typed by the commercial SSOP-PCR

(LABType[®] SSO B Locus, One Lambda, Inc.). We were able to detect *HLA-B*15:02* in all 24 samples and another 72 samples of other *HLA-B* alleles with 100% sensitivity and >99.9% specificity (Table 3). A representative gel electrophoresis is shown in Figure 2B.

HLA-B15 group is one of the most diverse families of HLA-B alleles. Identifying a broad *HLA-B*15* group might be a good choice to avoid the use of carbamazepine. However,

HLA-B*15:02 nested SSP-PCR S. Virakul et al.

Table 3 Numbers of samples defined by each method

A.II. 1. 2	Purified genomic	Whole
Allelesa	DNA ^b	blood ^c
B*07:02	0/2	_
B*07:05	0/8	0/2
B*08:01	0/1	_
B*13:01	0/8	0/15
B*13:02	0/4	_
B*15:01	0/3	0/6
B*15:02	20/20	24/24
B*15:11	0/2	_
B*15:13	0/1	0/1
B*15:21	0/1	_
B*15:25	0/2	0/7
B*15:32	0/1	0/1
B*18:01	0/7	0/9
B*18:02	0/1	0/1
B*27:04	0/3	0/6
B*27:06	0/3	_
B*35:01	0/4	0/2
B*35:03	0/2	_
B*35:05	0/7	_
B*38:02	0/5	0/4
B*39:01	0/1	0/3
B*40:01	0/8	0/12
B*40:02	_	0/1
B*40:06	0/7	_
B*44:03	0/7	_
B*46:01	0/23	0/20
B*48:01	0/1	0/3
B*49:01	0/1	_
B*51:01	0/4	0/5
B*51:02	0/1	0/2
B*52:01	0/5	0/3
B*54:01	0/1	_
B*55:01	0/1	_
B*56:01	0/1	_
B*57:01	0/4	0/3
B*58:01	0/11	0/9

HLA, human leukocyte antigen.

there have been false positive results for *HLA-B*15:01*, *15:11*, *15:12*, *15:13*, *15:18*, *15:21*, *15:25* and *15:32*, which are found in more than 1% of the Thai population. As a result, patients with false positive results of these alleles have to pay for expensive drugs that they may be allergic to. Moreover, the use of alternative drugs could result in other consequences.

For example, the exposure of valproate in utero was associated with increased risk of impaired cognitive function at 3 years of age (13). Therefore, the development of methods to specifically and accurately detect HLA-B*15:02 is important. Previous SSP-PCR methods have reported the use of at least six sets of primers in six separate reactions with 30 cycles from touchdown phase to detect HLA-B*15:02 (7, 8). We report an alternative method to specifically detect HLA-B*1502 without the use of multiple sets of primers. In this study, our in-house SSP-PCR required two reactions. With the help of nested PCR, the second reaction can specifically identify HLA-B*15:02. We have also validated that the use of as little as 1 µl whole blood in this alternative method gave clear and consistent results comparable to genomic DNA sampling. Although SSP-PCR is the most cost effective method, its DNA extraction step can become expensive depending on which DNA extraction kit is used. In addition, if a cheaper alternative technique such as a standard salting out method is used to extract DNA, this can result in a longer turnaround time. However, the nested SSP-PCR method carries a contamination risk, and it should be tightly controlled. Further development into a single closed tube is recommended.

In conclusion, *HLA-B*15:02* can be identified by our inhouse nested SSP-PCR method with 100% sensitivity and >99.9% specificity, from both purified DNA and whole blood. This technique also requires a smaller amount of the starting material compared to other methods. Patient benefits include the prevention of adverse events from taking carbamazepine, lower costs and shorter turnaround time.

Acknowledgments

This work was supported by the 90th Anniversary of Chulalongkorn University Fund (Ratchadaphiseksomphot Endowment Fund) and the Thailand Research Fund (Senior Research Scholar Grant – RTA5280002).

Conflict of interest

The authors have declared no conflicting interests.

References

- Chung WH, Hung SI, Hong HS et al. Medical genetics: a marker for Stevens-Johnson syndrome. *Nature* 2004: 428: 486.
- Chung WH, Hung SI, Chen YT. Human leukocyte antigens and drug hypersensitivity. Curr Opin Allergy Clin Immunol 2007: 7: 317–23.
- Man CB, Kwan P, Baum L et al. Association between HLA-B*1502 allele and antiepileptic drug-induced cutaneous reactions in Han Chinese. *Epilepsia* 2007: 48: 1015-8.
- 4. Locharernkul C, Loplumlert J, Limotai C et al. Carbamazepine and phenytoin induced Stevens-Johnson syndrome is associated

alt should also be noted that extremely rare alleles such as HLA-B*13:39, 15:20, 15:77, 15:85, 15:88, 15:121, 15:144, 15:154, 15:194, 15:204, 15:213, 15:214, 15:223 and 40:137 were not detected in this study.

^bThe first number is the number of samples detected by the new nested PCR method using purified genomic DNA as template, and the second number shows alleles defined by SSOP commercial technique.

^cThe first number is the number of samples detected by the new nested PCR method using whole blood as template, and the second number shows alleles defined by SSOP commercial technique.

S. Virakul et al. HLA-B*15:02 nested SSP-PCR

with HLA-B*1502 allele in Thai population. *Epilepsia* 2008: **49**: 2087–91.

- Alfirevic A, Jorgensen AL, Williamson PR, Chadwick DW, Park BK, Pirmohamed M. HLA-B locus in Caucasian patients with carbamazepine hypersensitivity. *Pharmacogenomics* 2006: 7: 813–8.
- Ferrell PB Jr, McLeod HL. Carbamazepine HLA-B*1502 and risk of Stevens-Johnson syndrome and toxic epidermal necrolysis: US FDA recommendations. *Pharmacogenomics* 2008: 9: 1543-6.
- Yu N, Ohashi M, Alosco S et al. Typing of HLA-B*15 alleles using sequence-specific primers. *Tissue Antigens* 1998: 52: 260-9.
- Bunce M, O'Neill CM, Barnardo MC et al. Phototyping: comprehensive DNA typing for HLA-A, B, C, DRB1, DRB3, DRB4, DRB5 & DQB1 by PCR with 144 primer mixes utilizing sequence-specific primers (PCR-SSP). *Tissue Antigens* 1995: 46: 355–67.
- Sayer DC, Cassell HS, Christiansen FT. HLA-B*27 typing by sequence specific amplification without DNA extraction. *Mol Pathol* 1999: 52: 300–1.
- Bu Y, Huang H, Zhou G. Direct polymerase chain reaction (PCR) from human whole blood and filter-paper-dried blood by using a PCR buffer with a higher pH. *Anal Biochem* 2008: 375: 370-2.
- Kermekchiev MB, Kirilova LI, Vail EE, Barnes WM. Mutants of Taq DNA polymerase resistant to PCR inhibitors allow DNA amplification from whole blood and crude soil samples. *Nucleic Acids Res* 2009: 37: e40.
- Robinson J, Mistry K, McWilliam H, Lopez R, Parham P, Marsh SG. The IMGT/HLA database. *Nucleic Acids Res* 2011: 39: D1171-6.
- Meador KJ, Baker GA, Browning N et al. Cognitive function at 3 years of age after fetal exposure to antiepileptic drugs. N Engl J Med 2009: 360: 1597–605.

- Gonzalez-Galarza FF, Christmas S, Middleton D, Jones AR. Allele frequency net: a database and online repository for immune gene frequencies in worldwide populations. *Nucleic Acids Res* 2011: 39: D913–9.
- Chandanayingyong D. HLA class II (DRB1, DQA1 and DQB1) allele and haplotype frequencies among HIV infected discordant couples in thais. 7th Asia-Oceania Histocompatibility Workshop and Conference. Karuizawa, Japan, 2003.
- Pimtanothai N, Charoenwongse P, Mutirangura A, Hurley CK. Distribution of HLA-B alleles in nasopharyngeal carcinoma patients and normal controls in Thailand. *Tissue Antigens* 2002: 59: 223-5.
- 17. Yang G, Deng YJ, Hu SN et al. HLA-A, -B, and -DRB1 polymorphism defined by sequence-based typing of the Han population in Northern China. *Tissue Antigens* 2006: **67**: 146–52.
- 18. Hu ZH, Liu ZH, Xiong YJ et al. A novel HLA-DRB1*15 allelic sequence isolated from the Han population of Guangdong, China. *Int J Immunogenet* 2005: **32**: 221–2.
- Canossi A, Piancatelli D, Aureli A et al. Correlation between genetic HLA class I and II polymorphisms and anthropological aspects in the Chaouya population from Morocco (Arabic speaking). *Tissue Antigens*. 2010: 76: 177–93.
- Romphruk AV, Romphruk A, Kongmaroeng C, Klumkrathok K, Paupairoj C, Leelayuwat C. HLA class I and II alleles and haplotypes in ethnic Northeast Thais. *Tissue Antigens* 2010: **75**: 701–11.
- 21. Yang G, Deng YJ, Qin H et al. HLA-B*15 subtypes distribution in Han population in Beijing, China, as compared with those of other populations. *Int J Immunogenet* 2010: **37**: 205–12.

ORGANIC LETTERS

2012 Vol. 14, No. 6 1440-1443

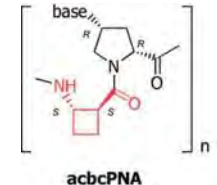
Pyrrolidinyl Peptide Nucleic Acid Homologues: Effect of Ring Size on **Hybridization Properties**

Woraluk Mansawat, † Chotima Vilaivan, † Árpád Balázs, † David J. Aitken, † and Tirayut Vilaivan*,†

Organic Synthesis Research Unit, Department of Chemistry, Faculty of Science, Chulalongkorn University, Phayathai Road, Patumwan, Bangkok 10330, Thailand, and Laboratoire de Synthèse Organique & Méthodologie, ICMMO – CNRS UMR 8182, Université Paris-Sud, 15 rue Georges Clemenceau, 91405 Orsay cedex, France

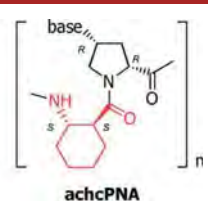
vtirayut@chula.ac.th

Received January 23, 2012





ABSTRACT



The effect of ring size of four- to six-membered cyclic β -amino acid on the hybridization properties of pyrrolidinyl peptide nucleic acid with an alternating $\alpha l \beta$ peptide backbone is reported. The cyclobutane derivatives (acbcPNA) show the highest $T_{\rm m}$ and excellent specificity with cDNA and RNA.

Nucleic acids form higher order structures in a predictable fashion as a result of the highly specific Watson-Crick type base pairing. This property is essential for the function of nucleic acids in the storage and transfer of genetic information in all living organisms. It is also the basis of various applications, ranging from biomedical sciences through biotechnologies to material sciences. In recent years, there has been considerable interest in the design of alternative nucleic acid recognition systems that may offer advantages over DNA or RNA in terms of chemical stability, binding affinities, and/or specificities toward different types of nucleic acids. Peptide nucleic acid (PNA) is a class of nucleic acid analogues in which a peptide-like backbone replaces the deoxyribose-phosphate backbone of DNA. In addition to being able to recognize its cDNA/RNA with high affinity and sequence specificity, the electrostatically neutral nonphosphate backbone of PNA gives rise to a number of unique properties not observed in other classes of DNA analogues,

such as complete resistance to nucleases and the relative insensitivity of PNA·DNA hybrids to ionic strength.² Conformational restriction of the N-aminoethylglycyl backbone of the original PNA (now known as aegPNA), for example, by incorporation of a cyclic moiety or one or more substituents along the PNA backbone, can provide PNA with an improved binding affinity as well as specificity.³⁻⁵

[†] Chulalongkorn University.

[‡] Université Paris-Sud.

⁽¹⁾ Reviews: (a) Silverman, S. K. Angew. Chem., Int. Ed. 2010, 49, 7180–7201. (b) Aldaye, F. A.; Palmer, A. L.; Sleiman, H. F. *Science* **2008**, *321*, 1795–1799. (c) Seeman, N. C. *Mol. Biotechnol.* **2007**, *37*, 246– 257. (d) Leumann, C. J. Bioorg. Med. Chem. 2002, 10, 841–854.

^{(2) (}a) Nielsen, P. E. Chem. Biodiversity 2010, 7, 796–804. (b) Lundin,

K. E.; Good, L.; Strömberg, R.; Gräslund, A.; Smith, C. I. E. Adv. Genet. 2006, 56, 1-51. (c) Egholm, M.; Buchardt, O.; Christensen, L.; Behrens, C.; Freier, S. M.; Driver, D. A., Berg, R. H.; Kim, S. K.; Norden, B.; Nielsen, P. E. *Nature* **1993**, *365*, 566–568.

⁽³⁾ Reviews: (a) Corradini, R.; Sforza, S.; Tedeschi, T.; Totsingan, F.; Manicardi, A.; Marchelli, R. Curr. Top. Med. Chem. 2011, 11, 1535–1554. (b) Efimov, V. A.; Aralov, A. V.; Chakhmakhcheva, O. G. Russ. J. Bioorg. Chem. 2010, 36, 663-683. (c) Kumar, V. A.; Ganesh, K. N. Acc. Chem. Res. 2005, 38, 404-412.

⁽⁴⁾ Selected examples of PNA incorporating cyclic structures in the backbone: (a) Pokorski, J. K.; Witschi, M. A.; Purnell, B. L.; Appella, D. H. *J. Am. Chem. Soc.* **2004**, *126*, 15067–15073. (b) Govindaraju, T.; Kumar, V. A.; Ganesh, K. N. *J. Am. Chem. Soc.* **2005**, *127*, 4144–4145.

⁽⁵⁾ Selected examples of PNA with backbone substituents: (a) Dragulescu-Andrasi, A.; Rapireddy, S.; Frezza, B. M.; Gayathri, C.; Gil, R. G.; Ly, D. H. *J. Am. Chem. Soc.* **2006**, *128*, 10258–10267. (b) Englund, É. Á.; Appella, D. H. Angew. Chem., Int. Ed. 2007, 46, 1414-1418. (c) Manicardi, A.; Calabretta, A.; Bencivenni, M.; Tedeschi, T.; Sforza, S.; Corradini, R.; Marchelli, R. *Chirality* **2010**, *22*, E161–E172.

Inspired by the discovery that oligomers of cyclic β amino acids can adopt well-defined helical conformations, ^{6,7} we previously developed a series of pyrrolidinyl PNA with an α/β peptide backbone consisting of an alternating sequence of nucleobase-modified proline and cyclic β -amino acid "spacer" such as 1-aminopyrrolidinecarboxylic acid (dapcPNA)⁸ or 2-aminocyclopentane-carboxylic acid (acpcPNA).⁹ These pyrrolidinyl PNAs bind to DNA with higher affinity and sequence specificity compared to aegPNA. 10 They also exhibited some unusual features, including the preference for binding to DNA over RNA as well as the inability to form selfhybrids. The failure of pyrrolidinyl PNA carrying acyclic spacers to recognize DNA/RNA targets¹¹ suggested that the cyclic five-membered ring spacer locks the conformation of the PNA into a form that is close to optimal for DNA binding. The work carried out so far has been limited to a five-membered ring spacer, and in order to gain further insight into the structural properties of these pyrrolidinyl PNA, an investigation of the effect of the ring size of the spacer part was warranted. Modification of the ring size should change both the rigidity and the torsional angle (θ) of the NH-C2-C1-CO which is an integral part of the PNA backbone⁷ and could in turn significantly affect the hybridization properties of the resulting PNA.

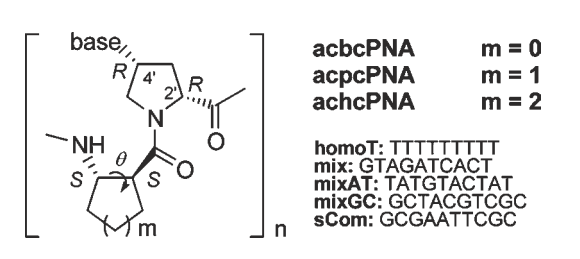


Figure 1. Structures and sequences of PNA.

We now report on the behavior of two new PNA manifolds, which incorporate 2-aminocyclobutane-carboxylic acid (ACBC) or 2-aminocyclohexanecarboxylic acid (ACHC) spacers, referred to here as acbcPNA and achcPNA respectively, and compare them with acpcPNA

which contains a 2-aminocyclopentanecarboxylic (ACPC) spacer (Figure 1). Since the (1S,2S) configuration was previously found to be optimal for the ACPC spacer,⁹ the same (1S,2S) configuration was a logical starting point for the new ring systems. Thus, the Fmoc-derivative of (1*S*,2*S*)-ACBC¹² was prepared, along with the known Fmoc-(1*S*,2*S*)-ACHC, ¹³ and each of these derivatives was combined with the (4'R)-nucleobase-modified (2'R)proline employing the Fmoc solid-phase peptide synthesis previously developed ¹⁴ to give eight new pyrrolidinyl PNA sequences as shown in Table S1, Supporting Information. All of these pyrrolidinyl PNA possess the same (2'R,4'R) configuration at the proline part except for *epi*acbcPNA-sCom. This latter PNA, with a (2'R,4'S) configuration, was synthesized in order to investigate the self-pairing abilities not observed in the (2'R,4'R) epimer of acpcPNA.¹⁵ The PNA was purified by HPLC (>90% purity), and the identities confirmed by matrix-assisted laser desorption ionization time-of-flight (MALDI-TOF) mass spectrometry. It is noteworthy that the intrinsically labile ACBC 16 is compatible with the basic conditions required during Fmoc group removal and nucleobase side chain deprotection procedures.

Table 1. Thermal Stabilities of DNA and RNA Hybrids of Homologous Pyrrolidinyl PNA a

entry	PNA	apDNA	pDNA	apRNA	pRNA
1	acbcPNA-homoT	73.8	_	n.d.	n.d.
		(72.5)	_	_	_
2	acbcPNA-mixAT	63.2	<20	50.8	25.8
		(54.2)	(<20)	(32.6)	(<20)
3	acbcPNA-mix	66.1	<20	58.2	31.7
		(53.3)	(<20)	(42.3)	(<20)
4	acbcPNA-mixGC	69.8	34.1	62.9	48.6
		(54.5)	(<20)	(48.0)	(32.9)
5	achcPNA-homoT	<20	_	n.d.	n.d.
		(72.5)	_	_	_
6	achcPNA-mix	<20	<20	<20	<20
		(53.3)	(<20)	(42.3)	(<20)

 $^aT_{\rm m}$ values of the corresponding acpcPNA hybrids under identical conditions are shown in parentheses, and ap and p are antiparallel and parallel, respectively. Conditions: 10 mM sodium phosphate buffer pH 7.0, 100 mM NaCl, and [PNA] = [DNA] = 1 μ M. $T_{\rm m}$ values are accurate to within ± 0.5 °C.

The hybridization properties of **acbcPNA-homoT** and **achcPNA-homoT** with cDNA (dA₉) were investigated by thermal denaturation experiments (monitored by UV-vis at 260 nm) (Table 1, entries 1 and 5). A well-defined thermal denaturation curve was observed only with **acbcPNA-homoT**. The melting temperature ($T_{\rm m}$) of

Org. Lett., Vol. 14, No. 6, **2012**

^{(6) (}a) Appella, D. H.; Christianson, L. A.; Klein, D. A.; Powell, D. R.; Huang, X.; Barchi, J. J., Jr.; Gellman, S. H. *Nature* **1997**, *387*, 381–382. (b) Cheng, R. P.; Gellman, S. H.; DeGrado, W. F. *Chem. Rev.* **2001**, *101*, 3219–3232.

^{(7) (}a) Vasudev, P. G.; Chatterjee, S.; Shamala, N.; Balaram, P. *Chem. Rev.* **2011**, *111*, 657–687. (b) Fülöp, F.; Martinek, T. A.; Tóth, G. K. *Chem. Soc. Rev.* **2006**, *35*, 323–334.

⁽⁸⁾ Vilaivan, T.; Lowe, G. *J. Am. Chem. Soc.* **2002**, *124*, 9326–9327. (9) (a) Vilaivan, T.; Srisuwannaket, C. *Org. Lett.* **2006**, *8*, 1897–1900. (b) Vilaivan, C.; Srisuwannaket, C.; Ananthanawat, C.; Suparpprom, C.; Kawakami, J.; Yamaguchi, Y.; Tanaka, Y.; Vilaivan, T. *Artif. DNA: PNA XNA* **2011**, *2*, 50–59.

⁽¹⁰⁾ Ananthanawat, C.; Vilaivan, T.; Hoven, V. P.; Su, X. *Biosens. Bioelectron.* **2010**, *25*, 1064–1069.

^{(11) (}a) Vilaivan, T.; Suparpprom, C.; Harnyuttanakorn, P.; Lowe, G. *Tetrahedron Lett.* **2001**, *42*, 5533–5536. (b) Vilaivan, T.; Suparpprom, C.; Duanglaor, P.; Harnyuttanakorn, P.; Lowe, G. *Tetrahedron Lett.* **2003**, *44*, 1663–1666. (c) Ngamwiriyawong, P.; Vilaivan, T. *Nucleosides, Nucleotides Nucleic Acids* **2011**, *30*, 97–112.

^{(12) (}a) Fernandes, C.; Pereira, E.; Faure, S.; Aitken, D. J. *J. Org. Chem.* **2009**, *74*, 3217–3220. (b) Declerck, V.; Aitken, D. J. *Amino Acids* **2011**, *41*, 587–595.

^{(13) (}a) Schinnerl, M.; Murray, J. K.; Langenhan, J. M.; Gellman, S. H. *Eur. J. Org. Chem.* **2003**, 721–726. (b) Xu, D.; Prasad, K.; Repič, O.; Blacklock, T. J. *Tetrahedron: Asymmetry* **1997**, *8*, 1445–1451.

⁽¹⁴⁾ Lowe, G.; Vilaivan, T. *J. Chem. Soc., Perkin Trans. I* **1997**, 555–560. (15) Taechalertpaisarn, J.; Sriwarom, P.; Boonlua, C.; Yotapan, N.; Vilaivan, C.; Vilaivan, T. *Tetrahedron Lett.* **2010**, *51*, 5822–5826.

⁽¹⁶⁾ Aitken, D. J.; Gauzy, C.; Pereira, E. *Tetrahedron Lett.* **2004**, *45*, 2359–2361.

73.8 °C is comparable to that of acpcPNA with the same sequence (72.5 °C). Circular dichroism (CD) experiments also clearly confirmed that the **acbcPNA-homoT**, but not **achcPNA-homoT**, could form a stable hybrid with dA₉ (Figure S9, Supporting Information). The melting curve of the hybrid between **acbcPNA-homoT** and dA₉, as monitored by CD spectroscopy, was in good agreement with that obtained from UV—vis experiments (Figure 2).

Although homopyrimidine PNAs generally form (PNA)₂·DNA triplexes by Watson—Crick/Hoogsteen base pairing, ¹⁷ UV and CD titrations of **acbcPNA-homoT** and dA₉ (Figure S10, Supporting Information) clearly showed that only the 1:1 duplex was formed. The lack of triplex formation is analogous to acpcPNA, which may be ascribed to the steric repulsion of the bulky acpcPNA/acbcPNA backbone that destabilizes such triplexes.⁹

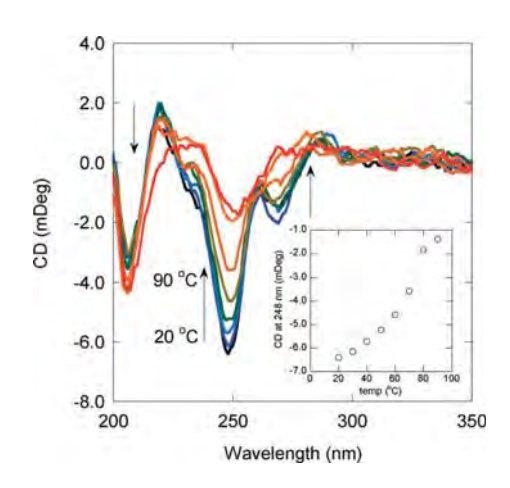


Figure 2. CD spectra of hybrid of **acbcPNA-homoT** and dA₉ at different temperatures (a) and change of CD signal at 248 nm as a function of temperature (b). Conditions: 10 mM sodium phosphate buffer pH 7.0, 100 mM NaCl, and [PNA] = [DNA] = 1μ M.

The binding studies of a mixed sequence PNA with DNA and RNA in both antiparallel and parallel orientations were performed on three different acbcPNA sequences with various G+C contents (acbcPNA-mixAT, acbcPNA-mix, acbcPNA-mixGC) and one achcPNA sequence (achcPNA-mix) (Table 1 and Figure S11, Supporting Information). The results were compared with the corresponding $T_{\rm m}$ values from acpcPNA with identical sequences. Several important observations were made. First, the acbcPNA binds to DNA and RNA preferentially in an antiparallel direction, although it can also form quite stable parallel acbcPNA·RNA hybrids. Second, both acbcPNA·DNA and acbcPNA·RNA hybrids show higher thermal stabilities than the corresponding acpcPNA hybrids. The extent of $T_{\rm m}$ increase depends on G+C content, ranging from 9 °C (20% G+C) to 15 °C (70% G+C) in acbcPNA·DNA hybrids and from 15 °C

(70% G+C) to 18 °C (20% G+C) in acbcPNA·RNA

The results from $T_{\rm m}$ experiments were also further confirmed by CD spectroscopy. The binding of **acbcPNA-mix** to antiparallel DNA, antiparallel RNA and parallel RNA resulted in a significant change in CD spectra compared to the sum of each component (Figure S12, Supporting Information). On the other hand, no such change was observed upon binding of **acbcPNA-mix** to parallel DNA as well as in all DNA and RNA hybrids with **achcPNA-mix** (Figure S13, Supporting Information).

Table 2. Thermal Stabilities of Mismatched DNA Hybrids of acbcPNA-mix

entry	DNA $(5' \rightarrow 3')$	$T_{\mathrm{m}}(^{\circ}\mathrm{C})^{a}$	$\Delta \: T_{\mathrm{m}} \: (^{\circ}\mathrm{C})^{b}$
1	dAGTGATCTAC	66.1 (53.3)	_
2	dAGTAATCTAC	40.4(26.4)	-25.7(-26.9)
3	dAGTTATCTAC	40.6(27.8)	-25.5(-25.5)
4	$dAGT\overline{C}ATCTAC$	42.8(31.0)	-23.3(-22.3)
5	$dAGT\overline{G}GTCTAC$	36.4(23.9)	-29.4(-29.5)
6	$dAGTG\overline{T}TCTAC$	46.6(29.4)	-19.5(-23.9)
7	$dAGTG\overline{C}TCTAC$	39.8 (23.8)	-26.3(-29.5)
8	$\overline{dAGTGAGCTAC}$	46.0(26.5)	-20.1(-26.8)
9	$dAGTGA\overline{A}CTAC$	47.0(28.4)	-19.1(-24.9)
10	$dAGTGA\overline{C}CTAC$	45.1 (28.8)	-21.0(-24.5)
11	$\overline{dAGTGATGTAC}$	41.2(26.4)	-24.9(-26.9)
12	dAGTGATATAC	38.3(24.2)	-27.8(-29.1)
13	dAGTGATTTAC	44.6(28.5)	-21.5(-24.8)

 $^aT_{\rm m}$ values of the corresponding acpcPNA hybrids under identical conditions 9 are shown in parentheses. Conditions: 10 mM sodium phosphate buffer pH 7.0, 100 mM NaCl, and [PNA] = [DNA] = $1\,\mu$ M. $^bT_{\rm m}$ (complementary) – $T_{\rm m}$ (mismatched). $T_{\rm m}$ values are accurate to within ± 0.5 °C.

Specificity is perhaps one of the most important aspects of any nucleic acid recognition systems. The $T_{\rm m}$ of hybrids between the PNA **acbcPNA-mix** and various DNA targets carrying a mismatched base at the positions 4–7 (Table 2) showed that the specificity (determined from the difference of $T_{\rm m}$ values between mismatched and cDNA hybrids) was comparable to acpcPNA. A $T_{\rm m}$ decrease of > 20 °C was observed in all but two cases (pT·dT and pA·dA mismatch, which showed $\Delta T_{\rm m}$ of –19.5 and –19.1 °C, respectively). This level of mismatch discrimination is better than the corresponding DNA and the original aegPNA (typical $\Delta T_{\rm m}$ –10 to –14 °C).²

Another unique property of acpcPNA is the inability to form self-pairing hybrids between two complementary acpcPNA sequences. This could lead to a number of useful applications in targeting DNA duplexes by a double duplex invasion mechanism that has been traditionally achieved with pseudocomplementary aegPNA bearing modified bases (2,4-diaminopurine/2-thiouracil). 18

hybrids. Third, the general preference for binding to DNA over RNA in the original acpcPNA was still observed in acbcPNA. Finally, the achcPNA with a mix sequence (achcPNA-mix) did not show any binding to cDNA or RNA in both antiparallel and parallel orientations.

The results from T_m experiments were also further con-

⁽¹⁷⁾ Kim, S. K.; Nielsen, P. E.; Egholm, M.; Buchardt, O.; Berg, R. H.; Nordén, B. *J. Am. Chem. Soc.* **1993**, *115*, 6477–6481.

⁽¹⁸⁾ Lohse, J.; Dahl, O.; Nielsen, P. E. Proc. Natl. Acad. Sci. U.S.A. 1999, 96, 11804–11808.

According to UV and CD melting studies, the PNA acpcPNA-sCom with a 10-mer self-complementary sequence showed no cooperative melting. On the other hand, acbcPNA-sCom showed a broad UV melting curve with apparent $T_{\rm m}$ of ca. 45 °C. At 20 °C, the same PNA showed a positive CD signal at 260 nm and a strong negative CD signal at 280 nm, which is distinctly different from the CD spectra of nonself-complementary acbcPNA (compare Figures S12 and S16, Supporting Information). These signals disappeared upon heating and reappeared upon cooling. The results suggest that acbcPNA-sCom can form a self-complementary hybrid. We also synthesized the (2'R,4'S) epimer of both acbcPNA and acpcPNA to compare the self-pairing behavior with the "normal" acpcPNA and acbcPNA. As shown in Table 3 and Figures S15 and S16, Supporting Information, the epi-acbcPNA-sCom self-pairing hybrid was considerably more stable than the corresponding epi-acpcPNA-sCom self-pairing hybrid. All self-complementary pyrrolidinyl PNAs can form stable hybrids with DNA with $T_{\rm m}$ values in the range of 67 °C (acpcPNA) to 73–78 °C (acbcPNA). In all cases, the PNA·DNA hybrids are more stable than the PNA · PNA hybrids at the same total strands concentration. The difference between T_{m} of PNA·DNA and PNA·PNA hybrids is smallest in epi-acbcPNA ($\Delta T_{\rm m} =$ 14 °C) and greatest in acpcPNA ($\Delta T_{\rm m} > 46$ °C).

Table 3. Thermal Stabilities of Self-Complementary and DNA Hybrids of acbcPNA and acpcPNA^a

entry	PNA	config	$T_{ m m}$ self	$T_{ m m}$ apDNA
1	acbcPNA-sCom	2'R,4'R	45.7	77.7
2	acpcPNA-sCom	2'R,4'R	<20	66.8
3	epi-acbcPNA-sCom	2'R,4'S	59.3	73.3
4	epi-acpcPNA-sCom	2'R,4'S	32.7	66.8

^a Conditions: 10 mM sodium phosphate buffer pH 7.0, 100 mM NaCl, and [PNA] = 2 μ M (self-hybridization) or [PNA] = [DNA] = 1 μ M (PNA·DNA hybridization). $T_{\rm m}$ values are accurate to within ± 0.5 °C.

Since the absence of NH in proline residues does not allow the formation of regular 11- and 14/15-helices usually observed in α/β peptides, ¹⁹ the preorganization into helical conformations of these α/β pyrrolidinyl PNA should be governed by the limited conformational space available to the cyclic β -amino acid spacer rather than hydrogen bonding. Based on our previous molecular dynamics simulations, ²⁰ the origin of stabilization of acbcPNA·DNA relative to acpcPNA·DNA hybrids

might be explained by a more favorable preorganization of acbcPNA as follows: Models of dapcPNA and acpcPNA showed the values of torsional angle NH-C2-C1-CO (θ) (Figure S17, Supporting Information) of the D-APC and (S,S)-ACPC spacers of 99.2 \pm 6.4° and 99.2 \pm 3.1° (averaged from 10 D-APC and 13 ACPC residues, respectively). A relatively large difference between these values compared to the corresponding θ figure from an X-ray structure of (R,R)-ACPC oligomer ($-85.9 \pm 12.2^{\circ}$; averaged from 6 residues)²¹ suggests that there must be a substantial conformational reorganization of the ACPC moiety to allow optimal binding to DNA. While the five-membered ring of ACPC is flexible enough to allow this, there is an entropic penalty associated with the conformational reorganization process. On the other hand, the torsional angle θ obtained from an X-ray structure of (R,R)-ACBC oligomer $(-95.5 \pm 3.7^{\circ})$; averaged from 8 residues)²² is closer to the optimal θ values shown above. Hence, the acbcPNA is better preorganized for binding to DNA when compared to acpcPNA. The torsional angle θ of ACHC obtained from an X-ray structure of (S,S)-ACHC hexamer was in the range of only $51.5-61.4^{\circ}$. The large deviation from the optimal θ , together with the rigidity of the cyclohexane ring system which does not allow efficient conformational reorganization, should explain the inability of achcPNA to pair with DNA. The origin of the greater stabilization of acbcPNA·RNA compared to acpcPNA·RNA hybrids cannot be explained without further structural information, but the ability to bind strongly to RNA in addition to DNA clearly suggests potential of applications of acbcPNA involving RNA targets.

In conclusion, we have successfully synthesized homologues of acpcPNA with four-membered ring (acbcPNA) and six-membered ring (achcPNA) spacers. The replacement of ACPC with ACBC resulted in a new pyrrolidinyl PNA with general binding properties similar to acpcPNA but with an increase of $T_{\rm m}$ with cDNA and RNA hybrids by 0.9-1.8 °C per modification without compromising the specificity. In contrast, the replacement of ACPC with ACHC resulted in total loss of binding to both DNA and RNA. The results are explained by a more favorable conformational preorganization of the ACBC residue compared to ACPC and ACHC.

Acknowledgment. Financial supports to this work come from the Thailand Research Fund (RTA5280002) (to T.V.) and the Ratchadaphiseksomphot Endowment Fund from Chulalongkorn University (postdoctoral fellowship to W.M.).

Supporting Information Available. Synthesis of Fmoc-(1S,2S)-ACBC-OH and NMR spectra, analytical HPLC and MALDI-TOF mass spectral data of PNA, and additional UV and CD spectra. This material is available free of charge via the Internet at http://pubs.acs.org.

Org. Lett., Vol. 14, No. 6, 2012 1443

⁽¹⁹⁾ Choi, S. H.; Guzei, I. A.; Spencer, L. C.; Gellman, S. H. *J. Am. Chem. Soc.* **2008**, *130*, 6544–6550.

(20) Siriwong, K.; Chuichay, P.; Saen-oon, S.; Suparpprom, C.;

Vilaivan, T.; Hannongbua, S. Biochem. Biophys. Res. Commun. 2008,

⁽²¹⁾ Appella, D. H.; Christianson, L. A.; Klein, D. A.; Richards, M. R.; Powell, D. R.; Gellman, S. H. J. Am. Chem. Soc. 1999, 121, 7574-7581.

⁽²²⁾ Fernandes, C.; Faure, S.; Pereira, E.; Théry, V.; Declerck, V.; Guillot, R.; Aitken, D. J. *Org. Lett.* **2010**, *12*, 3606–3609.

⁽²³⁾ Appella, D. H.; Christianson, L. A.; Karle, I. L.; Powell, D. R.; Gellman, S. H. *J. Am. Chem. Soc.* **1999**, *121*, 6206–6212.

The authors declare no competing financial interest.

Provided for non-commercial research and education use.

Not for reproduction, distribution or commercial use.



This article appeared in a journal published by Elsevier. The attached copy is furnished to the author for internal non-commercial research and education use, including for instruction at the authors institution and sharing with colleagues.

Other uses, including reproduction and distribution, or selling or licensing copies, or posting to personal, institutional or third party websites are prohibited.

In most cases authors are permitted to post their version of the article (e.g. in Word or Tex form) to their personal website or institutional repository. Authors requiring further information regarding Elsevier's archiving and manuscript policies are encouraged to visit:

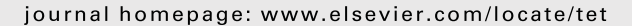
http://www.elsevier.com/copyright

Tetrahedron 68 (2012) 3988-3995



Contents lists available at SciVerse ScienceDirect

Tetrahedron





Clicked polycyclic aromatic hydrocarbon as a hybridization-responsive fluorescent artificial nucleobase in pyrrolidinyl peptide nucleic acids

Woraluk Mansawat^a, Chalothorn Boonlua^a, Khatcharin Siriwong^b, Tirayut Vilaivan^{a,*}

ARTICLE INFO

Article history: Received 1 December 2011 Received in revised form 2 March 2012 Accepted 19 March 2012 Available online 28 March 2012

Keywords: Click chemistry Fluorescence Polycyclic aromatic hydrocarbon Peptide nucleic acid

ABSTRACT

Pyrene as well as other aromatic hydrocarbons could be successfully incorporated into pyrrolidinyl peptide nucleic acid bearing a p-prolyl-2-aminocyclopentane carboxylic acid backbone (acpcPNA) as a base surrogate via a triazole linker employing Cu-catalyzed alkyne—azide cycloaddition (click chemistry). The labeling can be performed via a pre-clicked pyrene monomer or by post-synthetic modification of azide-containing acpcPNA on solid support. Thermal denaturation experiments suggested that the pyrene—triazole unit can behave as a universal base in the acpcPNA system. The mode of base-pairing has been proposed based on molecular dynamics simulations. Importantly, the fluorescence spectra of the pyrene-labeled single stranded acpcPNA and its hybrid with DNA are quite different. The ratio of emissions at 380 and 460 nm changed significantly (up to a factor of 7) upon hybrid formation with complementary DNA.

© 2012 Elsevier Ltd. All rights reserved.

1. Introduction

Polycyclic aromatic hydrocarbons, such as pyrene can behave as a universal base¹ in DNA that can 'pair' against all four natural nucleobases (i.e., adenine, cytosine, guanine, and thymine) without specific preference due to the lack of hydrogen bonding.^{2,3} When incorporated into peptide nucleic acid (PNA), an electrostatically neutral analogue of DNA with a peptide-like backbone, pyrene could also behave as a fluorescent universal base. 4,5 As the fluorescence properties of pyrene are very sensitive to its microenvironment, pyrene-modified DNA and PNA are potentially useful as fluorescence probes for DNA or RNA hybridization. 6 Our interest has long been focused on a conformationally restricted pyrrolidinyl alternating D-proline/2-amino-cyclopentanecarboxylic acid backbone (acpcPNA).^{7,8} We have demonstrated some unusual properties of this acpcPNA system⁹ and have reported interesting DNA-hybridization-responsive fluorescence properties of pyrene-containing acpcPNA. 10,11

In recent years, the copper(I)-catalyzed Huisgen azide—alkyne cycloaddition (CuAAC) reaction to give 1,4-disubstituted-1,2,3-triazole derivatives (known as 'click chemistry') has become one of the most useful tools in biomolecular research. $^{12-15}$ While it has

Scheme 1. Structure of acpcPNA with clicked pyrene (Tz^{Py}) as an artificial nucleobase.

a Organic Synthesis Research Unit, Department of Chemistry, Faculty of Science, Chulalongkorn University, Phayathai Road, Patumwan, Bangkok 10330, Thailand

b Department of Chemistry and Center for Innovation in Chemistry, Faculty of Science, Khon Kaen University, Khon Kaen 40002, Thailand

been extensively used for conjugation of DNA with various molecules, such as dyes and other reporter groups as well as for making DNA with modified backbones ^{16,17} and nucleobases, ^{18–22} the application of click chemistry in PNA research is relatively underexplored. ²³ The majority of click reactions involving PNA is usually performed via terminally azide or alkyne-labeled PNA, ^{24,25} although examples of internal labeling are known. ²⁶ In this work, we have developed methods based on click chemistry to incorporate polycyclic aromatic hydrocarbons, such as pyrene as a substitute for canonical nucleobases in acpcPNA (Scheme 1). In addition, we also investigated the ability of the clicked pyrene to behave as a fluorescent universal nucleobase and have modeled the system by molecular dynamics (MD) simulations.

^{*} Corresponding author. Tel.: +66 2 2187627x101; fax: +66 2 2187598; e-mail address: vtiravut@chula.ac.th (T. Vilaivan).

2. Results and discussions

2.1. Synthesis of TzPy and azide building blocks

In the first method, we decided to start with the pre-clicked pyrene (Tz^{Py}) monomer to be incorporated into acpcPNA by solid phase peptide synthesis. The Fmoc-protected acpcPNA monomer (4) was synthesized as outlined in Scheme 2. The synthesis started from the known intermediate **1**, which was obtained in four steps from *trans*-4-hydroxy-L-proline.²⁷ Nucleophilic substitution with sodium azide afforded the intermediate **2** in 95% yield. The Tz^{Py} chromophore was formed by clicking 1-ethynylpyrene to the azide 2 in the presence of CuI as a catalyst in 57% yield. Subsequent cleavage of the protecting groups followed by Fmoc protection and C-protecting group removal gave the desired clicked pyrene acpcPNA monomer (4) in 68% yield over three steps from 3. In the second method, we wished to explore the possibility of performing the click reaction after the acpcPNA synthesis but prior to the cleavage from the solid support ('post-synthetic click reaction'), hence the Fmoc-protected azide-substituted amino acid $(5)^{28}$ was also synthesized from 2.

carrying a cytosine base (C) and an azide group (N₃) in place of the Tz^{Py} , respectively, were also synthesized by the same protocol to be used as controls (**PNA2**: m/z calcd 4621.0; found 4621.9; **PNA3**: m/z calcd 4552.9; found 4554.4).

2.3. Thermal stabilities of pyrene-containing acpcPNA—DNA hybrids

The hybridization properties of **PNA1** bearing the triazole-linked pyrene (X=Tz^{Py}) at the middle position with oligodeoxynucleotides were investigated by thermal denaturation experiments (Table 1). The complementary DNA targets containing one of the four natural nucleobases opposite to the pyrene in **PNA1** were chosen to test the ability of pyrene to behave as a universal base. The absorbance at 260 nm versus temperature plots showed sigmoidal curves in all cases, which indicated co-operative dissociation of the base pairs similar to the unmodified acpcPNA. The $T_{\rm m}$ values revealed that each of the four nucleobases in the DNA strand can pair equally well to the pyrene in the PNA strand. The $T_{\rm m}$ values range from 68.1 °C (vs dT in **DNA4**) to 69.8 °C (vs dG in **DNA1**), with a $\Delta T_{\rm m}$ of 1.8 °C (Table 1, entries 1–4). On the other hand, the un-

DpmO
$$\stackrel{\bullet}{N}$$
 $\stackrel{\bullet}{N}$ $\stackrel{\bullet}{N}$

Scheme 2. Reagents and conditions: (a) NaN₃ 1.1 equiv, anhydrous K_2CO_3 1.2 equiv, dry DMF, 2–3 h, 70 °C under N_2 , 95%; (b) i. TFA in anisole, 2 h, rt, ii. FmocOSu 0.9 equiv, NaHCO₃ 2.5 equiv, CH₃CN/H₂O=1:1, overnight, rt, quantitative; (c) 1-ethynylpyrene, Cul (15 mol %), DIEA 2 equiv, CH₃CN, 12 h, 80 °C, 57%; (d) i. p-TsOH 3.2 equiv in CH₃CN, 3 h, rt, ii. FmocCl 1.3 equiv, DIEA 3.8 equiv, rt, 85%, iii. TFA/CH₂Cl₂=1:1 in anisole, 15 min, rt, 68%.

2.2. Solid-phase synthesis of pyrene-containing acpcPNA via a pre-formed clicked pyrene monomer

Starting from standard acpcPNA building blocks, together with the clicked pyrene monomer (4), the PNA1 with a sequence of Bz-GCATTATz^{Py}AGATAC-LysNH₂ was successfully synthesized on a Tentagel resin equipped with a Rink amide linker employing a standard Fmoc-solid phase strategy previously developed in our laboratory.²⁹ The monomer 4 was incorporated using 2-(1H-7-azabenzotriazol-1-yl)-1,1,3,3-tetramethyluronium hexafluorophosphate (HATU) as an activator during the coupling step. The successful synthesis of the PNA1 was confirmed by MALDI-TOF mass spectrometry (m/z calcd 4779.2; found 4782.3). The coupling efficiency per step was generally >95% as determined by spectrophotometry during the solid-phase synthesis. The low isolated yield (3.5%) was comparable to unlabeled PNA and was attributed to the loss during the HPLC purification step. The PNA2 and PNA3,

Table 1 $T_{\rm m}$ data of **PNA1**, **PNA2**, and **PNA3** (*N*-GCATTAXAGATAC-C) and their hybrids with **DNA1-4** (5'-GTATCTYTAATGC-3')

Entry	PNA	X	DNA	Y	$T_{\rm m}~(^{\circ}{\rm C})^{\rm a}$	$\Delta G_{\mathrm{binding}}$ (kcal/mol) ^b
1	PNA1	Tz ^{Py}	DNA1	G	69.8	-90.8
2		Tz^{Py}	DNA2	Α	69.0	-88.9
3		Tz^{Py}	DNA3	C	68.9	-87.7
4		Tz^{Py}	DNA4	T	68.1	-85.2
5	PNA2	C	DNA1	G	85.0	-94.0
6		C	DNA2	Α	72.0	-86.1
7		C	DNA3	C	69.0	-75.0
8		C	DNA4	T	65.7	-79.3
9	PNA3	N_3	DNA4	T	61.2	_

Conditions: 2.5 μM PNA, 3.0 μM DNA, 10 mM sodium phosphate buffer pH 7.0.
 Derived from 10 ns MD trajectories using MM—GBSA method and larger negative value indicates the higher thermodynamic stability.

modified PNA2 with a cytosine instead of the triazole-linked pyrene showed a strong preference for pairing with dG in the opposite DNA strand (**DNA1**) as shown by a high $T_{\rm m}$ of 85.0 °C (Table 1, entry 5). The three other mismatched hybrids between PNA2 and **DNA2**-**DNA4** showed a significant decrease in the $T_{\rm m}$ values by 13.0−19.3 °C, with the pC·dC pair being the most destabilized (Table 1, entries 6–8). The $T_{\rm m}$ of the mismatched hybrids of **PNA2** are in the same range as those of **PNA1** hybrids, although the $T_{\rm m}$ range is much smaller for the latter, indicating that the $Tz^{\rm Py}$ acpcPNA could form stable duplexes with little discrimination between the four natural DNA bases. To confirm the active role of the Tz^{Py} in pairing with the opposite base in the DNA strand, the $T_{\rm m}$ of the **PNA3** · **DNA4** duplex was also determined. The $T_{\rm m}$ value of only 61.2 °C for this 'abasic' PNA·DNA duplex compared to the $T_{\rm m}$ of 68.1 °C ($\Delta T_{\rm m}$ =6.9 °C) of the **PNA1 · DNA4** duplex suggested that the $\pi - \pi$ stacking provided by the triazole-linked pyrene is contributing to the duplex stabilities (Table 1, entries 4 and 9). In the case of **PNA2** · **DNA4** duplex, although the two opposite mismatched bases cannot form the Watson-Crick hydrogen bonding, there is still considerable stabilization of the duplex compared to that of the **PNA3** · **DNA4** duplex, which could also be explained by the presence of similar π – π stacking interactions.

2.4. Molecular dynamics simulations of pyrene-containing acpcPNA—DNA hybrids

To get further insight in the possible mode of pairing of the pyrenetriazole base in acpcPNA, molecular dynamics (MD) simulations were performed on various hybrids of **PNA1** and compared with **PNA2**. The $\Delta G_{\rm binding}$ values calculated from the MD trajectories using MM–GBSA approach^{30–32} are in good agreement with the thermal stabilities obtained experimentally (Table 1). The $\Delta G_{\rm binding}$ range for the hybrids of **PNA1** with DNA is –85.2 to –90.8 kcal/mol while the corresponding figures of **PNA2** were –75.0 to –86.1 kcal/mol (mismatched hybrids) and –94.0 kcal/mol (complementary hybrid). The model of **PNA1 DNA1** hybrid suggests that the pyrene is not directly interacting with the opposite nucleobase in the complementary DNA strand, but rather pointing out to the major groove (Fig. 1a) probably due to the bulkiness of the pyrene ring that does not allow effective pairing with the nucleobase despite the possibilities of obtaining further stabilization due to π – π

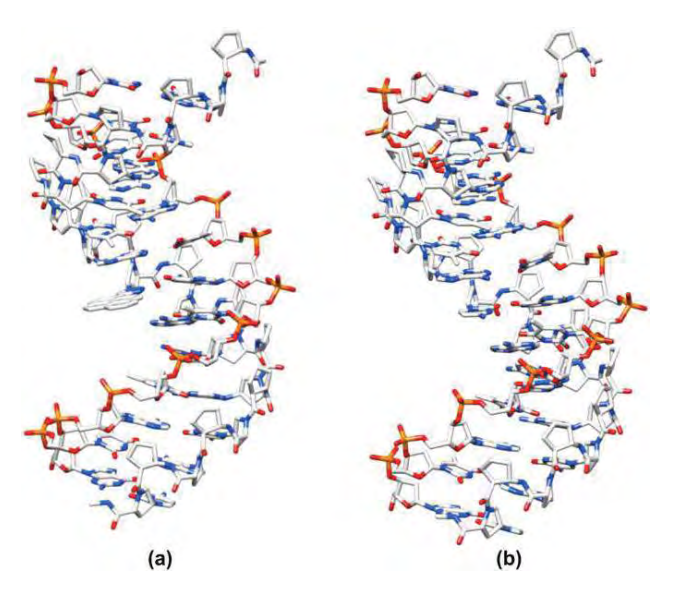


Fig. 1. Energy minimized structures of (a) **PNA1 · DNA1** (pTz^{Py}-dG) and (b) **PNA2 · DNA1** (pC-dG) duplexes.

stacking. The MD structures also show additional hydrogen bonding between the triazole part and the opposite nucleobase and a stacking interaction of the pyrene part with the adjacent base A in the same PNA strand. The triazole can form up to two hydrogen bonds with base G, and form one bond with other bases (Fig. S12). The hydrogen bond distance between the acceptor (nitrogen atom of triazole) and donor (nitrogen atom of the opposite G, A, C, and T bases) averaged over 10,000 structures of each MD trajectory were 3.32 ± 0.29 , 3.23 ± 0.25 , 3.30 ± 0.30 , and 4.58 ± 0.69 Å, respectively. Note that the criterion of hydrogen bond distance is within 3.5 Å. For PNA1 DNA4 hybrid, although some simulated structures of 10 ns MD trajectory (for example, the snapshot shown in Fig. S12) exhibit the hydrogen bond interaction between triazole and thymine, the average distance of 4.58 Å implies that the hydrogen bond strength is lower compared with those of others, which could explain the lower stability of PNA1 DNA4 system. Similarly, the two hydrogen bonds of Tz^{Py}-G in the duplex **PNA1** · **DNA1** may account for its higher stability than PNA1 DNA2 and PNA1 DNA3 duplexes, even though the average hydrogen bond distances of these two duplexes are slightly shorter. Generally, however, according to $\Delta G_{\text{binding}}$ values listed in Table 1, one can say that the stabilities of pyrene-triazole binding to nucleobases are not significantly different. The overall conformation of the Tz^{Py}-containing PNA1 DNA1 hybrid is similar to the normal duplex PNA2 DNA1 (Fig. 1b). The MD simulation thus clearly explains the role of the Tz^{Py} as a universal base in acpcPNA.

2.5. Optical properties of Tz^Py -containing acpcPNA DNA hybrids

It is expected that the environments of the pyrene chromophore in the single-stranded PNA should be quite different from that of its hybrid with DNA. One related study on Nielsen's type aegPNA⁴ with pyrene as an artificial nucleobase showed that the fluorescence emission of the pyrene is quenched (up to fivefolds) upon hybridization to its complementary DNA and RNA targets, which was explained by stacking of the pyrene unit within the PNA·DNA or PNA·RNA duplexes. Having demonstrated that the Tz^{Py} could behave as a universal base in acpcPNA, it would be interesting to study how the optical properties of the Tz^{Py} acpcPNA change in response to the hybridization event.

Absorption spectra of the single-stranded PNA1 showed a broad, unstructured pyrene peak with λ_{max} of ca. 350 nm due to the electronic coupling between the pyrene and the conjugated triazole (Fig. 2a). Upon excitation at 350 nm, the PNA1 displayed an emission spectrum showing both the pyrene monomer or locally excited state (LE) bands at λ_{max} =390, 410, and 435 nm, as well as another band that appeared as a weaker, broad shoulder around 460 nm (Fig. 2b). The latter emission band could be attributed to exciplex³³ or intramolecular charge transfer (ICT) species^{34,35} that are typically observed in non-polar solvents. We propose that the hydrophobic TzPy base in the single stranded acpcPNA is not free but associates with other nucleobases to avoid direct contact with water. This process is facilitated in single-stranded PNA due to the possibilities of folding of the PNA backbone into a compact structure.³⁶ Such folding is obviously unlikely in the much more rigid PNA-DNA duplex.

Interestingly, when the **PNA1** was hybridized with either of the complementary **DNA1**—**DNA4**, the absorption as well as the fluorescence spectra of the hybrid changed dramatically compared to the single-stranded PNA. The absorption spectra of the hybrids showed a splitting of the pyrene absorption band into two peaks of equal intensities at 354 and 368 nm. The bathochromic shift of the pyrene absorption indicated the presence of stacking interactions between the pyrene and the nucleobase, which is consistent with the MD simulation results. In addition, the CD spectrum of the

W. Mansawat et al. / Tetrahedron 68 (2012) 3988-3995

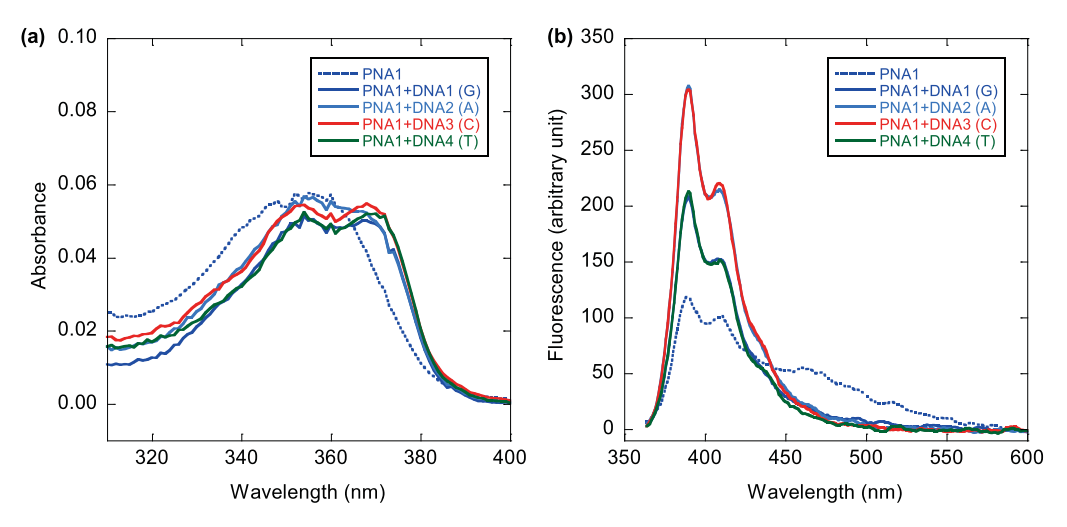


Fig. 2. Absorption (a) and fluorescence spectra (b) of **PNA1** and its hybrids with **DNA1–DNA4** (conditions: 2.5 μM PNA, 3.0 μM DNA in 10 mM sodium phosphate buffer pH=7.0, λ_{excit} =350 nm).

PNA1 DNA2 hybrid showed a weak, but definite, signal in the pyrene absorption region (Fig. 3), confirming the presence of interaction between the pyrene and the nucleobase. In the fluorescence spectra, the exciplex emission disappeared upon hybridization, with a concomitant increase of the monomer emission at 390 nm (1.8-2.6-folds). The increase of the monomer emission could be ascribed to the change of the environment of the pyrene to a more hydrophilic one upon hybridization as shown by the location of the pyrene moiety in the major groove, with only one face stacking to the adjacent A base in the N-terminal direction (Fig. 1a). Although the change of emission spectra at a single wavelength is relatively small, the ratio of the monomer (390 nm) to exciplex (460 nm) emissions changed quite significantly from 2.1 in single-stranded PNA1 to between 9.4 and 15.0 in its DNA hybrids, which translated to the response change from 4.4 to 7.0-fold (Table 2). Compared to conventional PNA with pyrene as a universal base, ⁴

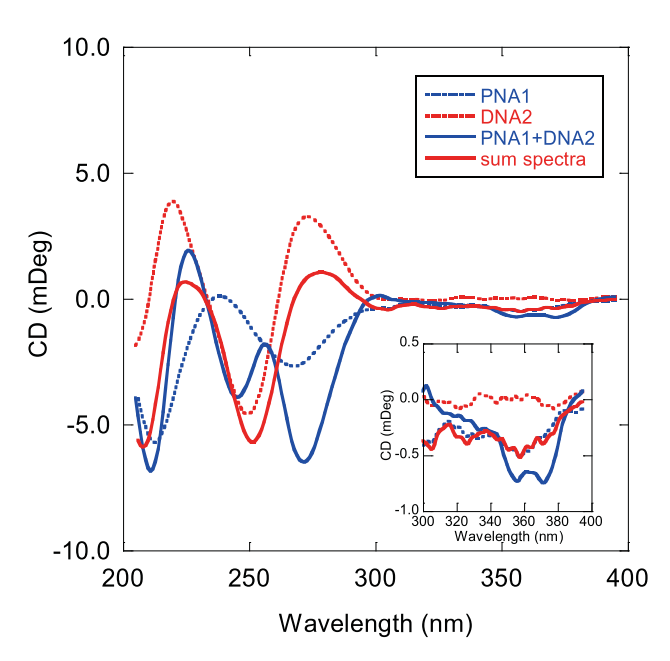


Fig. 3. CD spectra of PNA1 and its hybrid with DNA2 (conditions: 2.5 μM PNA, 3.0 μM DNA in 10 mM sodium phosphate buffer pH 7.0).

Table 2 Fluorescence data of **PNA1** (*N*-GCATTATz^{Py}AGATAC-*C*) and their hybrids with **DNA1**—**DNA4** (5'-GTATCTYTAATGC-3')

Entry	Y in DNA	I_{390}/I_{460}	$I_{390}/I_{390(ss)}$	$I_{460}/I_{460(ss)}$	$(I_{390}/I_{460})/(I_{390}/I_{460})_{\rm ss}$
1	ssPNA	2.1	1.0	1.0	1.0
2	G	9.4	1.8	0.40	4.4
3	Α	13.0	2.6	0.43	6.1
4	C	15.0	2.6	0.37	7.0
5	T	14.5	1.8	0.27	6.8

the present system of Tz^{Py}-modified acpcPNA behaves quite differently, and in a more advantageous way because the change in the fluorescence response can be monitored in a ratiometric fashion rather than at a single wavelength. The large difference between the monomer and exciplex emission (390 vs 460 nm) also means that not only the intensity, but also the color of the fluorescence change upon hybridization with DNA. Indeed, the fluorescence color change from green-blue to blue could even be observed by naked eyes under black light illumination (Fig. S11). Hence, the Tz^{Py} unit can behave as fluorescence universal artificial base in acpcPNA that exhibits fluorescence change upon pairing with all four natural nucleobases.

2.6. Synthesis of pyrene- and other aromatic-hydrocarbon-containing acpcPNA by post-synthetic click reactions on solid support

Although the synthesis and incorporation of the pyrenyl-triazole monomer into acpcPNA were straightforward, it would be highly desirable to develop a general strategy to perform a click reaction at a later stage of the PNA synthesis. This post-synthetic click reaction would allow attachment of a diverse set of chromophores on the same azide-containing acpcPNA intermediate, such as **PNA3** without having to synthesize all the monomers and oligomers separately. To explore this new strategy, the resinsupported and fully-protected azide **PNA3** was treated with 1-ethynylpyrene in the presence of Cu(I)—TBTA³⁸ complex in DMSO/^tBuOH/H₂O (3:1:1) (Scheme 3).³⁹ This solvent mixture was compatible with the solid support used in the PNA synthesis (Tentagel[®]), allowing efficient swelling to permit quantitative click reaction. The completeness of the reaction was monitored by HPLC (Fig. S9) and MALDI-TOF mass spectrometry (Fig. 4). In both

W. Mansawat et al. / Tetrahedron 68 (2012) 3988-3995

(synthesized from monomer 5)

$$Ar = \begin{bmatrix} Cu(I) - TBTA \\ Na ascorbate \end{bmatrix}$$

$$Ar = \begin{bmatrix} Tz^{Ph} \\ Tz^{Py} \end{bmatrix}$$

$$Tz^{An}$$

Scheme 3. Synthesis of aromatic-hydrocarbon-clicked acpcPNA via post-synthetic click reactions.

analyses, the signals due to the **PNA3** (t_R =53.0 min, m/z 4555.4) were completely absent with concomitant appearance of the new signal of the **PNA1** (t_R =62.1 min, m/z 4780.8) after a single click reaction performed overnight. The mass increase of 225.4 amu after the click reaction indicated a successful incorporation of the ethynylpyrene unit (MW 226.3). The **PNA1** prepared by this post-synthetic strategy is identical in all respects to the **PNA1** synthesized through the pre-formed monomer **4**. In addition, pyrene as well as other aromatic hydrocarbons including benzene and anthracene were successfully attached to another azide-containing PNA **PNA4** (GCATTT**N**₃TGATAC) via their ethynyl derivatives using the same strategy to afford **PNA5**, **PNA6**, and **PNA7**, which were labeled by pyrene-1-yl, phenyl and anthracene-9-yl triazoles, respectively (Table 3, Figs. S6—S8). While the single stranded Tz^{Ph}

PNA6 as well as its DNA hybrid is practically non-fluorescent, the Tz^{An} **PNA7** showed a weak emission at 420 nm in single stranded form, which increased only slightly upon hybridization with DNA. On the other hand, the characteristic switch between monomer/exciplex was observed in the Tz^{Py} **PNA5** and its DNA hybrid (Fig. S13), indicating the general fluorescence properties of the Tz^{Py} base irrespective of the identity of flanking bases (A/A in **PNA1** and T/T in **PNA5**).

3. Conclusion

In conclusion we had demonstrated that pyrene could be successfully incorporated into acpcPNA as a base surrogate via a triazole linker using 'click' chemistry via a pre-formed pyrene-labeled

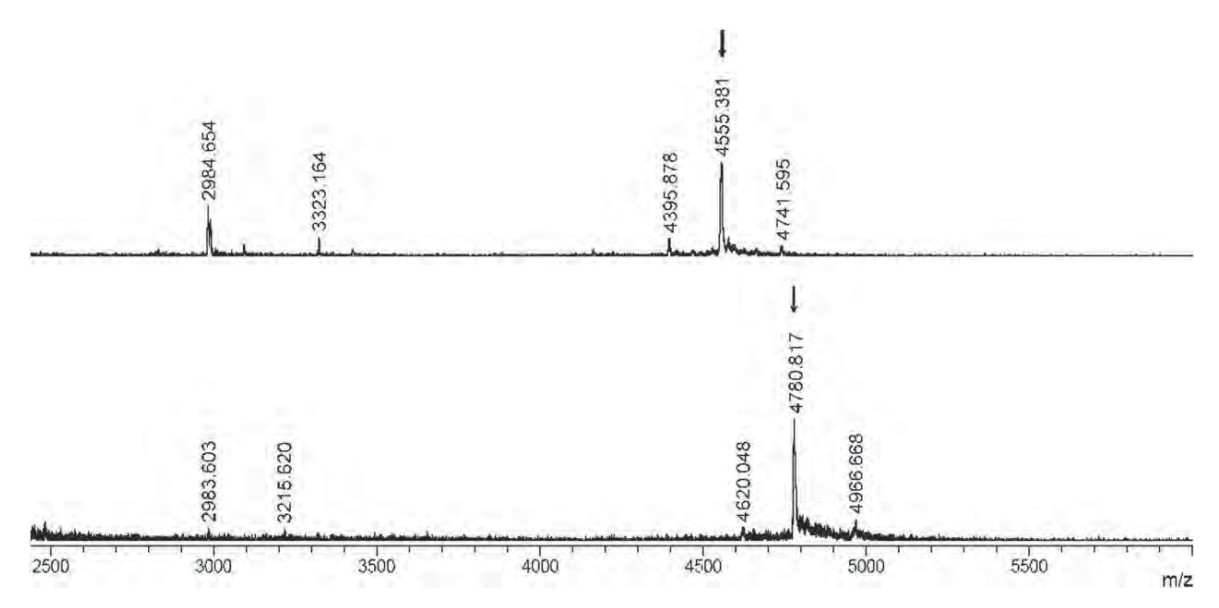


Fig. 4. MALDI-TOF mass spectra of crude PNA3 (Bz-GCATTAN₃AGATAC-LysNH₂) before (top) and after (bottom) the on-solid-support click reaction with 1-ethynylpyrene (MW 226.3). The peaks of interest are indicated by an arrow.

Table 3Characterization data of the clicked acpcPNA synthesized via post-synthetic click reaction

Entry	PNA	Sequence $(N \rightarrow C)^a$ GCATTY X YGATAC	m/z (calcd) ^b	m/z (found) ^c	Isolated yield ^d (%)
1	PNA1	X=Tz ^{Py} ; Y=A	4779.2	4779.4	4.4 (3.5)
2	PNA5	$X=Tz^{Py}$; $Y=T$	4761.2	4762.8	5.1
3	PNA6	$X=Tz^{Ph}$; $Y=T$	4637.0	4638.2	2.1
4	PNA7	$X=Tz^{An}\cdot Y=T$	4737.1	4738.2	2.8

- ^a All sequences were N-terminal benzoylated, C-terminal L-lysinamide capped.
- b Average mass calculated for [M+H+].
- ^c MALDI-TOF, CCA matrix, linear mode.
- ^d The yield in parentheses was obtained from the pre-formed monomer strategy.

monomer or by post-synthetic modification of azide-containing acpcPNA with 1-ethynylpyrene. The latter protocol allows attaching of pyrene, as well as other aromatic hydrocarbons including anthracene and benzene, to the same common azide-modified acpcPNA intermediate without the need for synthesizing each monomer separately. In addition, the click reaction protocol was conveniently carried out on the solid support, which allowed facile purification of the modified PNA from the excess reagents. Thermal denaturation experiments suggested that the pyrene-triazole unit can behave as a universal base in the acpcPNA system with little discrimination among the four canonical nucleobases. Molecular dynamics simulations suggested that the triazole can form weak hydrogen bonds with all nucleobases and that the pyrene was pointing away to the major groove rather than intercalating into the duplex. Furthermore, the fluorescence of the Tz^{Py} chromophore is sensitive to the hybridization state of the acpcPNA as shown by a significant increase of the pyrene monomer emission at 390 nm with concomitant decrease in the exciplex emission at 460 nm upon pairing with a complementary DNA carrying either A, T, C or G opposite to the pyrene.

4. Experimental section

4.1. General

Chemicals and solvents were purchased from standard suppliers and were used without further purification. RP-HPLC experiments were performed on a Water Delta $600^{\text{\tiny TM}}$ HPLC system. ^1H and ^{13}C NMR spectra were recorded on a Bruker Avance 400 NMR spectrometer operating at 400 MHz for ^1H and 100 MHz for ^{13}C . MALDI-TOF mass spectra were obtained on a Microflex MALDI-TOF mass spectrometry (Bruker Daltonics) using α -cyano-4-hydroxycinnamic acid (CCA) as the matrix. High resolution mass spectra were obtained on a Bruker Daltonics micrOTOF in positive ESI mode. IR spectra were recorded on Nicolet iS10 FT-IR spectrometer.

Oligonucleotides were obtained from Biodesign (Pathumthani, Thailand) and were used as received. The concentration of oligonucleotides and acpcPNAs was determined from the absorbance at 260 nm using the reported molar extinction coefficients at 260 nm (ϵ_{260}) for DNA monomers. The molar extinction coefficient of Tz^{Py} was obtained from the free monomer in methanol (2.84×10⁴ L mol⁻¹ cm⁻¹) was used for calculation of Tz^{Py}-containing acpcPNA. UV, fluorescence, and CD measurements were carried out in sodium phosphate buffer solution (10 mM, pH 7.0) using 10 mm quartz glass cuvettes. Absorption spectra and the melting temperatures (2.5 μ M PNA, 3.0 μ M DNA, 20–90 °C, 1.0 °C/min) were recorded on a Varian Cary 100 UV—vis spectrophotometer. CD spectra were measured on a Jasco-J815 spectropolarimeter and fluorescence spectra were measured on a Varian Eclipse spectrofluorimeter.

4.2. Synthesis

4.2.1. N-9-Fluorenylmethoxycarbonyl-(2'R,4'R)-[4-(pyren-1-yl)triazol-1-yl]-proline (4). A 50 mL round bottom flask was charged with compound 1 (0.55 g, 1 mmol), sodium azide (71.5 mg, 1.1 mmol), and anhydrous K₂CO₃ (0.17 g, 1.2 mmol) in 3 mL dry DMF. The slurry was heated at 70 °C with stirring under N_2 for 3 h. When the starting material was completely consumed (monitored by TLC), DMF was removed under reduced pressure. The reaction mixture was partitioned in dichloromethane/water and the dichloromethane layer was washed with water (three times). The organic layer was dried over Na₂SO₄ and concentrated in vacuo to get the azide intermediate **2** as a white solid (0.40 g, 95% yield); $\delta_{\rm H}$ (400 MHz; CDCl₃) 1.26 and 1.47 (9H, $2\times s$, CH₃ Boc rotamers), 2.16 and 2.20 [1H, $2 \times m$, $1 \times CH_2(3')$ rotamers], 2.37–2.52 [1H, $2 \times m$, $1 \times CH_2(3')$ rotamers], 3.43 and 3.52 [1H, $2 \times m$, $1 \times CH_2(5')$ rotamers], 3.67 and 3.76 [1H, $2 \times m$, $CH_2(2')$ rotamers], 4.15 [1H, m, CH(4')], 4.43 and 4.57 [1H, $2 \times m$, $1 \times CH(5')$ rotamers], 6.90 and 6.95 (1H, $2\times s$, CHPh₂ Dpm rotamers), 7.26–7.34 (10H, m, Ar CH Dpm). A mixture of 2 (0.40 g, 0.95 mmol), 1-ethynylpyrene (186 mg, 0.82 mmol), DIEA (0.35 mL, 2 mmol), and CuI (28.6 mg, 0.15 mmol, 15 mol %) were dissolved in CH₃CN (5 mL). The reaction mixture was heated at 80 °C under N₂ for 12 h (monitored by TLC). The solvent was removed and the residue was purified by column chromatography with EtOAc/hexanes (40:60) as eluent to obtain the Boc-protected intermediate 3 as a brown solid (0.31 g, 57% yield); δ_H (400 MHz; CDCl₃) 1.31 and 1.51 (9H, 2×s, CH₃ Boc rotamers), 2.53-2.72 [1H, m, $1 \times CH_2(3')$ rotamers], 3.05-3.17 [1H, m, $1 \times CH_2(3')$ rotamers], 3.99–4.15 [1H, m, $1 \times CH_2(5')$ rotamers], 4.28–4.37 [1H, m, $CH_2(2')$ rotamers], 4.61–4.76 [1H, $2 \times m$, $1 \times CH(5')$ rotamers], 5.41-5.50 [1H, m, CH(4')], 6.89 (1H, s, CHPh₂ Dpm), 7.07-7.30 (10H, m, Ar CH Dpm), 8.01-8.21 (9H, m, Ar CH Pyrene), 8.54 and 8.56 (1H, $2\times s$, CH Triazole rotamers). Compound **3** (0.27 g, 0.42 mmol) was then treated with p-TsOH (254 mg, 1.3 mmol, 3.2 equiv) in CH₃CN (5 mL) at room temperature. After 3 h, the Boc protecting group was completely removed (as monitored by TLC). DIEA (0.28 mL, 1.6 mmol, 3.8 equiv) was then added to the yellow slurry formed to give a brown solution followed by FmocCl (141 mg, 0.54 mmol). The reaction was stirred at room temperature until a brownish precipitate was observed (3 h). The solvent was removed and the residue was purified by column chromatography with EtOAC/hexanes (40:60) as eluent to receive a Fmoc-protected intermediate as a light yellow solid (0.27 g, 85% yield); $\delta_{\rm H}$ (400 MHz; CDCl₃) 2.55–2.78 [1H, m, $1 \times CH_2(3')$ rotamers], 2.97–3.17 [1H, m, $1 \times CH_2(3')$ rotamers], 3.90–4.77 [6H, m, $CH_2(5')$, CH(2'), Fmoc aliphatic CH and CH₂ rotamers], 5.24-5.44 [1H, m, CH(4')], 6.85 and 6.91 (1H, $2\times s$, $CHPh_2$ Dpm rotamers), 6.96–8.23 (27H, m, aromatic CH), 8.64 and 8.67 (1H, 2×s, CH Triazole rotamers). This intermediate (0.10 g, 0.13 mmol) was treated with 1:4:4 anisole/TFA/CH₂Cl₂ (2 mL) for 15 min at room temperature. After removal of the volatiles under a stream of N₂ gas, the residue was washed with Et2O to give the product 4 as a yellow solid (54.5 mg, 68% yield). The overall yield from $\mathbf{1}$ was 31%; R_f 0.22 (EtOAc/MeOH 9:1); ν_{max} (film) 3130, 3045, 2960, 2898, 1708, 1610, 1595, 1479, 1452, 1422, 1357, 1248, 1200, 1183, 1172, 1120, 1054 cm⁻¹; $[\alpha]_D^{24}$ -5.00 (*c* 0.50, MeOH); δ_H (400 MHz; DMSO- d_6) 2.74–2.92 [1H, m, $1 \times CH_2(3')$ rotamers], 3.05–3.21 [1H, m, $1 \times CH_2(3')$ rotamers], 4.09–4.16 [1H, m, $1 \times CH_2(5')$], 4.20–4.25 [1H, m, 1×CH₂(5')], 4.20–4.38 (3H, m, CH and CH₂ Fmoc), 4.44–4.48 and 4.61–4.65 [1H, $2 \times m$, CH(2') rotamers], 5.40–5.52 [1H, m, CH(4')], 7.32-7.38 (2H, m, Fmoc Ar CH), 7.40-7.46 (2H, m, Fmoc Ar CH), 7.68–7.75 (2H, m, Fmoc Ar CH), 7.91 (2H, d, I 7.6, Fmoc Ar CH), 8.12 (1H, t, J 7.6, pyrene CH), 8.25–8.40 (7H, m, pyrene CH), 8.90 (1H, d, J 9.7, pyrene CH), 8.94 (1H, s, triazole CH); $\delta_{\rm C}$ (100 MHz; DMSO- $d_{\rm 6}$) δ =34.5 and 35.5 [CH₂ (3') rotamers], 46.6 and 46.7 (CH Fmoc rotamers), 50.8 and 51.4 [CH₂(5') rotamers], 57.0 and 57.3 [CH(4')

rotamers], 57.7 and 57.8 [CH(2') rotamers], 67.0 and 67.3 [Fmoc CH₂ rotamers], 120.1 (Fmoc Ar CH), 123.8 (C), 123.9 (C), 124.3 (C), 125.0 (CH), 125.1 (CH), 125.1 (CH), 125.3 (Fmoc Ar CH), 126.5 (CH), 127.1 (CH), 127.2 (Fmoc Ar CH), 127.3 (CH), 127.7 (Fmoc Ar CH), 127.5 (C),128.0 (CH), 130.4 (C), 130.6(C), 130.9 (C), 140.7 (Fmoc Ar C), 143.6 (Fmoc Ar C), 146.3 (C), 153.8 (CO Fmoc), 172.3 and 172.8 (COOH rotamers); HRMS (ESI⁺) m/z: found 605.2218. C₃₈H₂₉O₄N₄ (M·H⁺) requires 605.2189.

4.2.2. Synthesis of PNA. All acpcPNA oligomers were synthesized manually from the corresponding Fmoc-protected acpcPNA monomers and β-amino acids spacers by Fmoc-solid phase peptide synthesis on a Tentagel resin equipped with an acid-labile Rink amide linker as described previously $(0.5-1.5 \mu mol scale)$. The acpcPNAs were end-capped by benzoylation. If required, the postsynthetic modification is carried out at this stage. After completion of the synthesis, the nucleobase side-chain was deprotected by treatment with 1:1 aq NH₃/dioxane at 60 °C overnight. After cleavage from the resin using 95% TFA (3×30 min), the PNA was precipitated using diethyl ether and purified by reverse-phase HPLC (C18 column 4.6×150 mm, 0.1% TFA in water/methanol gradient from 90:10 to 10:90 over 85 min with 5 min equilibration time). The purity was determined by MALDI-TOF mass spectrometry and by reverse-phase HPLC using the following conditions: C18 column 4.6×50 mm, particle size 3 μ ; mobile phase A=0.1% TFA in water; B=0.1% TFA in MeCN; gradient=10-90% B over 25 min with 5 min equilibration time at a flow rate of 0.5 mL/min.

4.2.3. Post-synthetic click reaction on-solid support. The reaction vessel for solid-phase synthesis was filled with resin-supported azide PNA (0.5 μmol). 1-Ethynylpyrene (150 μL, 50 mM), tris[(1-benzyl-1*H*-1,2,3-triazol-4-yl)methyl]amine (300 100 mM), tetrakis(acetonitrile)copper(I)-hexafluorophosphate (150 μL, 100 mM) (each in DMSO/tBuOH 3:1), and sodium-L-ascorbate $(150\,\mu\text{L},400\,\text{mM}\,\text{in}\,\text{H}_2\text{O})$ were added to the resin and the mixture was kept overnight at room temperature, with occasional agitation.³⁹ The completeness of the reaction was monitored by MALDI-TOF analysis of the sampled resin following TFA cleavage. After the starting azide PNA was completely consumed, the resin was washed with DMSO, H₂O, and MeOH (three times each) and dried under a stream of N₂ gas. Cleavage and purification was carried out as described above.

4.2.4. Molecular dynamics simulation. To get further information concerning the stability of duplexes in the molecular level, molecular dynamics (MD) simulations of PNA1·DNA and PNA2·DNA duplexes, in total eight systems, in aqueous conditions have been performed using AMBER 9 package.⁴¹ Since the three-dimensional structure of acpcPNA is not available, its starting structure was built up based on that of the DNA DNA duplex by one-to-one mapping of the PNA backbone atoms onto DNA backbone atoms. The coordinates of the missing atoms were added using geometric calculation. To improve the structure of this modified backbone, partial optimization was then performed using molecular mechanics calculations. The structure of pyrenyltriazole (Tz^{Py}) base was optimized with B3LYP/6-31G* calculation using Gaussian 09 program⁴² before inserting into the PNA backbone. The force field parameters of PNA and pyrenyltriazole were prepared within the standard procedure (for more details, see Ref. 32).

Each duplex was embedded into a rectangular box of water extended by 10 Å in each direction from the duplex and then neutralized by adding 12 Na⁺ counterions. We employed the force fields of FF03⁴³ complemented with the prepared parameters. The simulations were performed at the temperature of 300 K and pressure of 1 atm with the standard conditions described elsewhere.³² The unconstrained MD trajectories were generated for 10 ns and the snapshots were stored every 1 ps.

Binding free energy calculation: The binding free energy, $\Delta G_{\text{binding}}$, for a duplex can be calculated as

$$\Delta G_{\text{binding}} = G^{\text{duplex}} - G^{\text{strand1}} - G^{\text{strand2}}.$$
 (1)

Each free energy G^{x} was computed for the snapshots from the 10 ns MD trajectories, according to the following equation:

$$G^{x} = H_{\text{gas}}^{x} + H_{\text{trans/rot}}^{x} + G_{\text{solvation}}^{x} - TS^{x}$$
 (2)

where H_{gas} is the gas-phase energy calculated using the molecular mechanics (MM) method, and H_{trans/rot} corresponds to the energy due to six translational and rotational degrees of freedom, which is $6 \times 1/2RT$ and equals 1.79 kcal/mol at 300 K. $G_{\text{solvation}}$ is the solvation free energy estimated using a continuum approach based on the generalized Born/surface area (GB/SA) model developed by Onufriev et al.³⁰ The entropic term, TS, can be estimated by normal mode (NMODE) analysis⁴⁴ at 300 K. More details of the calculation and applied parameters have been described elsewhere. 31,32

Acknowledgements

Financial supports to this work come from the Thailand Research Fund (RTA5280002) (to T.V.), the Ratchadaphiseksomphot Endowment Fund from Chulalongkorn University (postdoctoral fellowship to W.M.), the Development and Promotion of Science and Technology Talents Project (DPST) (to C.B.), the Higher Education Research Promotion and National Research University Project of Thailand, Office of the Higher Education Commission, through the Advanced Functional Material Cluster of Khon Kaen University (to K.S.) and Advanced Organic Materials Cluster of Chulalongkorn University (AM1006A, to T.V.), and the Thai government stimulus package 2 (TKK2555, SP2) under the Project for Establishment of Comprehensive Center for Innovative Food, Health Products and Agriculture. The Center for Innovation in Chemistry (PERCH-CIC), and National Electronics and ComputerTechnology Center, National Science and Technology Development Agency (URL: http:// www.lsr.nectec.or.th) are acknowledged for providing computing resources. We also thank Prof. Polkit Sangvanich for obtaining HRMS spectra.

Supplementary data

Supplementary data associated with this article can be found in the online version, at doi:10.1016/j.tet.2012.03.062. These data include MOL files and InChiKeys of the most important compounds described in this article.

References and notes

- Loakes, D. Nucleic Acids Res. 2001, 29, 2437–2447.
 (a) Matray, T. J.; Kool, E. T. J. Am. Chem. Soc. 1998, 120, 6191–6192; (b) Schweitzer, B. A.; Kool, E. T. J. Am. Chem. Soc. 1995, 117, 1863–1872.
- Balakin, K. V.; Korshun, V. A.; Mikhalev, I. I.; Maleev, G. V.; Malakhov, A. D.; Prokhorenko, I. A.; Berlin, Y. A. *J. Biosens. Bioelectron.* **1998**, *13*, 771–778.
- Tedeschi, T.; Tonelli, A.; Sforza, S.; Corradini, R.; Marchelli, R. Artif. DNA PNA XNA **2010**, 1, 83-89.
- 5. MacKinnon, K. F.; Qualley, D. F.; Woski, S. A. Tetrahedron Lett. 2007, 48, 8074-8077.
- éstergaard, M. E.; Hrdlicka, P. J. Chem. Soc. Rev. 2011, 40, 5771-5788.
- Vilaivan, T.; Srisuwannaket, C. Org. Lett. 2006, 8, 1897-1900.
- Vilaivan, C.; Srisuwannaket, C.; Ananthanawat, C.; Suparpprom, C.; Kawakami, J.; Yamaguchi, Y.; Tanaka, Y.; Vilaivan, T. *Artif. DNA PNA XNA* **2011**, 2, 50–59.
- Taechalertpaisarn, J.; Sriwarom, P.; Boonlua, C.; Yotapan, N.; Vilaivan, C.; Vilaivan, T. *Tetrahedron Lett.* **2010**, *51*, 5822–5826. 10. Reenabthue, N.; Boonlua, C.; Vilaivan, C.; Vilaivan, T.; Suparpprom, C. *Bioorg*.
- Med. Chem. Lett. 2011, 21, 6465-6469.
- 11. Boonlua, C.; Vilaivan, C.; Wagenknecht, H.-A.; Vilaivan, T. Chem.—Asian. J. 2011, 6. 3251-3259.
- 12. Meldal, M.; Tornøe, C. W. Chem. Rev. 2008, 108, 2952-3015.
- Best, M. D. Biochemistry 2009, 48, 6571-6584
- 14. El-Sagheer, A. H.; Brown, T. Chem. Soc. Rev. 2010, 39, 1388-1405.

- 15. Gramlich, P. M. E.; Wirges, C. T.; Manetto, A.; Carell, T. Angew. Chem., Int. Ed. **2008**, 47, 8350-8358.
- Esobe, H.; Fujino, T.; Yamazaki, N.; Guillot-Nieckowski, M.; Nakamura, E. *Org. Lett.* **2008**, *10*, 3729–3732.
- 17. Nuzzi, A.; Massi, A.; Dondoni, A. QSAR Comb. Sci. 2007, 26, 1191–1199.
- Nakahara, M.; Kuboyama, T.; Izawa, A.; Hari, Y.; Imanishi, T.; Obika, S. *Bioorg. Med. Chem. Lett.* **2009**, *19*, 3316–3319.
- Spadafora, M.; Postupalenko, V. Y.; Shvadchak, V. V.; Klymchenko, A. S.; Mély, Y.; Burger, A.; Benhida, R. *Tetrahedron* **2009**, 65, 7809–7816. 20. Chittepu, P.; Sirivolu, V. R.; Seela, F. *Bioorg. Med. Chem.* **2008**, *16*, 8427–8439.
- Berndl, S.; Herzig, N.; Kele, P.; Lachmann, D.; Li, X.; Wolfbeis, O. S.; Wa-
- genknecht, H.-A. Bioconjugate Chem. 2009, 20, 558-564.
- éstergaard, M. E.; Guenther, D. C.; Kumar, P.; Baral, B.; Deobald, L.; Paszczynski, A. J.; Sharma, P. K.; Hrdlicka, P. J. Chem. Commun. 2010, 4929–4931.
- 23. Howarth, N. M.; Ricci, J. Tetrahedron 2011, 67, 9588-9594 and references cited
- 24. Gogoi, K.; Mane, M. V.; Kunte, S. S.; Kumar, V. A. Nucleic Acids Res. 2007, 35, e139.
- 25. Lim, S. Y.; Chung, W.-Y.; Lee, H. K.; Park, M. S.; Park, H. G. *Biochem. Biophys. Res. Commun.* **2008**, 376, 633–636.
- Gasser, G.; Hüsken, N.; Köster, S. D.; Metzler-Nolte, N. Chem. Commun. 2008, 26.
- Lowe, G.; Vilaivan, T. J. Chem. Soc., Perkin Trans. 1 1997, 547–554.
 Bonger, K. M.; Kapoerchan, V. V.; Grotenbreg, G. M.; van Koppen, C. J.; Timmers, C. M.; van der Marel, G. A.; Overkleeft, H. S. Org. Biomol. Chem. 2010, 8,
- Lowe, G.; Vilaivan, T. J. Chem. Soc., Perkin Trans. 1 1997, 555–560.
 Onufriev, A.; Bashford, D.; Case, D. A. J. Phys. Chem. B 2000, 104, 3712–3720.

- 31. Gohlke, H.; Case, D. A. J. Comput. Chem. 2004, 25, 238-250.
- 32. Siriwong, K.; Chuichay, P.; Saen-oon, S.; Suparpprom, C.; Vilaivan, T.; Hannongbua, S. *Biochem. Biophys. Res. Commun.* **2008**, 372, 765–771.
- van Daele, I.; Bomholt, N.; Filichev, V. V.; van Calenbergh, S.; Pedersen, E. B. ChemBioChem **2008**, 9, 791–801.
 Bag, S. S.; Kundu, R. *J. Org. Chem.* **2011**, 76, 3348–3356.
 Grabowski, Z. R.; Rotkiewicz, K.; Rettig, W. Chem. Rev. **2003**, 103, 3899–4031.

- Seitz, O. Angew. Chem., Int. Ed. 2000, 39, 3249-3252.
- Although the nucleobase side chain protection is probably not required during the click reaction, in view of potential instability of organic azides under high temperature conditions necessary for side-chain deprotection it is preferred to leave the protecting groups at this stage.
- Chan, T. R.; Hilgraf, R.; Sharpless, K. B.; Fokin, V. V. Org. Lett. **2004**, 6, 2853–2855.
- Beyer, C.; Wagenknecht, H.-A. Chem. Commun. 2010, 2230-2231.
- Egholm, M.; Nielsen, P. E.; Buchardt, O.; Berg, R. H. J. Am. Chem. Soc. 1992, 114, 9677–9678.
- Case, D. A.; Darden, T. A.; Cheatham, T. E., III; Simmerling, C. L.; Wang, J.; Duke, R. E.; Luo, R.; Merz, K. M.; Pearlman, D. A.; Crowley, M.; Walker, R. C.; Zhang, W.; Wang, B.; Hayik, S.; Roitberg, A.; Seabra, G.; Wong, K. F.; Paesani, F.; Wu, X.; Brozell, S.; Tsui, V.; Gohlke, H.; Yang, L.; Tan, C.; Mongan, J.; Hornak, V.; Cui, G.; Beroza, P.; Mathews, D. H.; Schafmeister, C.; Ross, W. S.; Kollman, P. A. AMBER 9; University of California: San Francisco, 2006.
 42. Gaussian 09, Revision B.01; Gaussian,: Wallingford, Connecticut, 2009.
 43. Duan, Y.; Wu, C.; Chowdhury, S.; Lee, M. C.; Xiong, G.; Zhang, W.; Yang, R.;
- Cieplak, P.; Luo, R.; Lee, T.; Caldwell, J.; Wang, J.; Kollman, P. J. Comput. Chem. **2003**, 24, 1999-2012.
- 44. Kottalam, J.; Case, D. A. Biopolymers 1990, 29, 1409-1421.



Contents lists available at SciVerse ScienceDirect

Biosensors and Bioelectronics

journal homepage: www.elsevier.com/locate/bios



Short communication

Label-free capacitive DNA sensor using immobilized pyrrolidinyl PNA probe: Effect of the length and terminating head group of the blocking thiols

Orawan Thipmanee ^{a,b,c}, Saluma Samanman ^{a,b,c}, Supannee Sankoh ^{a,b,c}, Apon Numnuam ^{a,b,c}, Warakorn Limbut ^{a,b,d}, Proespichaya Kanatharana ^{a,b,c}, Tirayut Vilaivan ^e, Panote Thavarungkul ^{a,b,f,*}

- ^a Trace Analysis and Biosensor Research Center, Prince of Songkla University, Hat Yai, Songkhla 90112, Thailand
- b Center of Excellence for Innovation in Chemistry, Faculty of Science, Prince of Songkla University, Hat Yai, Songkhla 90112, Thailand
- ^c Department of Chemistry, Faculty of Science, Prince of Songkla University, Hat Yai, Songkhla 90112, Thailand
- ^d Department of Applied Science, Faculty of Science, Prince of Songkla University, Hat Yai, Songkhla 90112, Thailand
- ^e Organic Synthesis Research Unit, Department of Chemistry, Faculty of Science, Chulalongkorn University, Bangkok 10330, Thailand
- f Department of Physics, Faculty of Science, Prince of Songkla University, Hat Yai, Songkhla 90112, Thailand

ARTICLE INFO

Article history: Received 8 June 2012 Accepted 13 June 2012 Available online 19 June 2012

Keywords:
Blocking thiol
acpcPNA
Self-assembled monolayer
Capacitance measurement
DNA sensor
Trace analysis

ABSTRACT

This paper reports, for the first time, the influence of the length and the terminating head group of blocking thiols on the sensitivity and specificity of a label-free capacitive DNA detection system using immobilized pyrrolidinyl peptide nucleic acid (acpcPNA) probes. A C-terminal lysine-modified acpcPNA was immobilized through four different alkanethiol self-assembled monolayers (SAMs), i.e., 3-mercaptopropionic acid (MPA), thioctic acid (TA), thiourea (TU) and mercaptosuccinic acid (MSA). The hybridization between the acpcPNA probes and the target DNA was directly measured using the capacitive system. Five blocking thiols of various lengths (C=3, 6, 8, 9 and 11), with the -OH terminating head group, i.e., 3-mercapto-1-propanol (3-MPL), 6-mercapto-1-hexanol (6-MHL), 8-mercapto-1-octanol (8-MOL), 9-mercapto-1-nonanol (9-MNL), 11-mercapto-1-undecanol (11-MUL) and another blocking thiol (C=11) with a $-CH_3$ terminating head group, and 1-dodecanethiol (1-DDT) were investigated. The blocking thiol with the same length as the total spacer of the immobilized acpcPNA gave the highest sensitivity and specificity with the -OH terminating head group providing a slightly better signal than the -CH₃ group. Under the optimized conditions, the immobilized acpcPNA probes provided a wide linear range for DNA detection $(1.0 \times 10^{-11} - 1.0 \times 10^{-8} \text{ M})$ with a very low detection limit in the picomolar range. The modified acpcPNA electrode could be reused through at least 58 cycles. The high sensitivity and very low detection limits are potentially useful for the analysis of ultratrace levels of DNA in samples. Preliminary studies were also performed to see the effect of probe concentration and target length.

 $\ensuremath{\text{@}}$ 2012 Elsevier B.V. All rights reserved.

1. Introduction

The development of sensors for specific DNA sequences has attracted a lot of attention due to their potential applications. A number of parameters can affect the sensitivity and specificity of the sensor, one of which is the way the probes were immobilized onto the transducer surface (Lucarelli et al., 2004, 2008; Tichoniuk et al., 2008). DNA probes can be immobilized onto a gold electrode sensor via a mixed binary monolayer of thiolated DNA and diluents (Wong et al., 2005). Alternatively the probes can be immobilized via a self-assembled monolayer (SAM) followed by the blocking of any free sensing surfaces using a thiol compound. The latter procedure has generally provided better DNA

E-mail address: panote.t@psu.ac.th (P. Thavarungkul).

hybridization than the first technique (Herne and Tarlov, 1997). This is because the blocking thiol can help to project the immobilized probes away from the electrode surface. This prevents nonspecific DNA-surface interactions and also helps the probes to be well packed onto the gold surface (Mannelli et al., 2005; Peeters et al., 2008). Both the length and the terminating head group of the blocking thiols have been reported to affect the hybridization and the discrimination efficiency of DNA sensors (Dharuman and Hahn, 2007, 2008; Degefa and Kwak, 2008; Dharuman et al., 2010).

Recently peptide nucleic acid (PNA) has gained considerable attention as a sensing probe. PNA is a DNA mimic in which the natural deoxyribose-phosphate backbone is replaced by a neutral pseudopeptide chain consisting of repeating *N*-(2-aminoethyl)-glycine units (aegPNA) linked by amide bonds (Nielsen, 2001). Pyrrolidinyl PNA with a conformationally rigid D-prolyl-2-aminocyclopentanecarboxylic acid (ACPC) backbone (acpcPNA) is a relatively new PNA system developed by our group (Suparpprom et al., 2005; Vilaivan and Srisuwannaket, 2006). Compared to DNA

^{*}Corresponding author at: Department of Physics, Faculty of Science, Prince of Songkla University, Hat Yai, Songkhla 90112, Thailand. Tel.: +66 7428 8753; fax: +66 74 55 8849.

and aegPNA, it provided a stronger binding affinity and better sequence specificity towards DNA.

The aim of this work was to develop a new platform for a DNA biosensor based on a combination of a highly sensitive, simple to operate and relatively inexpensive electrochemical capacitive transducer (Loyprasert et al., 2008; Numnuam et al., 2009; Wannapob et al., 2010; Samanman et al., 2011) and a acpcPNA probe. A simple protocol for immobilization between the acpcPNA probe and SAMs of four alkanethiols with various chain lengths is explored. This work also aimed to investigate the influence of the blocking thiols with various chain lengths and terminating head groups (–OH and –CH₃). Finally, the performances of the developed capacitive DNA sensor were studied. A preliminary study was also performed using different PNA probes and DNA targets with different sequence and lengths.

2. Experimental

2.1. Materials

The 9-mer lysine-modified acpcPNA (Ac-TTT TTT TTT-LysNH₂), PNA-T9 probe and the 12-mer mixed base lysine-modified acpcPNA (Bz-TGT CAA CTG ACT-LysNH₂), PNA-M12 probe, were synthesized by Mrs. Chotima Vilaivan at Chulalongkorn University, Thailand according to the published protocol (Vilaivan and Srisuwannaket, 2006).

Oligonucleotide target DNAs were purchased from the Bioservice Unit, National Science and Technology Development Agency and BioDesign Co., Ltd., Thailand. The sequences are mentioned below.

For the PNA-T9 probe Complementary DNA D6comp:5'-AAAAAA-3' D9comp:5'-AAAAAAAAA3' D12comp:5'-AAAAAAAAAAAAA3' D15comp:5'-AAAAAAAAAAAAAAAA3' D27comp:5'- AAAAAAAAAAAAAAAAAAAAAAAAAAAAAAA D27compM18a:5'-TTTTTTTTAAAAAAAAAATTTTTTTT-3' D27compM18b:5'-TGCTCAGCTAAAAAAAAAAATGCTCAGCT-3' Single mismatched DNA D9M1G:5'-AAAAGAAAA-3' D9M1C:5'-AAAACAAAA-3' D9M1T:5'-AAAATAAAA-3' Double mismatched DNA D9M2G:5'-AAAGAGAAA-3' D9M2C:5'-AAACACAAA-3' D9M2T:5'-AAATATAAA-3' Non-complementary DNA D9non-compa:5'-TTTTTTT-3' D9non-compb:5'-TATTATTAT-3' For the PNA-M12 probe Complementary DNA D9 comp: 5'-CAGTTGACA-3'D12comp:5'-AGTCAGTTGACA-3' D15compM3:5′-GCTAGTCAGTTGACA-3′ D30compM18:5'-GACTGCACCAGTCAGTTGACATGTTGCGAC-3' Single mismatched DNA D12M1T:5'-AGTCATTTGACA-3' D12M1C:5'-AGTCACTTGACA-3' D12M1A:5'-AGTCAATTGACA-3' Double mismatched DNA D12M2T:5'-AGTTATTTGACA-3'

D12M2CG:5'-AGTGACTTGACA-3'

D12M2A:5'-AGTAAATTGACA-3'

Non-complementary DNA D12non-comp:5'-TCAGTCAACTGT-3'

Five blocking thiols of various lengths (C=3, 6, 8, 9 and 11), with the –OH terminating head group, i.e., 3-mercapto-1-propanol (3-MPL), 6-mercapto-1-hexanol (6-MHL), 8-mercapto-1-octanol (8-MOL) and 9-mercapto-1-nonanol (9-MNL) were obtained from Aldrich (Milwaukee, USA) and 11-mercapto-1-undecanol (11-MUL) was from Aldrich (Steinheim, Germany). Another blocking thiol (C=11) with a different terminating head group (C+3), 1-dodecanethiol (1-DDT) from Aldrich (Milwaukee, USA) was also studied. Four alkanethiols, mercaptosuccinic acid (MSA, Fluka, Buchs, Switzerland), 3-mercaptopropionic acid (MPA, Aldrich, Steinheim, Germany), thioctic acid (TA, Aldrich, Milwaukee, USA) and thiourea (TU, Sigma, Saint Louis, USA) were used to prepare the SAM surface.

2.2. Immobilization of the acpcPNA

The PNA-T9 probe was used in the initial optimization as the model. The cleaned gold electrodes (diameter 3 mm, 99.99%) were immersed in 250 mM alkanethiol solutions of MSA (Shervedani and Hatefi-Mehrjardi, 2007), MPA and TA for 12 h and in TU for 24 h at room temperature (Limbut et al., 2006). The SAMs formed from MSA, MPA and TA were activated for amide bond formation with lysine acpcPNA using 0.05 M EDC/0.03 M NHS in phosphate buffer (pH 5.00) for 5 h. Glutaraldehyde was used to activate the amino group of TU for coupling to the acpcPNA probe. Then 20 μL of a 5.0 μM (Wittung-Stafshede et al., 2000; Hejazi et al., 2010) of the acpcPNA was placed on the SAMs for 24 h at 4 °C. The electrode with the SAM of TU was further treated with 1.0 mM ethanolamine pH 8.00 for 7 minutes to deactivate all the remaining aldehyde groups not coupled to the immobilized acpcPNA. Finally, all immobilized acpcPNA electrodes were immersed in 1.0 mM of the six blocking thiol solutions for 1 h.

A 12-mer mixed base sequence (PNA-M12) was also immobilized, under the optimal immobilization conditions and also with the best blocking thiol to represent a more realistic scenario in analyses of real DNA samples.

2.3. Capacitance measurement

The modified electrode was used as the working electrode in a flow injection system under the following operating conditions: 10 mM phosphate buffer pH 7.00 as the running buffer, sample volume 300 μL and flow rate $50~\mu L \, min^{-1}$. The capacitance was determined from the obtained current response when a potential step of 50 mV was applied to the working electrode as previously described (Limbut et al., 2006) (Supplementary data Fig. 1S). When DNA was injected into the flow system, it hybridized to the immobilized acpcPNA on the working electrode and the capacitance decreased. The capacitance change (ΔC) due to the PNA–DNA hybridization could then be determined. The regeneration solution, 300 μL of 50 mM NaOH (Ananthanawat et al., 2009b), was then applied to break the binding between the probe and the target DNA, ready for a new analytical cycle (Supplementary data Fig. 1S inset).

2.4. Sensitivity determination

To determine the influence of the chain length and the terminating head group of the blocking thiols, a calibration curve was first obtained by injecting 1.0×10^{-11} – 1.0×10^{-8} M (n=3) of complementary target DNA with a subsequent regeneration step.

The sensitivity, i.e. the slope of the plot between the capacitance changes (-nF cm $^{-2}$) versus the logarithm of concentration of the complementary target DNA (log M) (Supplementary data Fig. 1S inset), was used to indicate the efficiency of the hybridization of the target DNA and the immobilized acpcPNA probe. A higher sensitivity reflects a more efficient system.

2.5. Specificity determination

The % signal suppression (%SS) of the mismatched DNA response was calculated according to Eq.(1). A large %SS indicated a better specificity:

$$\%SS = \frac{\Delta c_{\text{complementary DNA}} - \Delta c_{\text{mismatched DNA}}}{\Delta c_{\text{complementry DNA}}} \times 100 \tag{1}$$

3. Results and discussion

3.1. Effect of the length of the blocking thiols

The effect of the chain length of the blocking thiols was evaluated in terms of the sensitivity of the capacitance change caused by the hybridization of the complementary DNA target to the immobilized PNA-T9 probe.

The PNA-T9 probe was immobilized using the SAM of four different alkanethiols, i.e., TA(6C), TU(1C+1N), MSA(2C or 3C) and MPA(3C) via an amide bond with the ε -NH $_2$ side chain of the C-terminal lysine residue. The spacer from these alkanethiols when combined with the lysine spacer of the immobilized acpcPNA (5C+1N) became 11C+1N, 11C+2N, 7C+1N or 8C+1N and 8C+1N, respectively (Fig. 1(a-d)). The effect of the six blocking thiols with different chain lengths, i.e., 3-MPL(3C), 6-MHL(6C), 8-MOL(8C), 9-MNL(9C), 11-MUL(11C) with their -OH terminating head group and 1-DDT(11C) with its -CH $_3$ terminating head group, were compared.

Fig. 2(a) shows the sensitivities of the MPA-acpcPNA electrode to the blocking thiols, the one with the same length as that of the total spacer, 9-MNL (9 atoms, 8C+1N), provided the highest sensitivity (20.4 ± 0.7 -nF cm⁻² (\log M)⁻¹). The blocking thiol with a shorter length, i.e., 3-MPL, 6-MHL and 8-MOL gave a lower sensitivity. This is also true for the blocking thiol with a longer length, i.e., 11-MUL and 1-DDT also gave lower sensitivities.

For the SAM of TA and TU with a total spacer length of 11C+1N and 11C+2N, respectively, the highest sensitivities of

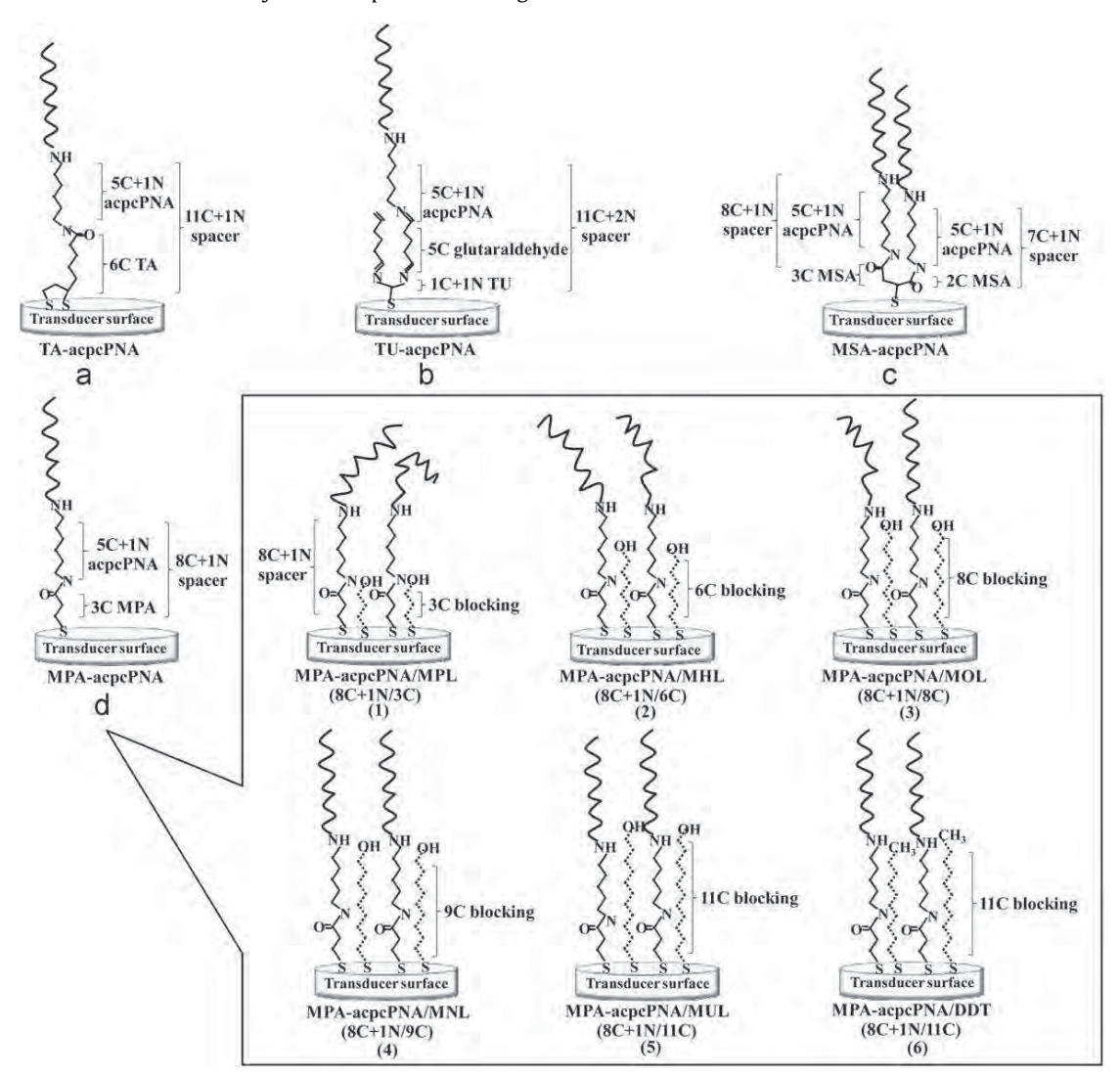


Fig. 1. The total spacer of the acpcPNA modified on four types of self-assembled monolayers (a) TA, (b) TU, (c) MSA and (d) MPA. Inset (d) schematic diagram of the six interfaces of the MPA immobilized acpcPNA electrode (total of 8C+1 N spacer) with different chain lengths of the blocking thiols, (d1) 3-MPL (3C), (d2) 6-MHL (6C), (d3) 8-MOL (8C), (d4) 9-MNL (9C), (d5) 11-MUL (11C) with the -OH terminating head group and (d6) 1-DDT (11C) with the -CH₃ terminating head group.

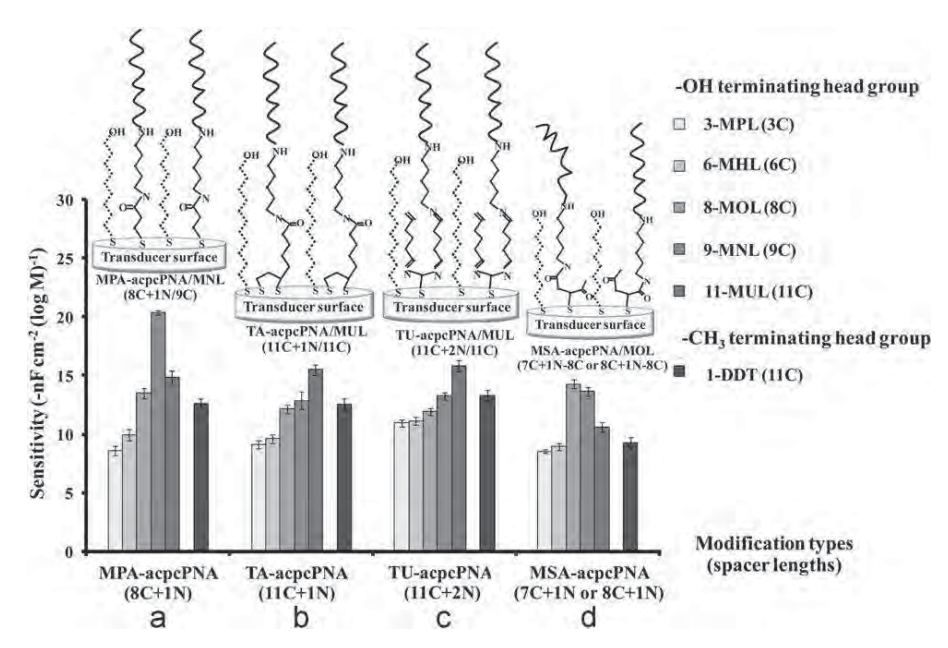


Fig. 2. Effect of the length and terminating head group of the blocking thiol on the sensitivity for the detection of the complementary target DNA.

 $15.5\pm0.5-nF\,cm^{-2}~(log\,M)^{-1}~for~TA~and~15.8\pm0.4-nF\,cm^{-2}~(log\,M)^{-1}~for~TU~were~obtained~using~the~longest~blocking~thiol~(11-MUL;~11C)~(Fig.~2(b)~and~(c)). Other blocking~thiols~with shorter chain length gave lower sensitivities. (Note: Longer blocking thiols (> 11C)~were~not~commercially~available.)$

In the case of MSA with a branched structure the total spacer of the immobilized acpcPNA is either 7C+1N or 8C+1N (Fig. 1(c)). The blocking thiols with the same length as the acpcPNA spacer (8-MOL or 9-MNL) showed the highest sensitivities of 14.3 ± 0.5 and 13.6 ± 0.3 -nF cm $^{-2}$ (log M) $^{-1}$, respectively (Fig. 2(d)). The two sensitivities were not much different since the immobilized acpcPNA probes could be attached on either the 7C+1N or 8C+1N spacer branches. Lower sensitivities were obtained from the use of blocking thiols with a shorter or longer length.

From the results it is clear that the blocking thiol with the same length as the total spacer of the immobilized acpcPNA showed the highest sensitivity. This is possibly because this length can help arrange the acpcPNA probes to be more readily available for hybridization. These results corresponded well with other reports, using various techniques to study the orientation of the probe, which showed that the use of blocking thiols or diluents helped to orient the probe to extend further into the solvent phase (Lee et al., 2006, 2007), making it more favorable for hybridization resulting in a maximum hybridization efficiency (Boozer et al., 2006; Gong et al., 2006; Su et al., 2005). For the blocking thiol with a shorter length than the total spacer, the end of the blocking thiol was further away from the acpcPNA probe. This could be explained by the probe not now being in an optimum position for access of the DNA target resulting in a lower sensitivity. For the blocking thiol with a longer chain length the lower sensitivity could be due to the overlapping of the blocking thiol with the base of the acpcPNA probes resulting in lower hybridization efficiency. The results are in line with the study made by Wong and coworkers on DNA-DNA hybridization (Wong et al., 2005).

3.2. Effect of the terminating head group

To test the effects of the terminating head groups, two blocking thiols with the same length were investigated, 11-MUL with an -OH terminating head group and 1-DDT with a -CH₃ terminating head group. The -OH terminating head group (with

the lone pair electron) consistently provided slightly better sensitivity than the –CH₃ terminating head group (without a lone pair electron) (Fig. 2(a–d)). This is possibly because of the more hydrophilic characteristic of the –OH terminating head group than the –CH₃ terminating head group (Dharuman and Hahn, 2007). This higher hydrophilicity will help the target DNA in an aqueous solution to move closer to the electrode surface (Gillmor et al., 2000), i.e., closer to the immobilized probe resulting in a more efficient hybridization. However, the effect is much less than the effect of the chain length of the blocking thiols.

3.3. Effect of PNA probe concentration

The amount of accessible immobilized probe is a major factor that would influence hybridization efficiency (Keighley et al., 2008; Liu et al., 2005). A preliminary study of the effect of concentration of the probe to be immobilized (3.0–7.0 μM) via the four SAMs, which should correlate with the amount of immobilized probe, was investigated. The sensitivity increased with concentration and leveled off at 5.0 μM (Supplementary data Fig. 2S). For all concentrations the blocking thiol with the same length as the total spacer of the immobilized PNA-T9 showed the highest sensitivity. The results indicated that a good sensor sensitively depends on both the probe concentration and the length of the blocking thiol.

3.4. Linear range and detection limit

The immobilized PNA-T9 probes $(5.0~\mu\text{M})$ using the blocking thiols that provided the highest sensitivities (Fig. 2) were tested i.e., MPA blocked with MNL, TA blocked with MUL, TU blocked with MUL and MSA blocked with MOL. The capacitance change was studied from 1.0×10^{-14} to 1.0×10^{-7} M of the target DNA. A linear relationship between the capacitance change and the logarithm of the target DNA was found between 1.0×10^{-11} and 1.0×10^{-8} M for all four systems and the detection limits (Buck and Lindner, 1994) of the four systems were between 6 and 10 pM (Supplementary data Table 1S). The proposed capacitive DNA sensor provided a much better detection limit than other methods such as QCM that gave a detection limit of 5 μ M and SPR that had a detection limit of 0.2 μ M studied by Ananthanawat

et al. (2009a,b) using a similar T9 acpcPNA probe. Therefore, this capacitive DNA sensor offers a promising alternative and more sensitive probe for the detection of ultra-trace levels of DNA.

3.5. Reusability

The reusability of the immobilized acpcPNA electrode was evaluated by repeatedly injecting the same concentration of complementary DNA ($1.0 \times 10^{-10}\,\mathrm{M}$) with a subsequent regeneration step. The electrodes modified with four SAMs with blocking solutions that provided the best sensitivities were tested. The reusability was evaluated in terms of the percentage of residual activity:

Residual activity (%) =
$$\frac{\Delta C_2}{\Delta C_1} \times 100$$
 (2)

where ΔC_1 and ΔC_2 were the capacitance change when the immobilized acpcPNA probe hybridized to the DNA target for the first time and after each regeneration, respectively (Supplementary data Fig. 1S inset). The electrodes could be reused for between 58 and 73 times with an average residual activity of \geq 98% (Supplementary data Table 1S). After the decrease of the response the electrode was tested (Supplementary data Fig. 3S(e)) and the cyclic voltammogram suggested that it is most likely caused by the loss of the SAM together with its attached acpcPNA from the gold electrode.

3.6. Reproducibility

The reproducibility of the responses of the PNA-T9 electrodes from two different preparations of MPA, TU and TA was tested by comparing the sensitivities. The sensitivities of the two electrodes were 20.4 ± 0.7 and $20.6\pm0.5-nF\,cm^{-2}~(log\,M)^{-1}$ for MPA; 15.8 ± 0.4 and $16.3\pm0.5-nF\,cm^{-2}~(log\,M)^{-1}$ for TU; 13.3 ± 0.5 and $13.5\pm0.4-nF\,cm^{-2}~(log\,M)^{-1}$ for TA. The sensitivities did not differ between each preparation, i.e., good reproducibility was obtained for different preparations.

3.7. Specificity

To investigate the specificity the PNA-T9 immobilized on MPA was employed because it provided the best sensitivity (Fig. 2(a)). Three blocking thiols with shorter length, the same length and longer length relative to the total spacer of the SAM modified PNA-T9 were also compared. The hybridization with the complementary target DNA, single and double base mismatched DNAs at 1.0×10^{-8} M were monitored. Fig. 3(a), (b), and (c) shows the results. The complementary DNA (D9comp) provided a much higher capacitance change compared to the single and double mismatched DNA target. The %SS obtained from the blocking thiol (9C) with the same length as the spacer (8C+1N) was the highest (76–79%) followed by the one with the next shorter length (8C) (70-74%) and the next longer length (11C) (68-69%). As expected, the %SS for the double mismatched target was higher than that for the single mismatched. Two different non-complementary DNAs were also tested (Fig. 3(b)) and gave the highest %SS of 99%.

PNA-M12 probe immobilized under optimal conditions obtained for the PNA-T9 probe, i.e. $5\,\mu\text{M}$ on MPA followed by blocking with MNL (the thiol with the same length as the spacer), was also investigated. In agreement with the results obtained

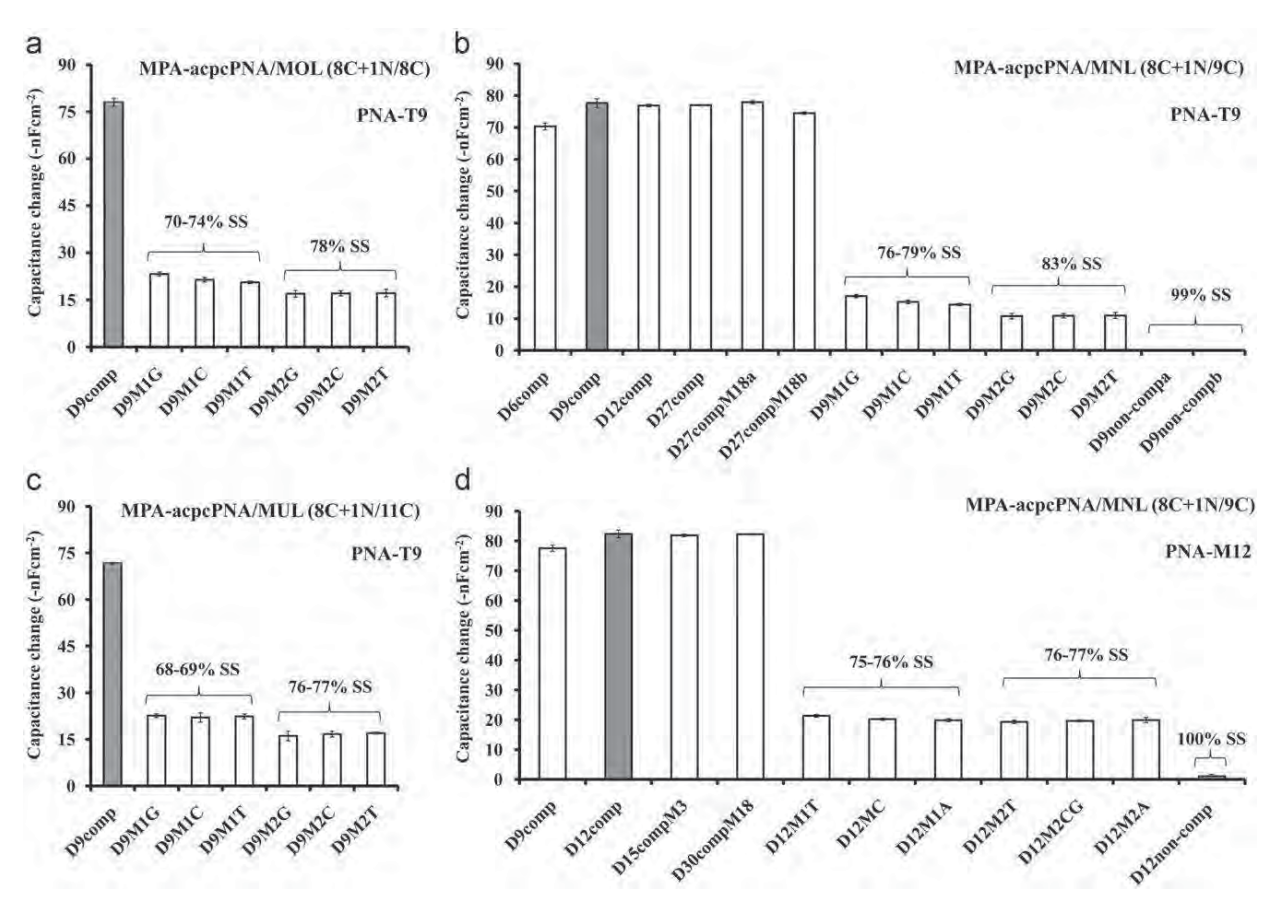


Fig. 3. The measured capacitance change (n=3) of the complementary, single, double mismatched and non-complementary target DNAs using immobilized acpcPNA probes (PNA-T9 and PNA-M12) on a MPA modified electrode (8C+1 N spacer) with different chain lengths of the blocking thiol, (a) 8-MOL (8C), (b) and (d) 9-MNL (9C), (c) 11-MUL (11C), tested at 1.0×10^{-8} M DNAs showing the %SS. Solid columns indicate the complementary target DNAs with the same length as the PNA probe.

with the 9-mer probe, good specificity was also obtained from this 12-mer mixed base probe, i.e., very high %SS for the single and double mismatched and a complete signal suppression for the non-complementary DNA (Fig. 3(d)).

3.8. Effect of target length

In the case of the complementary DNAs with different lengths, a shorter target length (D6comp for PNA-T9 and D9comp for PNA-M12) provided a lower capacitance signal than the fully complementary DNAs (D9comp for PNA-T9 and D12comp for PNA-M12) (Fig. 3(b) cf. 3(d)). This is because when the target DNA binds to the PNA probe, water and electrolyte molecules will be displaced by the DNA sample thereby giving a change in capacitance (Berggren et al., 1999). A longer duplex length caused a larger change since the water and electrolyte molecules were pushed further away from the electrode. It was of interest to observe that longer target DNAs gave a similar capacitance change to DNA with the same length as the probe. This implies that the overhanging unhybridized part of the DNA target, which is more flexible than the duplex, does not directly affect the performance of the biosensor, supporting the mechanism of capacitance change by water and electrolyte molecule displacement explained.

4. Conclusions

In this research, the effect of the length and terminating head group of the blocking thiol were studied using a highly sensitive capacitive system. The one with an equal length to the -OH terminating head group of the blocking thiol provided the highest sensitivity. The blocking thiol with an equal length also provided the highest %SS, so this also indicated the high binding specificity. These sensors based on acpcPNA probes provided very good performances such as they produced a linear concentration response over a wide linear range $(1.0 \times 10^{-11} - 1.0 \times 10^{-8} \text{ M})$, a very low detection limit (picomolar) and good reusability of at least 58 cycles. The high sensitivity and very low detection limits are potentially useful for the analysis of DNA at ultra-trace levels in samples. The hybridization response was also found to be correlated to the concentration of the probe to be immobilized and the length of the target DNAs. In this work, a probe concentration of 5.0 µM is sufficient to give maximum coverage of the sensor leading to the best response. As for the target length, there are correlations between the response and the length of the target that can form a duplex with the probe whereby a longer target length provided a larger response. No further increase in response was observed with targets carrying extra region that does not form hybrid with the probe. Further studies on this aspect would be useful.

Acknowledgements

The authors are grateful to Grants from the Thailand Research Fund (TRF, RTA528002); the Royal Golden Jubilee Ph.D-program (RGJ) supported by The Thailand Research Fund (3.C.PS/50/B.1 and 3.C.PS/51/B.1); the Office of the Higher Education Commission (CHE-SSR-Ph.D-THA); the Center of Excellence for Innovation in Chemistry (PERCH-CIC), the Office of the Higher Education Commission; the Higher Education Research Promotion and National Research University Project of Thailand, Office of the Higher Education

Commission; the Trace Analysis and Biosensor Research Center (TAB-RC), and Graduate School, Prince of Songkla University, Hat Yai, Thailand are all gratefully acknowledged. The authors thank Dr. Brian Hodgson, Prince of Songkla University, Hat Yai, Songkhla, Thailand for assistance with English.

Appendix A. Supporting information

Supplementary data associated with this article can be found in the online version at http://dx.doi.org/10.1016/j.bios.2012.06.021.

References

Ananthanawat, C., Vilaivan, T., Hoven, V.P., 2009a. Sensors and Actuators B:

Chemical 137, 215–221. Ananthanawat, C., Vilaivan, T., Mekboonsonglarp, W., Hoven, V.P., 2009b. Biosensors and Bioelectronics 24, 3544-3549.

Berggren, C., Stalhandske, P., Brundell, J., Johansson, G., 1999. Electroanalysis 11, 156-160.

Boozer, C., Chen, S., Jiang, S., 2006. Langmuir 22, 4694-4698.

Buck, R.P., Lindner, E., 1994. Pure and Applied Chemistry 66, 2527-2536.

Degefa, T.H., Kwak, J., 2008. Journal of Electroanalytical Chemistry 612, 37-41.

Dharuman, V., Hahn, J.H., 2007. Sensors and Actuators B: Chemical 127, 536-544. Dharuman, V., Hahn, J.H., 2008. Biosensors and Bioelectronics 23, 1250-1258.

Dharuman, V., Chang, B.Y., Park, S.M., HahnN, J.H., 2010. Biosensors and Bioelectronics 25, 2129-2134.
Gillmor, S.D., Thiel, T.C., Strother, T.C., Smith, L.M., Lagally, M.G., 2000. Langmuir

Gong, P., Lee, C.Y., Gamble, L.J., Castner, D.G., Grainger, D.W., 2006. Analytical

Chemistry 78, 3326-3334. Hejazi, M.S., Pournaghi-Azar, M.H., Ahour, F., 2010. Analytical Biochemistry 399,

Herne, T.M., Tarlov, M.J., 1997. Journal of the American Chemical Society 119,

8916-8920. Keighley, T.D., Estrela, P., Li, P., Migliorato, P., 2008. Biosensors and Bioelectronics

24, 906-911. Lee, C.Y., Gong, P., Harbers, G.M., Grainger, W.D., Castner, D.G., Gamble, L.J., 2006. Analytical Chemistry 78, 3326–3334.

Lee, C.Y., Nguyen, T.P.-C., Grainger, D.W., Gamble, L.J., Castner, D.G., 2007.

Analytical Chemistry 79, 4390–4400. Liu, J., Tian, S., Nielsen, P.E., Knoll, W., 2005. Chemical Communications, 2969–2971. Limbut, W., Kanatharana, P., Mattiasson, B., Asawatreratanakul, P., Thavarungkul,

P., 2006. Biosensors and Bioelectronics 22, 233-240. Loyprasert, S., Thavarungkul, P., Asawatreratanakul, P., Wongkittisuksa, B., Limsakul, C., Kanatharana, P., 2008. Biosensors and Bioelectronics 24, 78–86.

Lucarelli, F., Marrazza, G., Turner, A.P.F., Mascini, M., 2004. Biosensors and Bioelectronics 19, 515-530.

Lucarelli, F., Tombelli, S., Minunni, M., Marrazza, G., Mascini, M., 2008. Analytica Chimica Acta 609, 139–159.

Mannelli, I., Minunni, M., Tombelli, S., Wang, R., Spiriti, M.M., Mascini, M., 2005. Bioelectrochemistry 66, 129-138.

Nielsen, P.E., 2001. Current Opinion in Biotechnology 12, 16-20.

Numnuam, A., Kanatharana, P., Mattiasson, B., Asawatreratanakul, P., Wongkitti-suksa, B., Limsakul, C., Thavarungkul, P., 2009. Biosensors and Bioelectronics 24, 2559-2565.

Peeters, S., Stakenborg, T., Reekmans, G., Laureyn, W., Lagae, L., Van Aerschot, A., Van Ranst, M., 2008. Biosensors and Bioelectronics 24, 72-77.

Samanman, S., Kanatharana, P., Chotigeat, W., Decahmag, P., Thavarungkul, P., 2011. Journal of Virological Methods 173, 75-84.

Shervedani, R.K., Hatefi-Mehrjardi, A., 2007. Sensors and Actuators B: Chemical

Su, X., Wu, Y.J., Robelek, R., Knoll, W., 2005. Langmuir 21, 348-353

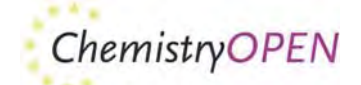
Suparpprom, C., Srisuwannaket, C., Sangvanich, P., Vilaivan, T., 2005. Tetrahedron Letters 46, 2833-2837.

Tichoniuk, M., Ligaj, M., Filipak, M., 2008. Sensors and Actuators 8, 2118-2135. Vilaivan, T., Srisuwannaket, C., 2006. Organic Letters 8, 1897–1900.

Wannapob, R., Kanatharana, P., Limbut, W., Numnuam, A., Asawatreratanakul, P., Thammakhet, C., Thavarungkul, P., 2010. Biosensors and Bioelectronics 26,

Wittung-Stafshede, P., Rodahl, M., Kasemo, B., Nielsen, P., Norden, B., 2000. Colloids and Surface A 174, 269-273

Wong, E.L.S., Chow, E., Gooding, J.J., 2005. Langmuir 21, 6957-6965.



DOI: 10.1002/open.201200016

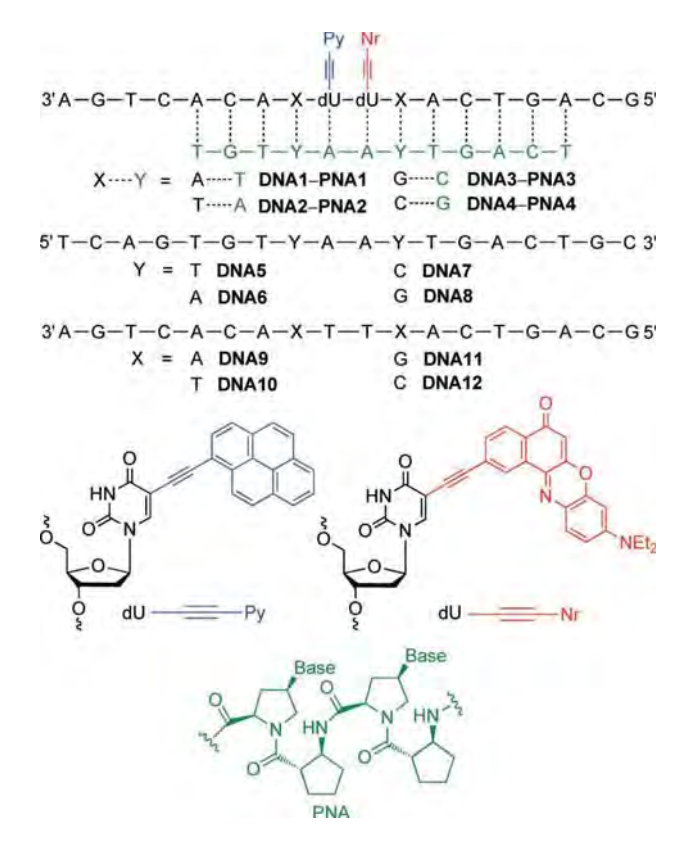
Conformational Control of Dual Emission by Pyrrolidinyl PNA-DNA Hybrids

Sabrina Sezi, [a] Reji Varghese, [a] Tirayut Vilaivan, *[b] and Hans-Achim Wagenknecht*[a]

The current interest in using nucleic acids as supramolecular scaffolds for the precise arrangement of chromophores is extremely high.^[1] This is triggered by the potential to control chromophore interactions through the geometry of the double helical structure and is also driven by the search for new multifluorescent probes for bioanalytics and for new multiluminescent organic materials. [2-6] However, the construction of nucleic acid-based multichromophores requires the understanding of photophysical interactions in chromophore pairs as the simplest unit along the helix. Wilhemsson et al. used rigid nucleic acid base analogues to study the influence of the relative orientation on energy transfer. [6] Recently, we published on white light-emitting DNA by combining ethynyl pyrene and ethynyl nile red as blue-green and red emitters.[4] Herein, we extend this concept to pyrrolidinyl PNA-DNA hybrids to study the influence of a conformationally restricted nucleic acid geometry.

Peptide nucleic acid (PNA) is a class of DNA analogues that consists of nucleobases attached to a peptide-like backbone. The original PNA with a flexible N-(2-aminoethyl)glycine backbone introduced by Nielsen et al. was shown to bind strongly to DNA and preferentially to RNA with high affinity and sequence specificity.^[7,8] We,^[9-11] as well as others,^[12-14] have shown that incorporating conformational rigidity into the PNA backbone could further improve the binding affinity, especially to DNA, as a result of decreased entropy loss upon hybridization. PNA systems derived from nucleobase-modified proline in (2'R,4'R) configurations in combination with cyclic β -amino acids including (R)-aminopyrrolidine-2-carboxylic acid (dapcP-NA),^[9] (2S)-aminocyclopentane-(1S)-carboxylic acid (acpcPNA)^[10] and (2S)-aminocyclobutane-(1S)-carboxylic acid (acbcPNA)^[11] formed very stable hybrids with complementary DNA. Much less stable hybrids were formed with RNA, and no self-pairing hybrids could be obtained in acpcPNA. [10] These properties have not been observed in other PNA systems. Recently, the artificial nucleobase 5-(1-pyrenyl)uracil was incorporated into acpcPNA to probe the sequence selectivity by fluorescence of hybrids with $\mathsf{DNA}.^{[15]}$

We applied, herein, dual-emitting oligonucleotides bearing ethynyl pyrene adjacent to ethynyl nile red to probe the differences in interactions in DNA duplexes compared to conformationally constrained acpcPNA-DNA hybrids. Using our published synthetic protocols, [4,10] we prepared doubly labeled oligonucleotides DNA1 to DNA4 and the corresponding acpcPNA counterstrands, PNA1 to PNA4. These strands can form fully complementary DNA-PNA hybrids in the binding region (e.g., DNA1-PNA1) in which the two fluorophores are embedded in four different sequential contexts (X-----Y, Scheme 1). DNA5 to DNA8 represent oligonucleotide counterstrands to DNA1 to DNA4, respectively, in order to compare the optical properties of the PNA-DNA hybrids with the corresponding doubly modified DNA duplexes (e.g., DNA1-DNA5). Additionally, PNA-DNA hybrids or DNA duplexes with two mismatches can be formed (e.g., DNA1-PNA2 or DNA1-DNA6). DNA9 to DNA12 represent reference oligonucleotides to measure the thermal stability of the unmodified acpcPNA-DNA hybrids (e.g,. DNA9-



Scheme 1. Sequences of modified oligonucleotides DNA1 to DNA4, acpcP-NA counterstrands PNA1 to PNA4, oligonucleotide counterstrands DNA5 to DNA8 and reference oligonucleotides DNA9 to DNA12.

Supporting information for this article is available on the WWW under http://dx.doi.org/10.1002/open.201200016.

© 2012 The Authors. Published by Wiley-VCH Verlag GmbH & Co. KGaA. This is an open access article under the terms of the Creative Commons Attribution Non-Commercial License, which permits use, distribution and reproduction in any medium, provided the original work is properly cited and is not used for commercial purposes.

 [[]a] S. Sezi, Dr. R. Varghese, Prof. H.-A. Wagenknecht Institute for Organic Chemistry, Karlsruhe Institute of Technology Fritz-Haber-Weg 6, 76131 Karlsruhe (Germany) E-mail: Wagenknecht@kit.edu

[[]b] Prof. T. Vilaivan Department of Chemistry, Faculty of Science, Chulalongkorn University Phyathai Road, Pathumwan, Bangkok 10330 (Thailand) E-mail: vtirayut@chula.ac.th

The optical properties of the acpcPNA-DNA hybrids in comparison with the corresponding DNA duplexes were characterized by UV/Vis absorption spectra, including melting temperatures (T_m) , and steady-state fluorescence spectroscopy (Table 1). The unmodified hybrids DNA9-PNA1 to DNA12-**PNA4** exhibit $T_{\rm m}$ values ranging from 71.8 °C to > 90 °C. Considering the fact that the PNA counterstrands PNA1 to PNA4 represent only a partial, 12 bases long complement, these $T_{\rm m}$ values are extremely high and show the extraordinary stabilizing effect of acpcPNA.^[10] On the other hand, it is highly interesting that the thermal stabilities of the acpcPNA-DNA hybrids contradict the known sequential effects in normal DNA. The only difference is that DNA9-PNA1 and DNA10-PNA2 contain two A-T base pairs where DNA11-PNA3 and DNA12-PNA4 bear two G-C base pairs. In normal DNA, an exchange of A-T by G-C base pairs increases the $T_{\rm m}$ values. With acpcPNA, the opposite effect is obtained, and the thermal stability is enhanced with A-T base pairs. The $T_{\rm m}$ values of PNA1 and PNA3 with their exactly complementary, unmodified DNA targets were 85.4 and 71.0 °C, respectively. These values are comparable to those obtained from the long target sequences used in this work, indicating that the binding should occur at the expected region. All four doubly labeled hybrids, DNA1-PNA1 to **DNA4-PNA4**, show reduced $T_{\rm m}$ values of 58.2–82.3 °C, due to

Table 1. Melting temperatures (T_m) and optical properties of acpcPNA-DNA hybrids in comparison with DNA duplexes.

Sequence ^[a]		<i>T</i> _m ^[b] [°C]	$\Delta A_{402}/\Delta A_{379}^{[c]}$	λ [nm] ^[d]	I ₆₆₅ /I ₄₄₀ ^[e]
DNA1	_	-	0.97	621	8.9
DNA1-DNA5	m	58.5	0.99	622	2.7
DNA1-DNA6	mm	48.7	1.02	624	9.0
DNA1-PNA1	m	82.3	0.92	618	3.6
DNA1-PNA2	mm	_[f]	0.96	622	9.1
DNA9-PNA1	m	86.0	-	-	-
DNA2	-	-	0.94	618	>10
DNA2-DNA6	m	57.2	0.97	620	4.3
DNA2-DNA5	mm	47.9	0.99	618	11.5
DNA2-PNA2	m	76.5	0.90	631	1.2
DNA2-PNA1	mm	_[f]	0.96	619	6.3
DNA10-PNA2	m	>90	-	-	-
DNA3		-	1.03	621	8.5
DNA3-DNA7	m	63.5	1.01	621	5.2
DNA3-DNA8	mm	51.2	1.06	622	> 10
DNA3-PNA3	m	58.2 _ ^[f]	0.95	623	2.2
DNA3-PNA4	mm		1.03	621	7.4
DNA11-PNA3	m	71.8	_	-	-
DNA4	_	_	0.91	622	> 10
DNA4-DNA8	m	64.3	0.98	623	1.7
DNA4-DNA7	mm	36.4	0.91	621	> 10
DNA4-PNA4	m	77.4	0.90	637	1.0
DNA4-PNA3	mm	_[f]	0.91	622	8.9
DNA12-PNA4	m	>90	=	_	-

[a] m = match, mm = mismatch. [b] Conditions: duplex (2.5 μM), buffer (10 mм Na-P_i, 250 mм NaCl, pH 7), 20–90 °C, 0.7 °C min⁻¹. [c] Absorption ratios at 402 nm versus 379 nm. [d] Absorption maximum of the nile red chromophore. [e] Fluorescence intensity ratios at 665 nm versus 440 nm. [f] $\Delta\Delta A < 0.05$.

the presence of the two fluorophores. On the other hand, the $T_{\rm m}$ values of these acpcPNA-DNA hybrids are generally higher compared with the corresponding doubly labeled DNA duplexes (i.e., DNA1-DNA5 to DNA4-DNA8, except DNA3-DNA7 in comparison with DNA3-PNA3). Mismatch-containing DNA duplexes (e.g., DNA1-DNA6) show strongly reduced thermal stabilities (-9.3 °C to -27.9 °C), while mismatch-containing acpcP-NA-DNA hybrids are not formed at all (e.g. DNA1-PNA2), as expected based on our previous results and as supported by the low absorption differences in the melting temperature experiments.[10]

The UV/Vis absorption of both the doubly modified acpcP-NA-DNA hybrids and the DNA duplexes show the presence of both chromophores at ~370-400 nm (ethynyl pyrene) and ~620 nm (ethynyl nile red). If excited at 380 nm, which is highly selective for ethynyl pyrene, the various single strands, hybrids and duplexes show dual emission at ~440 nm (ethynyl pyrene) and ~665 nm (ethynyl nile red) as the result of an energy transfer between both chromophores. In the most interesting case from the supramolecular point of view, the contributions of the blue-green and the red emission are equal, and thereby an emission of white light is generated. [4] A careful examination reveals two major differences in the UV/Vis absorption of the various samples (Figure 1 and the Supporting Information): Both the ratio of the two absorption bands of ethynyl pyrene at ~402 nm and ~379 nm as well as the maximum of nile red absorption varies significantly (Table 1). According to our previous results, the UV/Vis band at approximately 402 nm represents the absorption of an excitonically coupled complex of the ethynyl pyrene chromophore with one of the adjacent DNA bases.^[16] In the randomly folded single stranded DNA, these interactions are generally less pronounced. However, a higher extent of prestacking between the ethynyl pyrene and purines (A or G) exist in DNA1 and DNA3, respectively, as the corresponding absorption ratios $(\Delta A_{402}/\Delta A_{379})$ are higher compared with those of **DNA2** and DNA4. In principle, ground state interactions interfere with energy transfer, because the latter process requires the excitation of an uncoupled chromophore as energy donor (ethynyl pyrene) and subsequent transfer of excitation energy to an uncoupled and unexcited chromophore as acceptor (ethynyl nile red). Hence, it is not surprising that those single stranded oligonucleotides (DNA2 and DNA4), in which the ethynyl pyrene is less coupled in the ground state (according to the ratios $\Delta A_{402}/\Delta A_{379}$), exhibit better energy-transfer efficiencies (indicated by higher nile red emission, and displayed by higher fluorescence intensity ratios $I_{665}/I_{440} > 10$).

If the single strands DNA1 to DNA4 are annealed with the corresponding fully complementary counterstrands DNA5 to DNA8, the absorption side band at ~402 nm gets intensified, and the ratios $\Delta A_{402}/\Delta A_{379}$ increase accordingly. This is not a new result and has been reported previously. [14] However, intensified ground state interactions of the ethynyl pyrene chromophore with adjacent DNA bases in double stranded DNA inhibits energy transfer to ethynyl nile red. As a result, the fluorescence intensity at ~665 nm gets decreased significantly without a corresponding increase of the ethynyl pyrene emis-

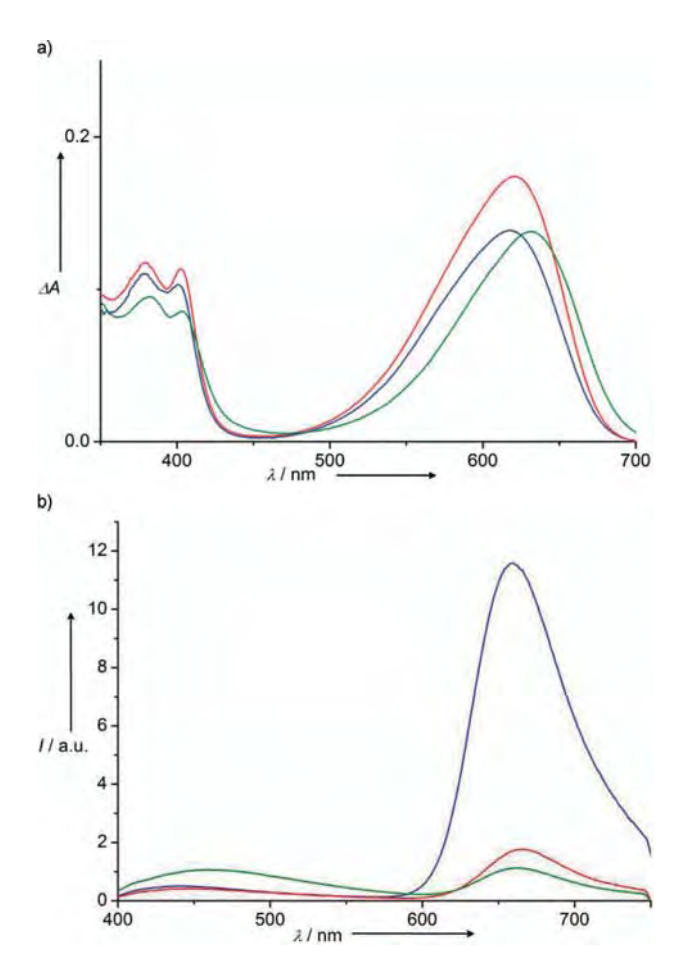
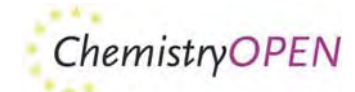


Figure 1. a) UV/Vis absorption and b) fluorescence representatively shown for single stranded DNA2 (----), double stranded DNA2-DNA6 (--**DNA2-PNA2** (——; 2.5 μм each) in buffer (10 mM Na-P_i, 250 mM NaCl, pH 7) at 20 °C and $\lambda_{\rm exc}$ 380 nm.

sion at \sim 440 nm. The ratio of the fluorescence intensities I_{665}/I_{665} I_{440} are reduced to values between 1.7 (**DNA4-DNA8**) and 5.2 (DNA3-DNA7). It is important to note here that the excitonic interactions do not require the fully matched DNA architecture around them, as they are formed also in the mismatched DNA duplexes (DNA1-DNA6 to DNA4-DNA7). However, in the latter duplexes they do not interfere with energy transfer. Obviously, transition dipole moments of the nonstacked subensemble can—due to higher conformational flexibility—adapt an orientation that is more suitable for efficient energy transfer. Thus, fluorescence intensity ratios I_{665}/I_{440} in the mismatched duplexes are similar to those of the corresponding single strands DNA1 to DNA4.

If the single strands DNA1 to DNA4 are annealed with corresponding fully complementary acpcPNA strands PNA1 to PNA4, the optical properties change quite significantly compared with the DNA duplexes. Except for **DNA1-PNA1**, the I_{665}/I_{665} I_{440} ratios are generally lower than that of the corresponding DNA duplexes, ranging between 1.0 (DNA4-PNA4) to 3.6 (DNA1-PNA1). The fluorescence intensity ratio bears no relationship to the duplex stability as can be seen by the lower I₆₆₅/I₄₄₀ ratio, despite the lower thermal stability of **DNA3**-PNA3 compared with DNA3-DNA7. In addition, the absorption side bands of ethynyl pyrene at ~402 nm get reduced and the absorption ratios $\Delta A_{402}/\Delta A_{379}$ get decreased accordingly. This observation indicates that the stacking interactions between the ethynyl pyrene chromophore and adjacent DNA bases are interrupted by the conformational constrain, which is introduced in acpcPNA-DNA hybrids. According to our discussion for the matched DNA duplexes above, this should yield stronger nile red fluorescence intensity at ~665 nm compared with DNA double strands. However, the opposite effect is observed: the red emission is also reduced in the acpcPNA-DNA hybrids. This result can be explained by two different effects that are probably combined to various extents in the different acpcP-NA-DNA hybrids. Firstly, except for DNA1-PNA1, the ethynyl pyrene fluorescence in acpcPNA-DNA hybrids increases slightly relative to DNA duplexes. The observed difference of the energy-transfer efficiencies is likely due to the change in the relative orientation of the chromophore dipole moments[3] upon duplex formation with PNA (helically twisted conformation), which partially prohibits an efficient energy transfer. With the published doubly modified DNA-DNA duplexes^[4] we observed that even if the difference in the energy transfer is small (according to the rather small increase of ethynyl pyrene fluorescence intensity), the significant drop of the red emission intensity in the duplex is due to the large molar extinction coefficient and the high fluorescence quantum yield of ethynyl nile red. Secondly, a careful examination of the ethynyl nile red absorption reveals changes of its maximum wavelength (most pronounced in DNA2-PNA2). This again supports ground state interactions between nile red and ethynyl pyrene, and thereby again interferes with ethynyl nile red emission induced by

The inspection of photophysical interactions in chromophore pairs is crucial for using the geometries of nucleic acid hybrids with artificial backbones for the development of multichromophore systems. From our results it becomes clear that the strong binding to DNA (high $T_{\rm m}$ values) and the pronounced sequence selectivity including mismatch discrimination of acpcPNA provides added value to the basic concept of self-assembled nucleic acid-based nanostructures and multichromophore arrangements. Among the samples presented herein, especially hybrids DNA2-PNA2 and DNA4-PNA4 show nearly equal contributions of the blue-green and red emission and, thus, represent white-light emitters with better thermal stability than the previously published white light-emitting DNA (WED).[4] These results demonstrate that the control of photophysical interactions between chromophores can be much better realized with the sterically constrained pyrrolidinyl PNA. Especially acpcPNA has a significant potential and should play an increasing role for the development of both fluorescent probes and nucleic acid-based nanomaterials.



Acknowledgements

This work was supported by the Alexander von Humboldt Foundation (R.V. and T.V.), the Deutsche Forschungsgemeinschaft (DFG) (GRK 640) and the Thailand Research Fund (RTA5280002).

Keywords: biosensors · fluorescence · nanomaterials · nucleic acids · peptides

- [1] a) R. Varghese, H.-A. Wagenknecht, Chem. Commun. 2009, 2615-2624; b) V. L. Malinovskii, D. Wenger, R. Haner, Chem. Soc. Rev. 2010, 39, 410-422; c) A. Ruiz-Carretero, P. G. A. Janssen, A. Kaeser, A. P. H. J. Schenning. Chem. Commun. 2011, 47, 4340-4347; d) T. J. Bandy, A. Brewer, J. R. Burns, G. Marth, T. Nguyen, E. Stulz, Chem. Soc. Rev. 2011, 40, 138-148.
- [2] a) M. E. Østergaard, P. J. Hrdlicka, Chem. Soc. Rev. 2011, 40, 5771 5788; b) S. P. Sau, P. J. Hrdlicka, *J. Org. Chem.* **2012**, *77*, 5 – 16.
- [3] a) Q.-H. Xu, B. S. Gaylord, S. Wang, G. C. Bazan, D. Moses, A. J. Heeger, Proc. Natl. Acad. Sci. USA 2004, 101, 11634-11639; b) M. Endo, T. Shiroyama, M. Fujitsuka, T. Majima, J. Org. Chem. 2005, 70, 7468-7472; c) T. Nguyen, A. Brewer, E. Stulz, Angew. Chem. 2009, 121, 2008-2011; Angew. Chem. Int. Ed. 2009, 48, 1974-1977; d) D. Navarathne, Y. Ner, J. G. Grote, G. A. Sotzing, Chem. Commun. 2011, 47, 12125 – 12127; e) W. Su, M. Schuster, C. R. Bagshaw, U. Rant, G. A. Burley, Angew. Chem. 2011, 123, 2764-2767; Angew. Chem. Int. Ed. 2011, 50, 2712-2715.
- [4] a) R. Varghese, H.-A. Wagenknecht, Chem. Eur. J. 2009, 15, 9307-9310; b) R. Varghese, H.-A. Wagenknecht, Org. Biomol. Chem. 2010, 8, 526-
- [5] R. E. Dale, J. Eichinger, Biopolymers 1974, 13, 1573 1605.

- [6] K. Börjesson, S. Preus, A. H. El-Sagheer, T. Brown, B. Albinsson, L. M. Wilhemsson, J. Am. Chem. Soc. 2009, 131, 4288-4293.
- a) P. E. Nielsen, M. Egholm, R. H. Berg, O. Buchardt, Science 1991, 254, 1497 – 1500; b) M. Egholm, O. Buchardt, L. Christensen, C. Behrens, S. M. Freier, D. A. Driver, R. H. Berg, S. K. Kim, B. Norden, P. E. Nielsen, Nature **1993**, 365, 566-568.
- [8] B. Hyrup, P. E. Nielsen, Bioorg. Med. Chem. 1996, 4, 5-23.
- [9] T. Vilaivan, G. Lowe, J. Am. Chem. Soc. 2002, 124, 9326-9327.
- [10] a) T. Vilaivan, C. Srisuwannaket, Org. Lett. 2006, 8, 1897 1900; b) C. Vilaivan, C. Srisuwannaket, C. Ananthanawat, C. Suparpprom, J. Kawakami, Y. Yamaguchi, Y. Tanaka, T. Vilaivan, Artificial DNA, PNA & XNA 2011, 2, 50 - 59
- [11] W. Mansawat, C. Vilaivan, Á. Balázs, D. J. Aitken, T. Vilaivan, Org. Lett. **2012**, 14, 1440 - 1443.
- [12] V. A. Kumar, K. N. Ganesh, Acc. Chem. Res. 2005, 38, 404–412.
- [13] J. K. Pokorski, M. A. Witschi, B. L. Purnell, D. H. Appella, J. Am. Chem. Soc. 2004, 126, 15067-15073.
- [14] R. J. Worthington, A. P. O'Rourke, J. Morral, T. H. S. Tan, J. Micklefield, Org. Biomol. Chem. 2007, 5, 249-259.
- [15] C. Boonlua, C. Vilaivan, H.-A. Wagenknecht, T. Vilaivan, Chem. Asian J. **2011**, *6*, 3251 – 3259.
- [16] a) E. Mayer, L. Valis, C. Wagner, M. Rist, N. Amann, H.-A. Wagenknecht, ChemBioChem 2004, 5, 865-868; b) C. Wagner, M. Rist, E. Mayer-Enthart, H.-A. Wagenknecht, Org. Biomol. Chem. 2005, 3, 2062-2063; c) A. Trifonov, M. Raytchey, J. Buchvarov, M. Rist, J. Barbaric, H.-A. Wagenknecht, T. Fiebig, J. Phys. Chem. B 2005, 109, 19490 - 19495.

Received: May 4, 2012

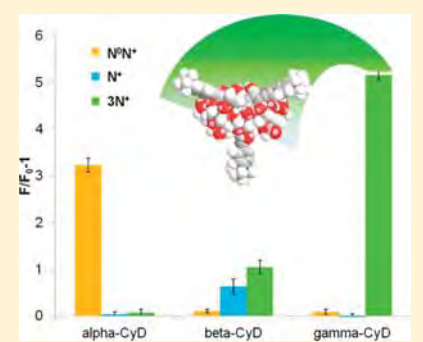
Published online on July 11, 2012

Inclusion Complexes between Amphiphilic Phenyleneethynylene Fluorophores and Cyclodextrins in Aqueous Media

Warathip Siripornnoppakhun, Nakorn Niamnont, Akachai Krumsri, Gamolwan Tumcharern, Samolwan T Tirayut Vilaivan,[†] Paitoon Rashatasakhon,[†] S. Thayumanavan,^{||} and Mongkol Sukwattanasinitt*^{,†}

Supporting Information

ABSTRACT: Binding events of cyclodextrins (CyD's) in aqueous media are important for designing and explaining the host-guest chemistry applied in sensing and controlled release systems. A water-soluble tricationic compound $(3N^+)$ with three branches of phenyleneethynylene fluorescent moieties and its related amphiphilic compounds $(3C^{-}, N^{0}N^{+}, N^{+}, and 2N^{+})$ are employed as molecular probes in the systematic characterization of the supramolecular interactions with CyD's $(\alpha, \beta, \text{ and } \gamma)$. The strong fluorescence enhancement, combined with induced circular dichroism (CD) signals and ¹H NMR data, is evidence of 1:1 static inclusion complexes of $3N^+/\gamma$ -CyD and $2N^+/\gamma$ -CyD. $3N^+$ presents a structural design which can form inclusion complexation with γ -CyD with one of the highest binding constants of 3.0×10^4 . The relatively moderate fluorescence enhancement, shift of ¹H NMR signals, and weak induced CD signals indicate fast exchange complexation of β -CyD with the amphiphilic guest molecules. The interaction with



 α -CyD is perceived only for $\mathbf{N}^{\mathbf{0}}\mathbf{N}^{+}$, the only nonbranched fluorescent guest model, via its strong fluorescence enhancement. However, the lack of ¹H NMR signal splitting and the lack of induced CD signals suggest the noninclusion mode of binding between N^0N^+ and α -CyD.

■ INTRODUCTION

Cyclodextrins (CyD's), a well-known class of host compounds used in sensing and controlled release applications, are cyclic oligosaccharides that selectively form inclusion complexes with guest molecules. Their unique configurations have a hydrophilic outer surface and a hydrophobic inner surface with the inner cavity diameters reported at 5.0, 6.2, and 8.0 Å for α -CyD, β -CyD, and γ -CyD, respectively.² In the aqueous phase, CyD's are amphiphilic and may interact with other chemical species that interfere with their collisional probability and hydration dynamics, leading to changes in their physical and chemical properties.³ These changes may be observed by various techniques to study the interactions between CyD's and guest molecules; examples include ¹H NMR, ⁴ mass spectrometry, ⁵ electrophoresis, ⁶ UV-vis absorption spectroscopy, ⁷ fluorescence spectroscopy, circular dichroism (CD) spectroscopy, X-ray crystallography, and computational calculations. Understanding the binding events of CyD's in aqueous media is crucial for employing their host-guest chemistry in sensing and controlled release systems. The inclusion complexes of CyD's have so far been held responsible for most spectroscopic changes observed in solution. In the solid phase, X-ray crystallography can generally provide unarguable proof of an inclusion complex. It is however trickier to have definitive

evidence of an inclusion complex in solution, due to its dynamic nature. We have thus taken the task of gathering evidence for inclusion complexes of CyD's in aqueous solution as our current research problem. We also aim to find structural attributes of the guest compounds that can enhance the stability of the inclusion complex in an aqueous system. Other parts, besides the hydrophobic cavity of the CyD structure (i.e., secondary hydroxyl groups on the wider rim, primary hydroxyl groups on the narrow rim, and the polar oxygen lone pair on the outer annulus)¹² may also take part in the binding events.

To study the inclusion complexes of CyD's in an aqueous system, amphiphilic molecular probes which allow comprehensive characterization by various spectroscopic methods are desirable. We have recently developed a water-soluble tricationic compound $(3N^+)$ with phenyleneethynylene fluorescent moieties which shows strong fluorescence responses upon protein and DNA binding. ¹³ Interaction of this amphiphilic fluorophore with the nanoconfined environment of CyD's is thus easily probed by fluorescence measurement. Extensive spectroscopic investigation of this compound and its

Received: June 12, 2012 Revised: September 6, 2012 Published: September 8, 2012

 $^{^\}dagger$ Department of Chemistry, Faculty of Science, Chulalongkorn University, Bangkok 10330, Thailand

^{*}Department of Chemistry, Faculty of Science, King Mongkut's University of Technology Thonburi, Bangkok 10140, Thailand

[§]Thailand National Nanotechnology Center, National Science and Technology Development Agency, Patumthanee 12120, Thailand

Department of Chemistry, University of Massachusetts at Amherst, Amherst, Massachusetts 01003, United States

family ($3C^{\circ}$, N^0N^+ , N^+ , and $2N^+$) provides useful information toward our objectives of obtaining evidence for CyD inclusion complexes in solution and molecular designs of suitable guest compounds.

■ EXPERIMENTAL SECTION

Absorption, Emission, and CD Spectroscopies. All spectroscopic measurements were performed on the solution samples in sodium phosphate buffer (pH 7, 10 mM) containing NaCl (100 mM) in a quartz cuvette (10 mm light path). The instruments used in data acquisition were a Varian Cary 50 UV—vis spectrophotometer, Varian Cary Eclipse spectrofluorometer, and JASCO CD spectrometer. The solutions of the fluorophore and CyD were thoroughly mixed and allowed to stand for 5 min before each measurement.

MS Spectroscopies. A mixture of each fluorophore/CyD pair was prepared in Milli-Q water at room temperature. The final concentrations of the fluorophores and CyD's are 10 and 40 μ M (fluorophore:CyD = 1:4). The MS data were acquired using the positive ion mode on a Micromass Quattro micro TM API electrospray ionization mass spectrometer (Waters, Milford, MA).

Synthesis. Synthesis procedures and characterization data of new amphiphilic fluorophores are described in the Supporting Information.

■ RESULTS AND DISCUSSION

We started our investigation by observing the changes of the fluorescence signal of $3N^+$ (5 μ M) upon the addition of α -, β -, and γ -CyD's (20 μ M). As shown in Figure 1a, γ -CyD dramatically enhanced the emission signal of $3N^+$, while β -CyD increased the signal only slightly and α -CyD did not create any changes of the spectrum at all. These results suggested that $3N^+$ interacted strongly with γ -CyD and only

weakly with β -CyD but may not interact with α -CyD. It is also interesting to note that the signal enhancement goes hand-in-hand with the blue shift, which implies the interaction with γ -CyD is involved in either a reduction of the π -conjugation length of the fluorophore or a reduction in its geometrical relaxation and intramolecular charge transfer (ICT). 3a,d,11,14

To identify the cause of this blue shift, the absorption spectra of $3N^+$ in the absence and presence of CyD's were recorded. The absorption spectra revealed that only γ -CyD caused a significant blue shift of the maximum absorption wavelength (λ_{max}) of the fluorophore from 370 to 364 nm (Figure 1b). This 6 nm (0.055 eV) shift is much smaller than the 40 nm (0.225 eV) shift present in the emission spectra, which indicates only a minor contribution of the change of the π -conjugation length to the blue shift of the emission maximum. The restriction of geometrical relaxation and the ICT process are thus the main contributors that indeed support the formation of an inclusion complex between $3N^+$ and γ -CyD in the aqueous medium.

In our next investigation, ¹H NMR spectra of 3N⁺ and its mixture with each CyD, at a 1:4 mole ratio, were compared. The $3N^+/\alpha$ -CyD mixture gave sharper and slightly downfield shifted ¹H NMR signals of 3N⁺, indicating some interactions between $3N^+$ and α -CyD. This interaction was not observed in the form of fluorescence enhancement as noted earlier, which is likely due to a much lower concentration (\sim 1/400) used in the fluorescence experiment. Therefore, the interaction between $3N^+$ and α -CyD is probably rather weak. For the mixture with β -CyD, all four aromatic signals of $3N^+$ became even sharper and more downfield shifted (Figure 2), which signified stronger interaction. In the case of $3N^+/\gamma$ -CyD, the four aromatic signals of 3N⁺ split into seven peaks which could be assigned to two sets of chemically inequivalent phenyleneenthynylene branches. One set consisted of the signals at 7.94, 7.71, 7.03, and 6.87 ppm (a, b, c, and d), and the other set contained the peaks at 7.83, 7.77, and 7.30 ppm (a', b', c', and d'). The peak pattern in the first set looked quite similar to those of the original $3N^+$, while the second set appeared with a quite different pattern. These two sets of peaks indicate unsymmetrical interaction of the three phenyleneethynylene branches of $3N^+$ with γ -CyD. The 2:1 integration ratio between the first and second sets also signifies that two phenyleneethynylene branches of 3N+ interact only weakly with γ -CyD while the other branch interacts quite strongly, probably via inclusion complexation. As the mixture contained excess γ -CyD (4 equiv), the ¹H NMR spectrum also showed the original signals of γ-CyD (for ¹H

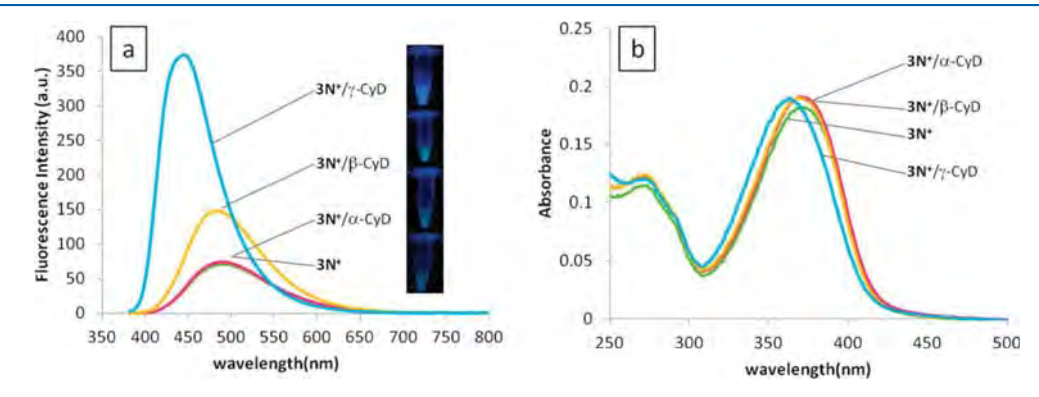


Figure 1. (a) Emission spectra and (b) absorption spectra of $3N^+$ (5 μ M) in the presence of α -, β -, and γ -cyclodextrins (20 μ M), excited at 370 nm. Inset: photographs of mixtures of $3N^+$ with CyD's under black light irradiation.